Perception and representation of temporally patterned odour stimuli in the mammalian olfactory bulb

Thesis submitted for the degree of Doctor of Philosophy

Andrew Erskine

University College London
Department of Neuroscience, Physiology and Pharmacology

Supervisor

Dr. Andreas T. Schaefer

Examiners

Dr. David Bannerman

Dr. Matt Grubb

Dedicated to the memories of my Grandparents, Dr. Norman Macleod (1926-2017) and Dr. Marion Macleod (1930-2017), who paved the way.

I, Andrew Erskine, confirm that the work presented in this thesis is my own. Where information has been derived from other sources, I confirm that this has been indicated in the thesis.

Signed:

Contents

List of Figures

List of Tables

Where data or analyses have been generated by others or in collaboration, specific contributions are given in the end matter experimental acknowledgements.

Abstract

Sensory stimuli in natural environments are dynamic and complex. The neural circuits of sensory systems in the brain are therefore adapted to extract meaningful information from this dynamic input. An attractive model system for understanding how such sensory input is processed in neural circuits is the mammalian olfactory bulb (OB). The OB has a convenient dorsal anatomical location for e.g. probe implantation, viral delivery and a well-defined circuit architecture. Furthermore, olfaction in rodent models is extremely behaviourally salient and OB circuit function can therefore be efficiently investigated in the context of behavioural response. Historically, investigation of OB function has focused on encoding of odour quality, utilising static, square pulse stimuli to explore this problem. This is in stark contrast to odour transmission in natural environments, which is governed by the chaotic structure of air turbulence, creating odour plumes. There are a number of lines of evidence suggesting that temporal information in odour plumes – the fluctuations in odour concentration within this structure – can be behaviourally relevant for olfactory based navigation and odour scene segmentation. I here posit that temporal correlations in concentration for mixtures of odours transmitted in plumes are a potential mechanism by which animals identify odour objects: mixtures of odours emanating from a common source. Using neuronal imaging, high-throughput behavioural methods, high-speed odour delivery and physical recording of odour plume dynamics, I show that temporal correlations exist between pairs of odours emanating from the same source; that mice can perceive this correlation structure and that temporal correlation is represented in the output cells of the olfactory bulb. These results indicate that mammalian olfaction operates at a higher temporal bandwidth than previously thought, and that detection of temporal features in odour signals may represent a potential mechanism for olfactory scene segmenetation.

Impact Statement

Natural sensory scenes are generally composed of complex, overlapping features which the brain must be able to segment and parse in order to generate useful perception and behavioural responses. A classic example is the auditory 'cocktail party problem': in a room full of multiple people holding separate, concurrent conversations how is the brain able to focus in on a single relevant conversation and filter out all the similar auditory stimuli in the room? A similar problem exists for the brain's olfactory system. Natural olfactory environments are generally made up of many different chemical volatiles emanating from separate, distinct sources but mixing together in air to create complex mixtures. How then can organisms hone in on individual odours of interest and determine that they come from a single source (e.g. food, predator) in the presence of a complex background odour environment? The broad finding of this thesis is that the temporal dynamics of odours signals - generated by natural air turbulence - are informative of the source and location of odour objects. It is shown here that these temporal dynamics are present in odour plumes; that they are predictive of odour source proximity; and that they are utilised in behaviour and represented by the neurons of the mouse olfactory bulb. This finding is predicted to have impact on the field of olfaction research as it demonstrates that the temporal dynamics of odour signals, while perhaps previously overlooked in mammalian olfaction research, are an important component of olfactory behavioural responses. More generally, the finding provides clues as to how the brain deals with and responds to complex sensory environments and may be of use in designing odour sensing robots with the ability to detect and locate certain chemical signatures in the environment (e.g. in bomb / drug detection).

In coming to this finding, a number of methodological advancements were made that have potential impact in the neuroscience and broader research communities. First, this thesis describes the development of AutonoMouse: a tool for con-

ducting high-throughput automated behavioural experiements in large cohorts of mice. AutonoMouse allows for high volumes of reliable behavioural data to be collected from mice without water restriction techniques and whilst minimising human presence during experiments. Although this tool is primarily used for olfaction research in this thesis, the technique is generally applicable to a range of other fields that utilise behavioural analysis methods (e.g. other areas of sensory neuroscience, pharmacology etc.) where it could likely also improve data throughput, as well as reproducibility and standardisation between labs. Furthermore, a new olfactometer design is introduced in this thesis based on high-speed injection valves. This new design allows for a significantly higher degree of fine-scale control over odour stimulus production in terms of output concentration and temporal bandwidth than has been reported previously. This is likely to be of particular utility to the olfactory research community. Finally, a method is here described for simultaneous detection of the temporal dynamics of two simultaneously occurring odours. This is achieved using fast photo-ionisation detectors and a simple computational algorithm to 'decompose' the signals of two individual odours mixed together in air. This will likely have impact on the olfaction research community - or anyone who requires careful calibration of the components of odour mixtures.

Part I.

Introduction

Thesis overview

The general objective of this thesis is to contribute to the understanding of how the brain processes sensory information and what behaviours can be achieved based on this input. I have chosen the early olfactory system in mice as a model system to explore these processes, comprising the olfactory sensory neurons of the nasal epithelium and the olfactory bulb - the primary information processing structure in olfaction and the area on which I will focus. The choice of an early processing stage as a model system has the advantage that information flow through it is largely defined by its sensory input, as opposed to e.g. cortical structures and their complex reciprocal interactions with other brain areas. This means that input-output characteristics of this system can be reliably and effectively probed with controlled stimuli. The olfactory bulb is a convenient structure to work on due to its anatomically isolated positioning in a dorsal region, allowing for easy access with various manipulation and recording techniques (Wilson and Mainen, 2006). Olfaction itself is also a useful sensory system to consider, given its tight relationship with behavioural responses in laboratory rodents, allowing for rapid training in a variety of behavioural tasks that can then be linked back to circuit function (Abraham et al., 2004, Uchida and Mainen, 2007, Abraham et al., 2010, Shen et al., 2013, Li et al., 2014, Rokni et al., 2014, Resulaj and Rinberg, 2015, Roland et al., 2016).

The majority of work in olfactory processing has asked how the neural circuits of the olfactory system allow for the quality of odour stimuli to be distinguished, asking how odour stimulus space - where space is the set of detectable odours - is represented in the brain (Yokoi et al., 1995, Bodyak and Slotnick, 1999, Uchida and Mainen, 2003, Abraham et al., 2004, Barnes et al., 2008, Abraham et al., 2010, Nunes and Kuner, 2015). Natural transmission of airborne odours is via mass air movement and turbulence, creating transmission structures known as 'plumes'. Plumes are random, chaotic structures due to their generation by turbulent flow (reviewed in Celani et al., 2014). However, there is evidence to suggest that temporal information within these plumes - in the form of the structure of their concentration fluctuations - contains highly salient signals that can be used in various olfactory sensory computations and behaviours (Hopfield, 1991, Moore and Atema, 1991, Fort and Rospars, 1992, Murlis, 1992, Hendin et al., 1998, Hopfield,

1999, Weissburg et al., 2002, Vergassola et al., 2007). I will ask what the extent is to which temporal features in odour transmission contain robust information about the environment of potential use to behaving animals; whether animals perceive these temporal features and use them to inform behaviour; and how temporal information is represented in the neural circuits of the early olfactory system.

1. Anatomy and function of early olfactory structures

1.1. Olfactory epithelium

In vertebrates, odour signals are drawn into the nasal cavity by respiration and across the nasal epithelium. The nasal epithelium is home to a specialised class of sensory neurons known as olfactory sensory neurons (OSNs) which are capable of detecting and responding to volatile odourants. There are roughly 5x10^6 OSNs in rodent nasal epithelium (Getchell and Getchell, 1991, Ressler et al., 1993, Shipley et al., 1995, Shepherd and Greer, 1998). These cells express olfactory receptors (OR), which bind to odour molecules and generate a second messenger response, causing excitation of OSNs (Raming et al., 1993). ORs are generally a G-protein coupled 7 transmembrane domain protein, and there exists a wide variety and number of types within this family with around 1000 OR genes present in rodents (Pevsner et al., 1988, Jones and Reed, 1989, Buck and Axel, 1991, Raming et al., 1993, Buck, 1996, Young et al., 2002). Each OSN expresses only a single type of OR out of this large family (known as the 'one-neuron, one-receptor' rule), resulting in a large heterogeneity of different OSN types (Ibarra-Soria et al., 2014, Saraiva et al., 2015). OSNs of different types (expressing different ORs) are organised into several broad zones within the nasal epithelium, but within these zones OSNs are organised in a seemingly random pattern (Ressler et al., 1993, Vassar et al., 1993, de Bruyne et al., 2001).

Though each OSN expresses a single OR, ORs are usually not solely activated by a single odour ligand. Rather, ORs bind to different odorants with unique affinity profiles (Malnic, 1999). Some OSNs therefore respond to many odours in a test set, and others to just one or two test odours (Pfaff and Gregory, 1971,

Revial et al., 1983, de Bruyne et al., 1999, Malnic, 1999, Uchida et al., 2000, de Bruyne et al., 2001, Wachowiak and Cohen, 2001, Wang et al., 2003, Araneda et al., 2004) [1]. Moreover, the set of odours that bind an OR generally cannot be classified according to a single molecular property and do not tend to respond to e.g. a particular functional chemical group or structure (Revial et al., 1983, Malnic, 1999, Araneda et al., 2000, Wetzel et al., 2001, Bozza et al., 2002, Araneda et al., 2004, Hallem et al., 2004, Yao et al., 2005).

1.1.1. Olfactory sensory neuron physiology

OSN types display heterogeneous baseline firing properties based on the type of OR they express (Hallem et al., 2004, Yu et al., 2004, Connelly et al., 2013). When activated by an odour ligand, a signalling cascade is initiated via a G-protein and type III adenylyl cylcase producing cAMP as the second messenger. This drives a Ca^{2+}-activated Cl^- channel, producing a slow depolarisation followed by a burst of action potentials (Tomaru and Kurahashi, 2005, Touhara and Vosshall, 2009, Connelly et al., 2013). OSNs respond in a graded manner, with higher action potential frequency induced by higher odorant concentrations (Ma et al., 1999, Imanaka and Takeuchi, 2001) and can therefore relay concentration information to the olfactory bulb.

In mammals, the delay between odour arrival in the nose and sensory response is governed by a number of factors: the shape of the turbinates within the nose and therefore the path the odour must take through the nose to bind to OSNs (Kent et al., 1996); the time taken for odour to diffuse into mucous membranes to reach receptors (Grosmaitre et al., 2006); the receptor-odor binding affinity and the signalling transduction pathway that occurs after binding; and the concentration of the odour stimulus (Spors et al., 2006, Connelly et al., 2013). It is therefore difficult to reach an exact lower bound on the response time of an OSN to odour presentation at the nose, but this can be approximated with existing behavioural and physiological studies.

Isolated mouse OSNs recorded on a suction pipette in solution while presented

[1] This result of course depends on the test set of odours used. There are 1000s of detectable volatile odorants and, while statistically unlikely, it is feasible that OSN receptive fields become more similar over a wider range of test odours (Wilson and Mainen, 2006)

with cineole show rapid depolarisation, reaching peak amplitude within 100ms (Reisert and Matthews, 2001). Given that the time for a switch between clean and odourised solution in this study was estimated to be ~70ms, this suggests that the entire process of odour-receptor binding, signal cascade and resulting cell depolarisation can happen on the order of 10s of milliseconds in mammalian OSNs (Reisert and Matthews, 2001). This process, however, can certainly be slower for different odour/receptor pairs. Using an intact epithelium preparation with targeted patch-clamp recordings of MOR23 cells, Grosmaitre et al., 2006 show that the response latency of these OSNs presented with their primary ligand (lyral) is on the order of 160ms. The authors of this study also show that a significant fraction of this response latency arises from the time taken for the odourised solution to reach OSN receptors after delivery by using a high K+ solution as a stimulus. In this case the response latency is ~75ms, suggesting that the process of receptor binding, internal signalling cascade and resulting depolarisation takes around 85ms in the case of MOR23 OSNs stimulated with lyral. In a different approach, Spors et al., 2006 image OSN glomeruli terminals by loading calcium Green-1 dextran presynaptically, allowing for observation of the activity of multiple OSNs simultaneously *in vivo.* In this approach, a variety of response time courses were observed depending on the odour and glomerulus imaged, but the T10 of responses (time to 10% of maximal response amplitude after odour presentation to the nose) were generally on the order of 50-100ms, with the lower bound of latencies seen for higher odour concentrations, again suggesting that OSN response latencies are in the 10s of milliseconds range. Postsynaptic from the OSN terminals, projection neurons of the olfactory bulb have also been observed to fire within 100ms after odour presentation in *vivo* (Fukunaga et al., 2012). Finally, combined physiology and behavioural work has shown that reliable cell- and odour-specific spike patterns occur in the OB within the first inhalation after odour presentation, with the first informative stimulus component arising in as little as 30-40ms (Cury and Uchida, 2010) - again suggesting that the temporal delay between odour arriving in the nose and detectable OSN depolarisation is on the order of 10s of milliseconds, in line with latency timescales reported for insect OSNs (Raman et al., 2010, Nagel and Wilson, 2011).

1.2. Olfactory bulb

1.2.1. Feedforward projections to mitral and tufted cells

Though OSNs are intermingled throughout the nasal epithelium in their spatial arrangement, axons from these cells converge and terminate on specific, focal locations in the olfactory bulb known as glomeruli. OSN axons target two mirror glomeruli on each OB hemisphere (Ressler et al., 1994, Vassar et al., 1994, Mombaerts et al., 1996), which are reciprocally linked by intrabulbar projections (Ressler et al., 1994, Vassar et al., 1994, Mombaerts et al., 1996, Lodovichi et al., 2003).

Within each glomerulus, OSN axons make excitatory synapses (directly or though polysnaptic pathways: see sections 1.2.2 and 1.2.3) onto the apical dendrites of mitral and tufted cells (M/TCs), the cell bodies of which reside in the mitral cell and external plexiform layer respectively. Mitral and tufted cells can also be distinguished by their dendritic and somatic morphology (Macrides and Schneider, 1982, Mori et al., 1984, Orona et al., 1984, Fukunaga et al., 2012, Kikuta et al., 2013), as well as their axonal projections (Haberly and Price, 1977, Nagayama et al., 2010). The projection of OSNs to M/TCs represents a massive convergence step, as the ratio of OSN terminals to glomeruli is ~5000:1 (Shepherd and Greer, 1998). M/TCs are glutamatergic and are the principal output neurons of the OB. M/TCs both extend a single primary dendrite into their associated glomerulus and therefore receive direct feedforward input from only one OSN type. The OSN synapse onto M/TCs is highly reliable (Murphy et al., 2004) which has lead to suggestions that the convergence from OSNs to M/TCs serves to amplify sensory input, or to extend the dynamic response range of glomerular output (Cleland and Linster, 1999).

This pattern of feedforward processing from the OSNs results in multiple parallel channels of odour information in the bulb with each glomerulus and associated M/TC group receiving input largely from a particular group of OSNs with affinity for a particular set of odours. OB responses therefore form a spatial 'map' related to incoming odours. Responses across this 'odour map' of processing channels exhibit complex spatiotemporal dynamics in the output circuitry of the bulb (Sachse and Galizia, 2002, Spors and Grinvald, 2002, Bozza et al., 2004).

A major factor in these spatiotemporal differences between odours appears to arise presynaptically from OSN dynamics in response to odour stimuli. Diverse temporal patterns in responses are observed with selective OSN axon terminal imaging, with individual glomeruli displaying differences in latency and rise time of odour-response within timescales similar to animal reaction times in olfactory discrimination tasks (Spors et al., 2006).

1.2.2. Mitral and tufted cell physiology

In addition to morphology, M/TCs can be differentiated based on physiological properties. M/TC firing is tightly coupled to the respiration cycle (Onoda and Mori, 1980, Fukunaga et al., 2012) and typically shows rhythmic bursting at this frequency (4-8Hz). Although many base physiological properties such as input resistance, action potentials fired per inhalation cycle and peak to peak membrane voltage are largely similar between these cell types, the phase of firing within a respiration cycle of M/TCs is a distinguishing characteristic, with TCs firing much earlier than MCs in the sniff cycle. Odour stimulation has the effect of increasing spike rate and respiration phase locking in both cell types, though increasing odour concentrations advance MC phase progressively (Fukunaga et al., 2012). These differences in firing patterns between M/TCs correspond to classic morphological identifiers of the cell types (Macrides and Schneider, 1982, Onoda and Mori, 1980, Mori et al., 1984) and likely arise due to differences in local network connectivity from GABAergic interneurons such as PG cells as differences in phase of firing are largely abolished under GABA clamp (Fukunaga et al., 2012). Recent evidence also suggests that differences of firing phase may also result from differences in synaptic pathways from OSN terminals, with TCs being the recipient of monosynaptic OSN connections and MCs being targeted through polysynaptic connections via external tufted cells (Gire et al., 2012). The monosynaptic connections to TCs may confer them with the ability to response with a lower latency than MCs to incoming odour stimuli. Like OSNs, M/TCs have heterogeneous baseline firing rates, with approximately 1/3rd of M/TCs falling into the classification of 'silent' cells: neurons that can respond to odour but rarely produce any spontaneous action potentials (Kollo et al., 2014). M/TCs belonging to the same glomerulus can often be electrically coupled and display highly

correlated spiking patterns (Ma and Lowe, 2010).

1.2.3. Glomerular layer inhibitory networks

A number of interneuron types mediate lateral interactions in the glomerular layer (GL) of the OB, collectively known as juxtaglomerular (JG) cells and generally falling into 3 categories with heterogeneous morphology: periglomerular (PG), superficial short-axon (sSA) cells and external tufted (ET) cells.

PG cells form the majority of JG cells in the GL (Parrish-Aungst et al., 2007). These cells generally extend their dendrites into a single glomerulus. PG cells are inhibitory and their dendrites contain both pre- and postsynaptic sites which release γ-aminobutyric acid (GABA), dopamine or both (Shipley and Ennis, 1996, Shepherd and Greer, 1998). OSNs form connections with PG cells which can retrogradely inhibit release from OSN axons (Nickell et al., 1994, Wachowiak and Cohen, 1999, Aroniadou-Anderjaska et al., 2000, Ennis et al., 2001, Wachowiak and Shipley, 2006).

While PG cells generally make local connections onto single glomeruli, sSA cells (despite their name) send long-range excitatory glutamatergic projections with their axons synapsing on PG cells and tufted cells up to 30 glomeruli away (Banerjee et al., 2015).

1.2.4. Glomerular layer physiology

PG cells exhibit heterogeneous morphologies and protein expression patterns (Kosaka et al., 1995, 1997, 1998, Toida et al., 1998, 2000). In terms of physiology, PG cells can be split into 2 broad categories. The majority of PG cells receive bursting synaptic input without monosynaptic OSN input, while a minority receive monosynaptic OSN input and receive individual synaptic events (Hayar, 2004a).

sSA cells exhibit similar physiology to those PG cells that receive rhythmic bursting synaptic input and also do not receive monosynaptic OSN input (Hayar, 2004a,b). ET cells receive monosynaptic input from OSNs (Hayar, 2004b) and intrinsically generate rhythmic bursts of action potentials, regardless of synaptic input (Hayar,

2004a). Activation of ET cells is sufficient to trigger burst firing in MCs within the same glomerulus suggesting a role in feedforward excitation in the bulb (De Saint Jan et al., 2009, Gire et al., 2012). A number of recent lines of evidence challenge the classical idea that the majority of MCs receive direct OSN input and instead are part of a polysnaptic ET-MC pathway (Gire et al., 2012). sSA cells also appear to be important players in this pathway. Experiments targeting DAT+ interneurons (known to correspond to SA cells) have shown some evidence for electrical coupling between sSA cells and ET cells, and that this connection is responsible for regulating M/TC responsiveness and orchestrating glomerular output normalisation (Banerjee et al., 2015). A similar approach in older mice has demonstrated strong electrical coupling directly from sSA cells to M/TCs but negligible sSA to ET cell coupling (Liu et al., 2016). These results also imply a number of polysynaptic pathways involving connections from sSA cells to ET cells and PG cells, which can mediate long-range interactions between M/TCs of different glomeruli.

1.2.5. External plexiform layer inhibitory networks

In addition to their primary apical dendrite, M/TCs extend secondary horizontal dendrites through the external plexiform layer (EPL) and form dendrodendritic interactions with GABAergic granule cells (GCs). These cells are confined to the EPL and lack an axon (Shepherd and Greer, 1998). Though granule cell (GC) dendrites tend to form local connections with M/TCs, the long-range span of M/TC secondary dendrites means that indirect lateral connections between M/TCs can be mediated by GCs (Orona et al., 1984, Shepherd and Greer, 1998).

1.2.6. External plexiform layer physiology

The circuit physiology of the EPL is defined by the reciprocal dendrodendritic synapses between MCs and GCs. When excited sufficiently, MCs release glutamate onto associated GC dendrites which in turn release GABA back onto the MC (Isaacson and Strowbridge, 1998, Chen et al., 2000, Isaacson, 2001). Different levels of MC discharge will differentially excite associated GCs resulting in a wide range of modes of inhibition, from recurrent self-inhibition (Jahr and Nicoll,

1980, 1982, Isaacson and Strowbridge, 1998) to local or global lateral inhibition between MCs of different glomeruli (Jahr and Nicoll, 1982, Woolf et al., 1991, Isaacson and Strowbridge, 1998, Chen et al., 2000, Egger et al., 2003). Interactions between MCs via GC reciprocal synapses means lateral inhibition in the EPL is gated in an activity dependent manner, and that inhibition is enhanced when GC connected MC pairs show correlated activity (Arevian et al., 2008).

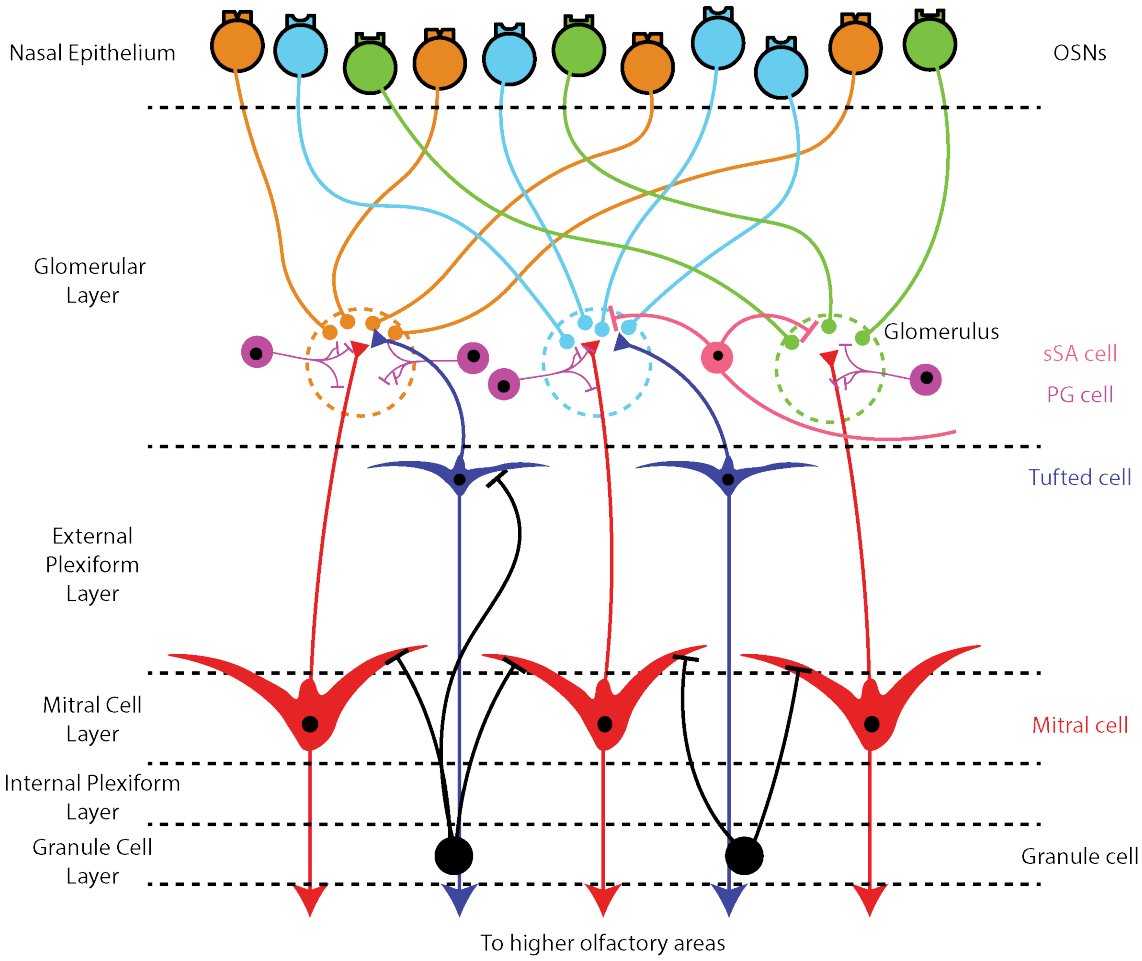

Figure 1.1.: Anatomy of the early olfactory system. Adapted in part from Nagayama et al., 2014. The early olfactory system is comprised of the nasal epithelium containing olfactory sensory neurons (OSNs), and the olfactory bulb (OB). Axons from OSNs expressing a particular olfactory receptor (OR) terminate in defined foci in the OB known as glomeruli (dotted line circles). The output cells of the OB, the mitral and tufted cells, send an apical dendrite into their associated glomerulus, which is synapsed onto by OSN axons. Mitral and tufted cells relay incoming odour signals from the OSNs to higher olfactory areas. The OB is also home to a network of heterogeneous inhibitory cells. Periglomerular (PG) cells provide local inhibition onto glomeruli. Superficial short axon (sSA) cells mediate longer range inhibitory interactions between glomeruli. Granule cells (GCs) in the deeper layers form dendrodendritic synapses with the secondary horizontal dendrites of mitral and tufted cells, effecting lateral inhibition between the output neurons of the OB.

2. Computation in the early olfactory system

What is the function of the neuronal circuitry in early olfactory system? Clearly, one function is to be able to detect and identify specific odorants in the environment; but the range of olfactory behaviours performed by animals, as well as the complex interplay between excitatory and inhibitory cell types, suggest that more subtle computations are being performed by this network.

2.1. Olfactory discrimination

A basic but important olfactory behaviour exhibited by many organisms is the ability to identify and discriminate the quality / identity of an odorant. Detection of odour identity is crucial for survival in many animals in order to be able to discriminate e.g. an odour that likely emanates from a predator rather than from a food source or conspecific, even if these odours happen to have similar chemical structure. Related and of similar importance is the ability to identify an odorant regardless of the concentration at which it is detected; as odours in natural environments will rarely be encountered at some static concentration level.

2.1.1. Discrimination behaviour

In line with its biological importance, olfactory discrimination can occur extremely rapidly in rodents. Measures of exploratory sniffing in rats reveal that discrimination of a novel odour from one to which the animal has previously been exposed can occur in as little as 140ms, with the bulk of this response time arising from the

time taken to inhale an odorant and for it to bind to OSNs (Wesson et al., 2008b). When discriminating between two pure monomolecular odorants, rodents generally only require a sampling time of 125-200ms (the equivalent of a single inhalation cycle or sniff) to achieve high accuracy levels (Uchida and Mainen, 2003, Abraham et al., 2004, Zariwala et al., 2013). Additionally, this sampling time is relatively constant regardless of the similarity of the two odorants in terms of their representation overlap in the bulb (Uchida and Mainen, 2003, Rinberg et al., 2006, Resulaj and Rinberg, 2015); however this time increases on the order of 70-100ms when discrimination is between similar mixtures of odours (Abraham et al., 2004, 2010). In these studies it is shown that although reaction time increases, high levels discrimination accuracy can still be achieved between similar mixtures. This suggests two interesting features of olfactory computation: 1) that stimuli producing overlapping representations in the early olfactory system can be distinguished from one another and 2) that some form of temporal integration by the neuronal circuit is required to achieve this.

Aside from discrimination of odour quality, rodents are also able to distinguish between absolute odour concentration at remarkably fast time scales. For odours with a 10-fold difference in concentration, discrimination can occur in a little as 70-140ms (Resulaj and Rinberg, 2015). Although they are able to perceive differences in concentration, it also appears that odour identity can be generalised over a similar magnitude of concentration difference and that mixtures can be perceptually classified according to the ratios of their components (Uchida and Mainen, 2007).

2.1.2. Circuit basis of olfactory discrimination

The basis for the ability to discriminate between a wide range of odours primarily arises from the 'labeled-line' organisation of the early olfactory system. As each glomerulus is supplied with input from an OSN expressing a particular OR, each glomerulus will have a different and separable response to different odours (Wachowiak and Cohen, 2001, Wachowiak et al., 2004). The high convergence ratio between OSNs and their focal point in a glomerulus likely enhances odour detection ability, especially at low input concentrations, by overcoming signal-to-noise issues in OSN transduction (Drongelen, 1978). Glomerular signals are relayed

to higher olfactory areas by the output M/TCs associated with each glomerulus. This results in several parallel feedforward pathways in the early olfactory system that can be read out collectively as an indication of which odours are present in the nose. Indeed, for natural blends of odours that elicit patterns of OB activation involving up to 20 glomeruli, these responses can be explained as a sum of glomerular responses to the individual components of the mixture (Lin et al., 2006). The inhibitory network in which the output circuitry of the bulb is embedded also plays a role in processing odour information for discrimination behaviours. For example, genetically increasing lateral inhibition onto M/TCs via the dendrodendritic synapses of GCs has been shown to decrease reaction times for discrimination of similar odour mixtures (Abraham et al., 2010, Nunes and Kuner, 2015).

This same inhibitory network has classically been implicated in contrast enhancement of odour responses through lateral inhibition, in part due to its similarity in terms of circuit structure to the retina (DeVries and Baylor, 1993). This contrast enhancement could be the basis of the ability to discriminate similar mixtures, as strongly overlapping patterns of glomerular activation could be decorrelated by sharpening output tuning. Dendrodendritic reciprocal interactions between GCs and MCs have been shown to mediate a form of centre-surround suppression for similar odours (Yokoi et al., 1995), enhancing tuning specificity in M/TCs[1]; though more recent studies have suggested that contrast enhancement through lateral inhibition may arise largely from PG cells in the glomerular layer which are better positioned to modulate mapping of glomerular input to M/TC output (Linster and Gervais, 1996, Linster and Hasselmo, 1997).

Given that animals are able to discriminate odour concentration as well as identity, the function of the early olfactory system circuitry cannot be limited to odour identity processing alone. Indeed, differences in stimulus concentration lead to distinct spatiotemporal patterns in OB projection cell firing including changes in phase of firing with relation to the respiration cycle (Bathellier et al., 2008). Firing rates of both M/TCs increase in response to increased concentration; however,

[1] Yokoi et al., 1995 claim that this centre-surround suppression is based on similar chemical features, e.g. a M/TC that is excited by an odourant with a particular carbon chain length may be inhibited by other molecules with different chain length. This suggests a level of chemotopy in early olfactory processing, though this functional architecture has been challenged in more recent work (Laurent, 1999, Cleland and Linster, 2005)

the phase of MC firing is progressively advanced in response to increasing concentration of odours while TC phase remains largely unaffected (Fukunaga et al., 2012). This change is mediated by the inhibitory network of the OB which progressively delays MC firing as input intensity is increased.

2.1.3. Redundancy of odour coding

An ongoing discussion on the topic of odour coding and discrimination is the extent to which the odour identity code is redundant. Given the established mechanism of odour transduction and processing in the brain, it seems probable that odour identity coding involves some degree of redundancy (as opposed to a strict 'labeled-line' coding and readout strategy), since OSNs can respond to more than one odour and odours can activate multiple OSNs; resulting in overlapping representations of odours in the olfactory bulb glomerular map (Duchamp-Viret and Duchamp, 1997, Friedrich and Korsching, 1997, Malnic, 1999, Laurent et al., 2001, Nara et al., 2011). While it is generally true that odours are encoded in the olfactory system by the activity of small, unique groups of OSNs and glomeruli; there is also evidence that certain pheromonal or particularly behaviourally salient odour cues are encoded in a non-redundant fashion by narrowly tuned OSNs (Nara et al., 2011, Dewan et al., 2013). How do these different levels of redundancy affect odour perception? Results of lesioning experiments (Lu and Slotnick, 1998, Slotnick and Bodyak, 2002, Bisulco and Slotnick, 2003, McBride and Slotnick, 2006, Slotnick, 2007) in mouse OB and from knockout mice with OSN axon guidance defects (Knott et al., 2012) have been interpreted as evidence that relatively large disruptions of the olfactory bulb leave a great deal of olfactory function intact (Laurent, 1999, Wilson and Mainen, 2006). In turn, this suggests that there is a large degree of redundancy in odour coding which transfers to perception: when components of a combinatorial, overlapping odour code are degraded, the base odour percept remains. By contrast, other studies that challenge the early olfactory system report conflicting results (Johnson and Leon, 2007) and suggest that early OB lesion studies fail to account for the possibility that simple odour discrimination is a trivial task for the mammalian olfactory system, and that these discriminations can be easily and quickly learned after lesions, though the odour percept may change significantly. For example, Bracey et al., 2013 show that

major olfactory epithelium disruptions are required to produce deficits in odour recognition and discrimination, whilst minor disruptions largely affect *recognition* of previously encountered odours. This result suggests that although odours are represented in the brain via combinatorial, overlapping patterns, perception of odour identity is largely non-redundant and is based on precise template matching of glomerular spatial map activity. This is further confirmed by the observation that target odours can be efficiently detected even in the presence of a large number of background odours which have glomerular representation patterns overlapping with the target odours (Rokni et al., 2014). In summary, it appears that although representation of odours in the brain results from overlapping patterns of glomerular activity that are therefore redundant with one another, perception of odour identity is specific to these complete patterns and is largely non-redundant - i.e. removing or adding a glomerular unit from a certain odour's response pattern results in a different identity perception. This has been demonstrated in experiments where mice are required to discriminate between optogenetic stimulation of a glomerular focal point vs. absence of activation in the presence of an odour background: where the odour background overlaps with the optogentically activated glomerulus, animals are unable to discriminate between the stimuli; but if the optogenetic activation is non-overlapping and therefore adds separate glomerular unit activity simultaneous with the response to the background odour, discrimination can be performed (Smear et al., 2013). Together, these later results suggest that the redundancy of odour representation does not transfer to redundancy in perception; however, a systematic exploration of graded olfactory bulb lesioning/challenge in multiple odour/task contexts is needed to reconcile the diverging views in the literature.

2.2. Odour source localisation

Many organisms rely on olfaction as their primary source of sensory information about the environment. In these animals, olfaction acts as an important sensory cue for navigation and detection of the location of sources of incoming odours.

2.2.1. Odour source localisation behaviour

The ability to navigate towards an odour source has been demonstrated in a number of model organisms in various experimental preparations. Moths, for example, are capable of robustly tracking emitted pheromones over long-distances relative to their body size (Vickers, 2006). Birds and fish are also capable of utilising olfactory cues for long-distance navigation (Hasler et al., 1978, Papi, 1990, Wallraff, 2004). Olfactory navigation is also present in rodents. Rats can be trained to run directly towards an odour source positioned at the end of a linear track, even when the odour source position is changed or background odours are introduced (Bhattacharyya and Singh Bhalla, 2015). This has also been demonstrated in blind eastern American moles, also showing that blocking of a nostril, as well as crossing the inputs to the nostrils, causes significant deviance away from the correct path to the odour (Catania, 2013). This suggests that bilateral sampling of odour signals may be necessary for orientation towards an odour source. Aside from navigation towards distant odour sources, rodents are also able to robustly track odour trails, with a strategy that involves multiple back-and-forth crossings over the trail (Khan et al., 2012). This behaviour also appears to require bilateral sampling as nostril block creates a deficit in trail following accuracy.

Where odour signals are presented directly to the nose rather than from a trail or distant source, animals can spontaneously orient towards the direction of the odour source (Gardiner and Atema, 2010, Esquivelzeta Rabell et al., 2017). Humans are also able to report the direction of an odour stimulus during active sniffing (Frasnelli et al., 2009).

2.2.2. Circuit basis of odour source localisation

Given that bilateral sampling of the odour environment appears to be important for olfactory based orientation, interhemispheric connections between olfactory input streams (Ressler et al., 1994, Vassar et al., 1994, Mombaerts et al., 1996, Lodovichi et al., 2003) may play a key role in extracting spatial information from smell. While there are no direct interhemispheric between the olfactory bulbs, the anterior commissure contains interhemispheric connections between the anterior

olfactory nucleus and piriform cortex, areas that are downstream and have feedback connections to the OB (Esquivelzeta Rabell et al., 2017). Transection of the anterior commissure has been shown to abolish the ability of mice to orient towards odour stimulus direction, without affecting spontaneous responses to novel odours, while optogenetic activation of the anterior olfactory nucleus (AON) triggers nostril movement towards the side of stimulation (Esquivelzeta Rabell et al., 2017).

2.3. Olfactory scene segmentation

Olfaction is a 'remote-sensor' and allows animals to detect the presence of objects some distance away. At the point of detection, however, odours are drawn into a focal point in the nose and any information about the spatial distribution of odours is seemingly lost; in contrast to, for example, vision in which the arrangement of the retina allows a topographic relationship between the spatial pattern of incoming light and the pattern of neuronal firing (Wässle, 2004). Furthermore, natural olfactory scenes are composed of multiple odour sources and the natural olfactory stimulus is therefore a complex, dynamic mix of a variety of odours (Wright and Thomson, 2005, Lin et al., 2006, Shen et al., 2013). Olfactory scene segmentation is a crucial task for survival in many organisms (Howard et al., 1968, Blaustein, 1981, Apfelbach et al., 2005). Given the obstacles described here, how is it that animals are able to form a stable representation of odour objects in their environment? The perceptual segmentation of visual (Wolfson and Landy, 1998, Crouzet and Serre, 2011) and auditory scenes (Elhilali and Shamma, 2008, McDermott, 2009) have been studied extensively, but in olfaction the mechanisms by and extent to which odour objects can be segmented from sensory input is less well explored (Laing and Francis, 1989, Jinks and Laing, 1999).

2.3.1. Olfactory scene segmentation behaviour

Much of the behavioural work on olfactory scene segmentation has approached this question from the angle of determining whether olfaction is a synthetic or analytical sense (Laurent, 1999, Rokni et al., 2014). In the analytical scenario, odour

percepts of mixtures are built in some predictable way from their individual components and these components can be reliably identified within the mixture. In the synthetic case, odour mixtures take on an entirely different perceptual quality than their components making detection of the individual odours within the mixture a problematic task.

Early perceptual studies in humans suggest a significant synthetic component to olfaction. These studies show that in the presence of mixtures of several odours, subjects have extreme difficulty in attending to a familiar odour in the mixture (Jinks and Laing, 1999, 2001) and many subjects are unable to name components of mixtures composed of commonly encountered odorants (Laing and Francis, 1989). More recent work, however, has shown that detection of a target odour against an unpredictable background is robustly performed in rodents, even with a mixture of up to 16 odours (in almost 50,000 possible combinations) (Rokni et al., 2014). Optogenetic activation of a single glomerulus can also be reliably detected against an odour background (Smear et al., 2013). Interestingly, the ability to detect target odours against a background appears to be significantly more robust when the odours are differentially positioned temporally, with some delay between presentation (Kay et al., 2005, Shen et al., 2013).

2.3.2. Circuit basis of olfactory scene segmentation

Some degree of odour pattern separation exists already in the output of the early olfactory system. For example, M/TC firing to a complex odour mixture can be decorrelated with the removal of a single odour component (Barnes et al., 2008). Further, in response to similar mixtures with overlapping glomerular activation patterns, M/TCs decorrelate the response pattern in their output (Gschwend et al., 2015). Enhancing GC inhibition with optogenetic or pharmacogenetic methods results in a greater degree of pattern separation in M/TC output, whilst silencing GCs result in decreased pattern separation (Gschwend et al., 2015).

3. Temporal dynamics in olfaction

The majority of studies presented so far have dealt largely with perception and processing of odour identity. The result is that odour stimuli used in many of these experiments are static in nature: long stimuli (relative to the respiration cycle) with low variability in concentration over time. This is in stark contrast to the way in which odours are encountered in natural environments - within odour plumes that have complex spatiotemporal patterns of transmission (figure 3.1). In general, an understanding of natural statistics of sensory signals is of great utility in probing the function of neuronal circuits as sensory systems are adapted to extract information from environments in which they find themselves. An under explored area of olfaction is the nature of temporal features of odour signal transmission, their effect on behaviour and representation in the brain.

3.1. Natural transmission of odours

At the length scales relevant for most organisms, diffusion of odours plays a minimal role in long-range odour transmission. Rather, transmission of odours in natural environments is largely governed by general air movement patterns, and the natural turbulent processes within those patterns. The result is that odours are transmitted as 'plumes', with complex distributions of odour concentration that are dynamic in both space and time (Villermaux and Innocenti, 1999). An approximation of how animals encounter these plumes can be gained by placing a detector downwind of an odour source (or some other source type also transmitted as a plume) and recording signal intensity fluctuations over time (Murlis, 1992, 1997, Justus et al., 2002, Celani et al., 2014). This reveals a structure characterised by wild fluctuations in odour concentration over time with a highly intermittent

profile. This scenario is complicated further when one considers that these dynamic plumes from different sources blend together in increasing degrees as they travel (Kree et al., 2013) and begs the question of how organisms can generate a stable perception of the olfactory environment in the face of this spatiotemporally dynamic signal structure. One convincing argument is that animals do not make sense of their olfactory environment by aiming to build a stable picture of concentration levels, e.g. by time-averaging, but rather utilise the dynamics of odour plumes themselves to generate an internal map of olfactory space (Hopfield, 1991, Murlis, 1992, Hopfield, 1999, Vergassola et al., 2007).

This is possible because turbulent flow has a continuous effect on odour transmission and as an odour plume travels its odour molecules are increasingly dispersed and mixed with air over time, while the gross structure of the plume shifts in space (Murlis, 1992). The effect on the plume is a progressively widening structure in which patches of odourised air become increasingly mixed with surrounding clean air and the concentration of odour in any patch progressively decreases. Thus, despite the chaotic nature of air turbulence, robust statistical features are observed along the plume length with infrequent packets of high odour concentration more likely at the base of the plume, and more frequent encounters with low concentration odour packets more likely as the plume travels. This effect has been observed in aquatic plumes (Moore and Atema, 1991, Weissburg et al., 2002) and, to a lesser extent, in airborne plumes as well (Murlis, 2000, Vickers et al., 2001). Importantly, there is evidence of a number of instantaneous components of odour concentration that vary reliably with distance of a detector from an odour source, in particular pulse slope and height (Moore and Atema, 1991). Additionally, intermittency of odour encounters increase with distance from the plume center (Justus et al., 2002). These components can be detected in a much shorter time window than calculating a stable estimate of mean concentration and are therefore likely to be of behavioural significance to an animal orienting itself in odour space.

3.2. Perception of temporal dynamics

Of course, the temporal dynamics arising in naturally occurring odour signals can only be considered behaviourally informative if animals are able to detect and perceive them. There has been relatively little work on perception of temporal features by vertebrates, but a number of theoretical works as well as studies in insects and crustaceans have shown that temporal features of odour plumes may be a key information source for behaviour.

3.2.1. Navigation behaviour

In many cases organisms do not just account for temporal dynamics in odour signals, but rather seem to actively utilise them in behaviour, particularly in navigation. Insects navigating to an odour source, when exposed to laminar, uniform odour stimuli will typically respond as if no odour signal is present and begin crosswind casting, only resuming normal navigation when exposed to repeated odour pulses (Willis and Baker, 1984, Baker et al., 1985). Studies in aquatic crustaceans also show an ability to use dynamic features of odour plumes to navigate (Weissburg et al., 2002). The strategies used by animals in these studies appears to be relatively constant across invertebrate species. Rather than attempting to determine odour plume (and therefore odour source) orientation by repeatedly sampling a small spatial window to determine absolute concentration, animals will exhibit a casting behaviour in which they cross the plume in a diagonal fashion and reorient when they reach the plume edge (David et al., 1983, Kuenen and Carde, 1994, van Breugel and Dickinson, 2014). The speed at which this behaviour occurs suggests that actual contact with odourised air is relatively transient with this strategy, and that animals must be able to quickly detect odour onsets and offsets to orient correctly. There may also be a component of bilateral sampling in these kinds of orientation behaviours (Gardiner and Atema, 2010). Casting behaviour is also consistent with a theoretical strategy for locally maximising odour information with regards to odour source orientation (Vergassola et al., 2007).

3.2.2. Olfactory scene segmentation

A fundamental conceptual problem in understanding the mechanism of olfactory scene segmentation in vertebrates is that, although odours are differentially distributed in space according to where they emanate from, at the point of detection the entire mixture of all odours is drawn into a relatively small focal point in the nose. One hypothesis is that odours in a mixture can be attributed to different sources based on differences in concentration fluctuation over time (Hopfield, 1991, Fort and Rospars, 1992, Hendin et al., 1998, Hopfield, 1999). Although the turbulence that creates and carries odour plumes is a random, chaotic process; odour sources that are proximal in space will be acted on locally by roughly similar patterns of air movements. Therefore, individual odour concentration fluctuations in a plume emanating from a single source are more likely to show temporal correlations than the same odours with separate and spatially distributed sources. By detecting these temporal correlations, animals could identify which components of the inhaled mixture arise from the same source, and which emanate from other sources or are atmospheric background odour. Conceptually, this presents an extremely powerful mechanism by which odour scene segmentation and figure-ground separation can be achieved quickly and efficiently without physically moving between odour sources in the environment to determine their respective locations. Furthermore, if utilised this mechanism would be strongly selected for in a great number of organisms as it would allow for e.g. determination that an odour is dispersed from a food source or conspecific rather than a predator, even if those two odour profiles have overlapping components.

At the time of writing, there is no direct evidence in vertebrates that temporal correlations can be detected and used to perform odour scene segmentation. There are, however, a number of lines of evidence that suggest this mechanism is utilised in biology. In molluscs, there is evidence that spacing of odour components (and therefore correlation in the resulting plume) has an effect on perception of the mixture, with a physical mixture of the components perceived differently to the individual components separated but closely spaced (Hopfield and Gelperin, 1989). In honeybees, extremely small delays in stimulus onset for two odours on the order of 6ms are sufficient to elicit a difference in perceptual quality vs. the two odours presented in synchrony (Szyszka et al., 2012).

3.2.3. Detection and neuronal representation of temporal information

Aside from work that suggests the utility of temporal information in behaviour, further evidence comes from the observation of detection and neuronal representation of temporal features in odour signals. A number of studies in mice have shown, using optogenetic methods in lieu of temporally structured olfactory stimuli, that fine differences in temporal structure are perceptible. With optogenetic activation of a single glomerulus via its associated OSNs, latency differences relative to the sniff cycle of as little as 25ms can be discriminated above chance (Smear et al., 2013). Differences in optogenetic OSN activation at scales of around 10ms can also be detected, regardless of synchronisation to the respiration rate, with some M/TCs reflecting these stimulus length differences in their firing rates (Li et al., 2014). Interestingly, odour stimulus duration differences on the order of 100ms can also be detected by humans for relatively high concentrations (Frasnelli et al., 2006). With direct optogenetic stimulation of M/TCs over a relatively broad region of OB, mice are able to detect the difference between synchronous activation of two M/TC populations vs. asynchronous activation with high accuracy, even where the time delay for asynchronous activation is as little as 13ms (Rebello et al., 2014).

For many behaviours that are assumed to be based on detection of temporal information, there is evidence of neural correlates. In the case of perception of small stimulus onset differences (Szyszka et al., 2012), it has been further shown that asynchronous mixtures produce distinct response patterns from the same odours presented in synchrony (Stierle et al., 2013). In lobster antennae, a subset of bursting olfactory sensory neurons (bOSNs) are tuned to specific stimulus intervals and, as a population, can encode a wide spectrum of temporal characteristics in an odour plume (Park et al., 2014), which may account for the ability of lobsters to navigate in the intermittent structure of a plume (Park et al., 2016). Electroantennograms in locusts have shown that insect OSNs are also capable of tracking fast fluctuations in odour concentration typically found in natural odour stimuli (Huston et al., 2015), with odor transduction occurring at less than 2ms and frequencies of more than 100Hz being faithfully tracked in the firing response (Szyszka et al., 2014). Direct measurements of principal neurons (PNs) in locusts

has also revealed a subset of PNs that reliably encode rapidly fluctuating odour stimuli (Geffen et al., 2009).

There is less direct physiological evidence of neuronal representation of temporally patterned odour signals in the mouse model system but a number of adjacent lines of evidence exist. In particular, one requirement for accurate coding of temporal information in the OB is that its projection neurons operate with some degree of temporal precision proportional to the bandwidth of temporal stimuli they are capable of encoding. Historically, olfaction has been considered a 'slow' sensory modality, in the sense that the responses of projection neurons in the OB appear to operate with less temporal precision than in other early sensory areas such as the vibrissal system (Bale et al., 2015) or visual system (Butts et al., 2007). This assumption has held in part because olfactory input in mammals is governed by the inhalation phase of respiration, and respiration varies cycle-by-cycle in duration, amplitude and waveform shape. Therefore, M/TC responses may appear temporally imprecise due this variation. Shusterman et al., 2011 extract spike-times of M/TC responses to odour stimuli while recording animal respiration. By warping time in these recordings such that all respiration cycles align in time according to their phase, spike-time data can then be considered in respiration-phase time rather than absolute time following an odour stimulus. In this 'sniff-warped' time, M/TC firing patterns are diverse across cells and odours with firing peaks that tile the entire timecourse of the sniff cycle. Furthermore, the jitter or temporal precision of spiking in these cells is much reduced compared to precision in absolute time, with a mean of ~12.5ms. This suggests a precision of firing in OB projection neurons comparable with other sensory systems (Wehr and Zador, 2003, Butts et al., 2007). Furthermore, given that the respiration rate of a normal, awake mouse lies within ~3-15Hz, this level of temporal precision could feasibly allow for sub-sniff temporal information to be generated by M/TC firing. In the case of Shusterman et al., 2011, determining the ability of M/TCs to encode temporal odour information is limited as the delivered odour stimuli were static, and still necessarily patterned by the animals' respiration cycle. Gupta et al., 2015 provide further insight by delivering odour stimuli with a time-varying pattern (fluctuating at up to 20Hz) and decouple the effect of respiration by controlling animal respiration with a double tracheotomy. The authors show here that responses to temporal odour patterns for M/TC cells can be predicted by simple

convolution of a cell's odour response kernel with the odour waveform. These responses are waveform and odour specific, suggesting that M/TCs can track temporal features of odour patterns, not simply the presence or absence of a particular odour. Projection neurons have also been found in the OB which respond as concentration change detectors (Parabucki et al., 2017) and allow concentration changes in odour stimuli to be read out at the timescale of a single sniff. Taken together, these studies reveal that projection neurons in the OB are capable of temporal firing precision comparable to other sensory systems and that temporal patterns in odour concentration change can likely be encoded. However, a systematic study of that ability of these neurons to encode temporal features of odour stimuli including temporal bandwidth, preferred stimulus features and relation to natural odour signals does not currently exist. Furthermore, the studies presented here regarding temporal encoding properties of OB projection neurons have generally utilised extracellular or jextuacellular electrophysiology methods, meaning that a detailed exploration of the physiological and network properties of neurons capable of encoding temporal features of odour stimuli is not available.

3.2.4. The early olfactory system in the context of temporally patterned odour information

If, as posited in this chapter, temporal dynamics are an important feature of the olfactory environment and provide behaviourally salient information then the early olfactory system should be capable of encoding some features of these temporal dynamics, as well as static features such as odour identity and stable odour concentration. This begs the question of whether the early olfactory system posesses and appropriate anatomy and physiology to encode these dynamic signals.

The temporal bandwidth of individual OSNs is limited by their response latency (here defined as time from odour arrival in the nose to depolarisation) and refractory period. Response latency in mammalian OSNs is likely on the order of 10s of milliseconds (see subsection 1.1.1), but OSN refractory periods appear to be the main limiting factor in the frequency at which they can track odour pulses in their depolarisations - recordings of dissociated OSNs responding to pulsed odour stimulation show that they are unable to track pulses at higher frequen-

cies than ~2Hz (Ghatpande and Reisert, 2011). This temporal resolution may be increased or decreased for different odours (the authors of Ghatpande and Reisert, 2011 use cineol stimulation) but the level reported here is low relative to the waking sniff rates of mice (3-15Hz). Even for individual OSNs with low temporal resolution, however, the population response may allow for encoding of faster olfactory dynamics given the convergent anatomy of the early olfactory system. If each successive odour event in the nose activates a small subpopulation of OSNs, then fast pulses can be encoded by successive activation of more and more OSNs, regardless of the response kinetics of individual cells. As the axons of OSNs of a given type converge onto OB glomerular foci (see subsection 1.2.1), projection neurons associated with a glomerulus will be driven by the pooled activity of all projecting OSNs, and therefore have access to the dynamics of this successive activation. Therefore, fast odour dynamics can in theory be read out by OB preojection neurons even with OSNs displaying low temporal bandwidth. It remains to be seen whether projection neurons in the OB do in fact encode temporally patterned odour input and whether they can do this whilst the majority of their response is driven by the respiration cycle (Fukunaga et al., 2012). However, as outlined in subsection 3.2.3, projection neurons in the OB possess a number of features that suggest they are capable of encoding this information: that they spike with temporal precision comparable to other sensory systems; that their firing profile differs between different temporal patterns of olfactory stimuli; and that they can report concentration changes in incoming odour input, at least at the temporal resolution of the sniff cycle.

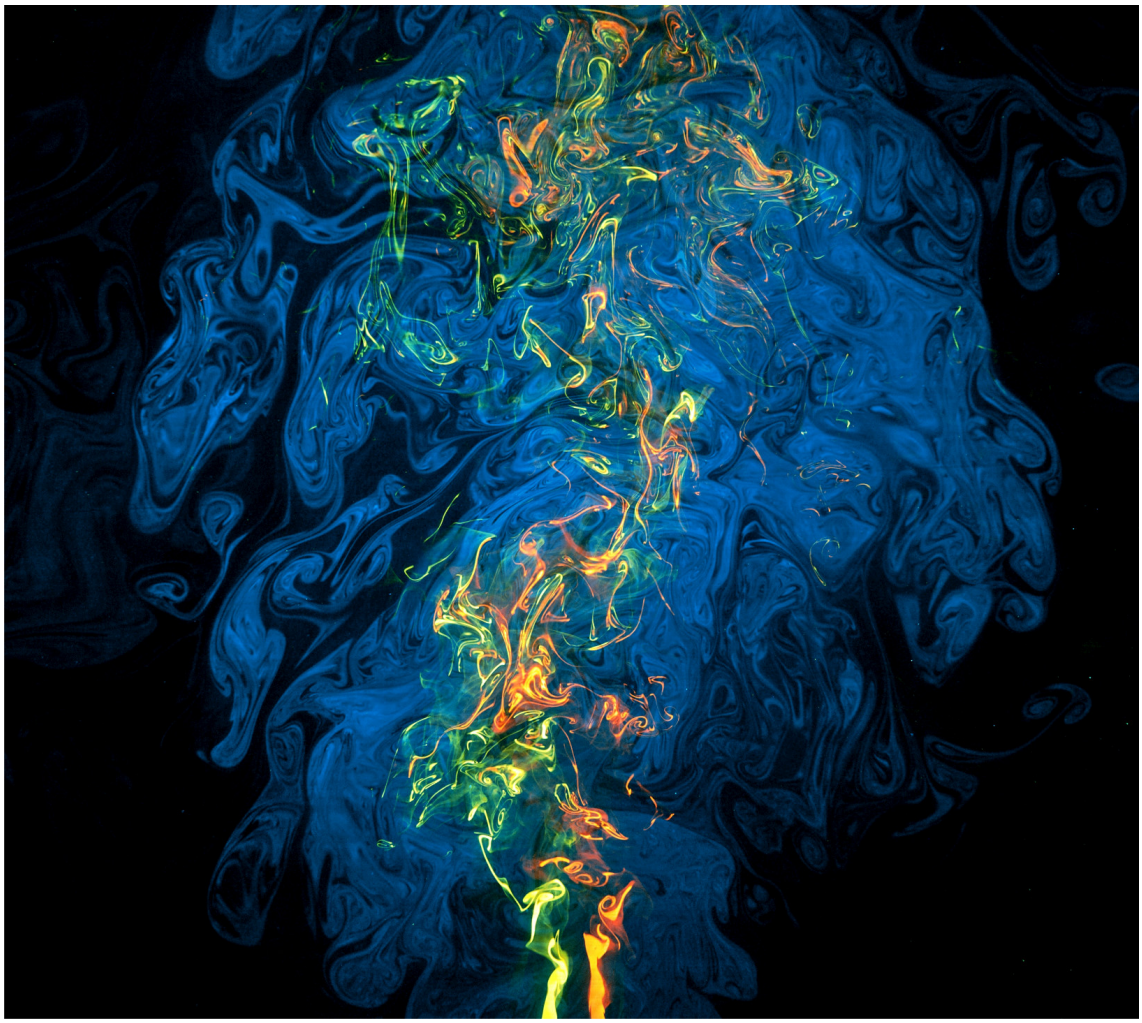

Figure 3.1.: Odour plume structure. In this image, adapted from Kree et al., 2013, plume structure is imaged with two fluorescent dyes released from separate sources (bottom of image) in water. The turbulent flow that carries the plume results in a complex, intermingling structure with dynamic fluctuations of tracer concentration.

4. Summary and aims

The works presented here demonstrate the utility of the early olfactory structures as a model system for understanding sensory processing. Study of these structures has led to key insights into processing of sensory information by heterogeneous circuit architectures, the role of inhibition in neural circuits and the behavioural abilities that can be achieved based on this processing. It does also appear, however, that a key feature of olfactory stimulus space - the temporal component - has been significantly underexplored, particularly in mammalian olfaction. Given the results of studies presented in chapter 3, it is likely that certain temporal features of odour transmission may contain significant behavioural information that can be extracted and utilised by organisms in the environment. In particular, temporal correlations in the concentration fluctuations of distinct chemical volatiles appear likely to be a highly informative signal regarding prediction of whether these chemicals emanate from the same or separate sources. In the following work I aim to provide physical evidence that naturally occurring odour plumes exhibit a rich temporal structure, and that temporal correlations in this structure are associated with source separation. Because odour objects in the environment are themselves mixtures of separate odour plume sources, the significance of showing that temporal correlations predict source separation is that it will identify a potential mechanism by which odour objects can be perceived against a background of non-object odours. Perception of temporal correlation in odour signals might therefore be a basis for many olfactory computations, including figure-ground separation and odour object perceptual binding.

These temporal features of odour signals can only be considered as a basis for certain sensory perceptions if animals are able to detect them. I therefore also aim to show that animals are capable of perceiving temporal correlations in odour signals at ethologically relevant frequencies, using a number of behavioural tests to determine their accuracy in perceiving temporal odour correlations, and per-

ceptual thresholds for the frequency of these correlations. Finally, I will explore the neural representation of temporally structured odour information in the olfactory bulb, an area of the brain concerned with early olfactory information processing, to attempt to understand the basis of any perception of temporal features in odour signals.

Part II.

Methods

5. General

5.1. Animals

All animal procedures performed in this study were approved by the UK government (Home Office) and by Institutional Animal Welfare Ethical Review Panel. All mice used were C57/Bl6 males unless otherwise specified in the text.

5.2. Odours

All odours were obtained in their pure form from *Sigma-Aldrich*, *St. Louis MO, USA.* Unless otherwise specified, odours were diluted 1/5 with mineral oil. Odours used were:

Ethyl butyrate - EB

Isopentyl acetate - AA

Eucalyptol - CN

Eugenol - EU

Acetophenone - ACP

2-Heptanone - 2H

Guajacol - Guaj.

Cinnamaldehyde - Cinn.

Valeric acid - Val.

Pelargonic acid - Pel.

Vanillin - V

Phenylethyl alcohol - P

2-Phenylethanol - 2P

α-Terpinene - αT

5.3. Analysis

Data analysis was performed with custom MATLAB (*Mathworks, Natick MA, USA*) software unless specified in the text. All control / GUI software was written in Python.

6. AutonoMouse

6.1. Overview

AutonoMouse is an automated system for simultaneous behavioural training and testing of large cohorts of mice in operant conditioning tasks, such as the go/no-go training paradigm. This system is used throughout this thesis for conducting behavioural experiments. In this chapter, construction of the system is described; as well as the architecture of the control software and general operating principles. Later methods chapters describe in detail the application of AutonoMouse to specific experimental problems.

6.2. Technical Development

The design for AutonoMouse was originally conceived as a modification to existing semi-automated conditioning boxes (Bodyak and Slotnick, 1999; *Knosys, Washington*) for single animals. Originally the extent of the modification from the authors of Abraham et al., 2004 was to include RFID detection for ease of recording animal identity during behavioural sessions. A later prototype built by Thorsten Bus and Andreas Schaefer (MPI Heidelberg) included the ability to group house animals and to gate their entry to a behaviour port by means of an IR-beam triggered entryway. Jan Herb, Thorsten Bus and the MPI mechanical / electrical workshops updated this prototype (MPI Heidelberg, National Institute for Medical Research, UK) to form the structure and design that is outlined here. The inital software prototype was implemented in Igor by Andreas Schaefer (MPI Heidelberg, National Institute for Medical Research, Francis Crick Institute).

Following the lesion experiment described in this thesis, a total software rehaul was undertaken by myself. The software was rewritten in Python and the structure redesigned to increase flexibility and modularity to allow for implemenation of a greater range of experiments rather than simple olfactory go/no-go tasks. The olfactometer was also redesigned by myself and Tobias Ackels (Francis Crick Institute) as described in Results chapter 16 and Methods chapter 9.

6.3. Design overview

AutonoMouse is designed with a set of key features in mind. The system is designed to:

- Simultaneously train groups of mice in operant conditioning tasks, whilst being able to track performance of each mouse in the group individually
- Operate in a completely automated fashion, such that any manual experimenter intervention is kept to a minimum
- Allow for efficient maintenance of experiment progress (including e.g. cleaning, mouse health monitoring)
- Produce high volumes of reliable behavioural data
- Operate for long-periods of time continuously such that large-scale experiments are feasible.

In AutonoMouse (see figure 13.1), groups of mice (up to 25) are housed in a common home cage. Prior to housing in AutonoMouse, each mouse is implanted with a radio-frequency identification (RFID) chip subcutaneously, allowing each mouse to be individually and automatically identified. Within the common home cage of AutonoMouse, mice have free access to food, social interaction and environmental enrichment. Water is not freely available in the home cage, but can be gained at any time by completion of user-defined behavioural tasks. To access these behavioural tasks, mice must leave the home cage and enter a behavioural area. This behavioural area contains hardware for delivering any stimuli (e.g. an odour port for odour discrimination tasks) and a lick port through which water rewards can be released. The lick port is also connected to a lick sensor which

registers the animals response (its lick rate) in response to the task stimuli. As animals must gain their daily water intake by completing behavioural tasks, mice are motivated to complete long sequences of trials without manual water restriction.

6.3.1. Terminology

Reference will be made throughout this thesis to various aspects of behavioural data generated with AutonoMouse. A few commonly used terminologies are listed here to aid the reader in understanding these references:

- Experimental group / cohort: A set of mice that are housed together in AutonoMouse for a series of behavioural tasks.

- Behavioural task: A sequence of trials designed to test some behavioural response. For example, an odour discrimination behavioural task might consist of some set of rewarded and unrewarded trials (paired differentially with two odours).

- Schedule: The pre-defined set of trials that makes up a particular behavioural task. A schedule is a list of many trials, and a behavioural task can consist of several consecutive schedules.

- Trial: A single test of mouse response to a stimulus e.g. a particular odour. On each trial, some stimulus is delivered with some reward valence and the response of the animal to that stimulus is recorded. Each behavioural task has some pre-defined logic that determines how AutonoMouse will respond to a mouse's response to a particular stimulus condition on a particular trial, e.g. by delivering a water reward or delivering a timeout punishment.

- Reward valence: Whether a trial is assigned as rewarded (S+) or unrewarded (S-).

6.4. Construction

6.4.1. Main structure

6.4.1.1. Home cage

The home cage chamber of AutonoMouse was an 52x62x17cm enclosure constructed from aluminium profiles (*MayTec Aluminium Systemtechnik GmBH, Dachau, Germany*) and walled with clear acrylic panels. The home cage contained floor-bedding (*Alpha Dri, LBS Biotechnology, UK*), environmental enrichment (running wheels, tunnels, soft bedding, 'homes', chew blocks) and a metal cage containing diet. The home cage was connected to a pre-chamber area constructed from acrylic panels by a wooden ramp. The pre-chamber was connected to the behaviour port via an acrylic tunnel. Access to the tunnel/behaviour port was controlled by a swing door, actuated by a rotary magnet (*GDRX 050 X20 D02 24V 100%, Magnet-Schultz*, *Woking, UK*) and controlled with custom electronics. A custom infra-red (IR) beam strip lined the walls of the access tunnel to detect animal presence. All behaviour was monitored in the behaviour port, which consisted of a custom plastic open faced enclosure housing an IR beam emitter/detector (*PIE310/PID310D, Kodenshi, Nagoya, Japan*), an RFID detector coil, a lick port, and some stimulus delivery device installed according to the desired behavioural task (e.g. odour port, speaker).

6.4.2. Control modules

6.4.2.1. Door module

Actuation of the door was controlled with custom electronics. This module received input from IR sensors and actuated the rotary magnet according to sensor input. When an animal was present in either the access tunnel or behaviour port, an IR beam was broken and the door was closed ensuring that only 1 animal had access to the behaviour port at a time.

6.4.2.2. IR module

Inputs from the IR beams were managed with custom electronics. This module powered and received input from IR beam detectors and relayed the on-off logic to other modules.

6.4.2.3. RFID module

The identity of the animal in the behaviour port was read out with an RFID detector and decoder (*Trovan LID-665 OEM Single Coil Compact Decoder, RFID Systems Ltd.*, *Yorkshire, UK*). The decoded RFID was relayed to the software via a serial port.

6.4.2.4. Lick module

Animal licking and water delivery was via a lick port housed in the behaviour port. The lick port was a hollow metal tube, open on the side facing the animal and connected to a water reservoir and gear pump (*MZR-2521, Harton Anlagentechnik GmBH, Alsdorf, Germany*) on the other side. The gear pump was controlled with a micro-controller (*S-ND, Harton Anlagentechnik GmBH, Alsdorf, Germany*) which could receive analog input via the AutonoMouse software to drive speed and duration of water delivery.

6.4.2.5. Digital / Analog Acquisition

All sensor data, digital I/O control and analog I/O control was via a peripheral component interconnect (PCI) data acquisition (DAQ) device (*PCI-6229*, *National Instruments, Austin TX, USA*) with a Bayonet Neill-Concelman (BNC) interface (*BNC 2090A, National Instruments, Austin TX, USA*), except for RFID reading and day-night cycle control which was via direct serial interface with a PC.

6.5. Software and experimental control

AutonoMouse was controlled with custom Python software. The primary role of the software was to:

- Build and manage schedules of trials for animals in the system to perform
- Manage a database of the animals housed in the system and assign schedules of trials to them
- Control delivery of trials to appropriate animals, read in and store resulting data
- Track performance of the animals housed in the system

The software is made up of two main packages: 'schedule generator' and 'autonomouse control'.

6.5.1. schedule-generator

The purpose of schedule-generator is to generate schedules of trials to fulfill a particular behavioural task. schedule-generator has a module based design in which users define 'trial widgets': self-contained code modules that follow a common pattern. In a trial widget the user defines a set of trial parameters (e.g. fraction of trials rewarded), stimulus parameters (e.g. stimulus length) and internal logic as to how sequences of trials will be constructed (e.g. no more than 3 unrewarded trials in a row). The trial widget also contains internal logic as to how to translate stimulus parameters into hardware output. For example, one stimulus parameter might be frequency of a stimulus pulse which would be some real number. The trial widget's internal logic would then be defined with some algorithm for creating a time sequence of pulses based on the desired frequency.

The output of schedule-generator is a data structure containing a sequence of trials and a pointer that describes how each of those trials should be converted into hardware output (e.g. a set of digital commands for driving a group of solenoid valves).

6.5.2. autonomouse-control

The purpose of autonomouse-control is to hold a database of animals housed in AutonoMouse, by reference to their implanted RFID chip. The software can then be used to assign schedules of trials to each of these animals to create a behavioural task for each animal. Individual mouse specific parameters such as water rewarded on each correct trial can also be set within the software. autonomouse-control is also responsible for implementing the behavioural 'loop':

1. Idle until animal detected (IR beam break)
2. On animal detected: initiate RFID decoding and read in current animal's unique identifier (ID)
3. Look up that animal in the database
4. Determine which trial in the schedule has not yet been performed by that animal
5. Parse the parameters for that trial into hardware commands (e.g. stimulus production)
6. Deliver the trial to the animal, and record from all installed sensors including the lick sensor
7. Determine how the animal performed in the trial (e.g. correct lick to a rewarded odour)
8. Deliver water rewards appropriately
9. Save the result of the trial and all recorded data to the database, and mark the current trial as completed
10. Return to 1.

The database within autonomouse-control can be used to track animal performance in the system - in terms of both performance accuracy and raw volume of trials performed per day.

6.6. Animal preparation

All animals taking part in a particular AutonoMouse cohort were weaned together from 3 weeks of age as a group and housed from this point on in a group cage to avoid disruption of social hierarchy and aggression later in the experiment. Animals underwent RFID implant surgery and were transferred to AutonoMouse at 5-6 weeks of age.

6.7. RFID implant surgery

Before being housed in AutonoMouse, all mice underwent an RFID implant surgery such that they could be individually identified by the system. Mice were anaesthetised under isoflurane (induction: 5% in O_2 2l/min, maintenance: 2%) and placed on a heat pad for maintenance of body temperature during the surgery. The fur around the base of the neck and scruff was shaved away and the skin cleaned with chlorhexidine (1%) and then dried with a sterile swab. A pre-sterilised needle (*IM-200, RFID Systems Ltd., Yorkshire, UK*) containing an RFID chip (*ID-100B, RFID Systems Ltd., Yorkshire, UK*) was then loaded onto a plunger and inserted into the loose skin at the base of the neck. The plunger was used to push the chip out of the needle before removing the needle, leaving the RFID chip implanted under the skin. Forceps were then used to pinch shut the incision made by the needle and medical superglue (*Vetbond, 3M, Maplewood MN, USA*) was applied to seal the wound. Animals were returned to an individual cage for 10 minutes following the surgery to recover from anaesthesia and for the superglue to dry. Once righting reflex was regained and the wound was confirmed as properly sealed the mouse was returned to the group cage with its cohort.

6.8. Experiment initiation and maintenance

For a generalised AutonoMouse experiment, the sequence of steps needed to initiate and maintain an experiment are here described.

First, a sequence of schedules for the desired behavioural task was generated in schedule-generator. In autonomouse-control, the RFID codes of the experimental cohort were entered into the database, as well as their assigned schedules. Animals were then weighed and transferred from their group cage into the common home cage of AutonoMouse. In general, the first behavioural task assigned to all animals was a 'pre-training' task designed to train animals to reliably gain their water intake from the behavioural port. The schedules for the pre-training task were designed as follows:

1. Water delivered as soon as animal detected in behaviour port (10 trials)
2. Animal must lick at least once to gain water reward once detected in the behaviour port (50 trials)
3. The percentage of total trial time (2s) that the animal must lick to gain a water reward is increased (up to 10% of trial length) (100 trials)

Each water reward was initially 15μl. This was adjusted to 10-30μl depending on animal performance (to ensure all mice performed roughly the same number of trials per day). During performance of these trials, animal weight was monitored daily, in addition to number of trials performed, to ensure that animals were indeed gaining their necessary daily water from the water rewards in the behaviour port. If any animal dropped in weight from the previous day, it was removed from the system and given water *ad libitum* for 10 minutes before being returned to the system. Any animal that consistently performed <100 trials per day or consistently dropped in weight (more than 2 days in a row) was isolated in the behaviour port and manually given water rewards from the lick port. Any animal that still dropped in weight or performed <100 trials per day after this treatment was removed from the cohort and culled.

For the first two weeks of any AutonoMouse experiment, animal weights were checked daily to ensure health status of the cohort. After two weeks, weight was checked more infrequently (every 4-5 days) but total trials performed was monitored daily to ensure animals had all performed >100 trials in the last 24 hours. Any animals not meeting this criterion were given water *ad libitum* for 10 minutes and then returned to the system. Any animals consistently performing few trials per day were removed from the cohort and culled.

The system was cleaned weekly. Animals were transferred to a temporary group

cage along with any loose bedding. Any areas with animal contact were removed and soaked in disinfectant (*Trigene, Ceva, Glenorie NSW, Australia*), cleaned and dried. The (AutonoMouse) cage floor bedding was removed and replaced. Animals were then transferred back into the system along with loose bedding.

For the most part, the door mechanism of the AutonoMouse system ensured that only 1 animal at a time was able to perform trials. In some rare cases, mice entered the access tunnel simultaneously resulting in two animals able to access the behaviour port. On these occassions, trial initiation could result in an error in RFID decoding (two RFID chips simultaneously next to the antenna, resulting in 'default' code). Alternatively, as the two animals both attempted to perform trials in the behaviour port, switching of the decoded RFID code from trial-to-trial was observed. As this situtation could confound behavioural results, 'default' trials and periods where RFID code rapidly switched from trial-to-trial are excluded from further analysis.

To determine whether mice gained body weight normally in the system (and were therefore comparable healthy to non-AutonoMouse housed animals), 3 cohorts of mice were raised either in separate single houses; colony housing as a group; or within the AutonoMouse system (see seubsection 13.3.4). The 3 cohorts were housed separately in standard group cages until P22, and then transfered into single cages (n = 8); a different group cage (n = 20); or the AutonoMouse system (n = 20). Mice in the AutonoMouse housing group were maintained as described above.

7. Lesion study

7.1. Overview

The aim of the lesion study (chapter 14) was to examine olfactory discrimination performance after disruption of the olfactory bulb with excitotoxic lesions. In particular, we aimed to determine changes in performance in response to olfactory discrimination in particular contexts, for example in response to a previously learned odour pair, or a completely novel odour pair. We also aimed to investigate the extent of performance change in response to variable sizes of lesion. To this end, mice were trained in AutonoMouse on a series of olfactory discrimination behavioural tasks prior to lesion induction to determine baseline performance. Mice then underwent a lesion surgery to induce damage to the olfactory bulb via injection of an excitotoxic solution or - in the control case - a sham surgery in which only the dilution solution was injected. After recovery from surgery, mice were re-housed in AutonoMouse and subjected to a further battery of behavioural tasks to determine changes in performance accuracy.

7.2. Task and trial structure

7.2.1. General trial structure

All tasks followed a standard go/no-go training paradigm. Animals were presented with either S+ rewarded odour or S- unrewarded odour (reward is reversed for roughly half the experimental group, e.g. in a group of 20 learning an EB vs. AA task, 10 are trained on EB as the S+ stimulus and 10 are trained on AA as the S+ stimulus) triggered by animal presence in the behavioural port. A water reward

could be gained by licking in at least 3 of the response period quarters following S+ odour presentation. Licking in at least 3 of the response period quarters during S- presentation resulted in an increased 'timeout' inter-trial interval (8-12s), in all other response cases the inter-trial interval was 4s and no water reward was delivered.

7.2.2. Task structures

Various kinds of discrimination tasks were presented to the experimental cohort. The terminologies, structures and primary purposes of these tasks are listed below.

7.2.2.1. Initial

The initial task was the first olfactory discrimination task presented after pre-training was complete. The purpose of this task was primarily to determine that all animals were capable of olfactory discrimination, and served as an initial version of the novel task.

7.2.2.2. Novel

A novel task was any olfactory discrimination between two pure odours in which the odours had never been previously presented to the animal. The purpose of this task was to determine the speed of task acquisition and confirm ability to perform discrimination for multiple odour pairs.

7.2.2.3. Familiar

A familiar task was any olfactory discrimination between two pure odours in which the animal had previously performed a discrimination task with the same two odours. The purpose of this task was to probe recognition and memory of acquired task learning.

7.2.2.4. Non-trigeminal simple (NTS)

An NTS task was any olfactory discrimination between two pure odours in which the two odours were non-trigeminally activating (vanillin and phenyethyl alcohol, Chen and Halpern, 2008). The purpose of this task was to dissect out any contribution to learning and odour detection from stimulation of the trigeminal nerve.

7.2.2.5. Mixture

A mixture task was an olfactory discrimination in which animals were asked to discriminate between mixture ratios of two odours. For example, S+ might be odour 1 and odour 2 mixed together in a 60%:40% ratio, and S- might be the same odours in a 40%:60% ratio. The purpose of this task was to be a more behaviourally demanding version of olfactory discrimination.

7.2.2.6. Non-trigeminal mixture (NTM)

An NTM task was the same as a mixture discrimination task, but both odours were non-trigeminally activating. The purpose of this task was both to be a more behaviourally demanding version of olfactory discrimination while dissecting out any contribution to learning and detection from stimulation of the trigeminal nerve.

7.2.2.7. Auditory

In an auditory task, animals were asked to discriminate between two pure audio sine waves at different frequencies. The purpose of this task within this experimental context was to ensure that any changes in olfactory discrimination performance were due to changes in olfactory ability rather than changes in general ability to perform GNG tasks.

7.2.2.8. S+ / S- Detection

In a detection task, animals were asked to discriminate between an odour and clean air. This discrimination was either performed with the odour as S+ (S+

detection), or with the clean air as S+ (S- detection). The purpose of this task was to determine an animal's ability to simply detect an odour, rather than discriminate between two odours.

7.2.3. Training schedules

Over the course of the lesion study, 3 different cohorts underwent a set of behavioural tasks. The precise training schedule for these 3 groups is shown in table 7.1, 7.2, 7.3.

Task (Group 1)	Odours / Hz	Task type
1	Cinn vs. ACP	Initial
2	EB vs. AA	Novel
3	EB vs. AA	Mixture
4	Time delay (25 days)	N/A
5	EB vs. AA	Familiar
6	V vs. P	NTS
7	V vs. P	NTM
Lesion		
8	EB vs. AA	Familiar
9	CN vs. EU	Novel
10	V vs. P	NTS
11	V vs. P	NTM
12	CN vs. EU	Familiar
13	CN vs. EU	Mixture
14	EB vs. AA	Familiar

Table 7.1.: Training schedules (group 1). The sequence (numbered) of behavioural tasks for cohort 1 in the lesion study is shown (n = 6 female). The task type according to subsection 7.2.2 is shown for each, as well as the odour pair or auditory frequency used. 'Lesion' row indicate the point at which lesions were induced. Task 4 is a time delay - intended to investigate performance in a familiar odour task after a period of not performing odour discrimination.

Task (Group 2)	Odours / Hz	Task type
1	EB vs. AA	Initial
2	CN vs. EU	Novel
3	EB vs. AA	Familiar
4	EB vs.AA	Mixture
Lesion		
5	CN vs. EU	Familiar
6	EB vs. AA	Familiar
7	EB	S+ detection
8	EB	S- detection
9	0.3 vs. 3 kHz	Auditory
10	5 vs. 10 kHz	Auditory

Table 7.2.: Training schedules (group 2). As in table 7.1 for cohort 2 (n = 14).

Task (Group 3)	Odours / Hz	Task type
1	EB vs. AA	Initial
2	CN vs. EU	Novel
3	EB vs. AA	Familiar
4	N/A	Odour block
5	EB vs. AA	Mixture
Lesion		
6	CN vs. EU	Familiar
7	ACP vs. 2H	Novel
8	V vs. P	NTS
9	V vs. P	NTM

Table 7.3.: Training schedules (group 3). As in table 7.1 for cohort 3 (n = 9). Task 4 is an odour diversion task (see figure 14.5d) intended to act as a control to ensure animals were truly using odour information to perform discrimination.

7.3. Odour delivery

Odour stimuli were delivered with a custom-built 8 channel olfactometer (see figure 14.3a) with two parallel input lines. Parallel lines were controlled separately and one odour input from each line could therefore be delivered to the odour carrier air stream simultaneously. Odour concentration delivered to the main odour carrier air stream was controlled by varying the flow and pressure levels in the

parallel input lines. The stimulus given to the behaving animal was controlled by switching between a clean air and odourised air flow line via a 5-way solenoid valve (*VK3210, SMC, Tokyo, Japan*).

Where pure odours were delivered to the animal (e.g. in a pulse of EB), the final odour stimulus was generated by triggering (at random) one valve from each parallel input line connected to the odour source of choice. Where binary mixtures of odours were delivered (e.g. in an EB/AA 6/4 pulse) the valve choice was also randomised but each input line delivered a separate odour. Each input line contained two S+ sources and two S- sources. Therefore, the sequence of valves used to deliver either an S+ or S- stimulus had 4 possible combinations for pure odour stimuli, and 8 possible combinations for binary mixtures. Chosen at random, these combinations ensured that animals were unlikely to learn to discriminate the noise of valve opening rather than odour stimulation.

7.3.1. Control stimuli

To ensure that the odour stimuli were the only salient signals that were learned in the discrimination task, control stimuli were designed in which the number of active valves was gradually increased. Initially, animals would be trained on only 4 valves (1 odour 1, 1 odour 2, 2 blank), typically for several hundred trials. At some point during training, 2 new valves were introduced to stimulus production and training continued. Finally another 2 valves were added and the full set of 8 was used to generate stimuli. The transition between valve numbers was automated so there was no additional time delay from one case to the other. By comparing performance before and after introduction of new valves, we could confirm that mice were truly using only the odour signals to discriminate. If performance dropped after introduction of the new valves it was an indication that some extraneous cue to do with e.g. the noise of valve switching was being learned in addition to or instead of the odour signal.

7.4. Lesion induction

Prior to surgery all utilised surfaces and apparatus were sterilised with 1% trigene. Surgical instruments were sterilised in an autoclave. Surgery was carried out with standard aseptic technique.

A glass injection pipette, pulled on a capillary tube puller (*P-1000, Sutter Instrument, CA USA*) and broken off to approx. 15μm diameter was back-filled with either NMDA (*Sigma-Aldrich*, *St. Louis MO, USA*) (10mg/ml diluted in 1% PBS) or 1% PBS and inserted into the injector apparatus (*Nanoject II, Drummond Scientific, PA USA*). Mice were anaesthetised with ketamine/xylazine solution via intraperitoneal injection (Vetalar/Rompun; 80mg/kg / 10mg/kg) and placed on a warm heat pad. Depth of anaesthesia was monitored throughout the procedure by testing toe-pinch reflex. The fur on the skull extending from the base of the head to the tip of the nose was shaved away and cleaned with 1% clorhexidine scrub. Mice were then placed on a thermoregulator (*DC Temp. Controller, FHC, ME USA*) heat pad controlled by a temperature probe inserted rectally. While on the heat pad, the animals were inserted into a stereotaxic frame (*900LS, Kopf Instruments, CA USA*) and a sterile surgical cover (*Buster op cover, Kruuse, Langeskov, Denmark*) was placed over the body of the animal. The scalp was incised and held away from the skull with arterial clamps and two craniotomies were made with a dental drill (*Success 40, Osada, Tokyo, Japan*) above the 2 olfactory bulb hemispheres. The craniotomies were covered with 1% phosphate-buffered saline (PBS) to prevent drying of brain tissue during the surgery. Depending on the desired lesion size, injections of either N-Methyl-D-aspartic acid (NMDA, *M3262, Sigma-Aldrich*, *St. Louis MO, USA*) or PBS were made to several injection sites in the bulbs (see table 7.4).

After injection completion, the craniotomy was resealed using silicone elastomer (*KwikCast, World Precision Instruments, FL USA*) and the skin incision was sutured closed (*Silkam 7/0, Braun, Tuttlingen Germany*) and cleaned with 1% clorhexidine scrub. Animals were given meloxicam (Metacam; 2mg/kg) injected subcutaneously for post-operative analgesia. Mice were removed from the stereotaxic apparatus and placed in a warm recovery chamber (*Thermo Scientific, MA USA*) (36ºC) until recovery from anaesthesia was observed (righting reflex regained). Following surgery, animals were singly housed for 3 days, and then

Coordinate ID	1	2	3	4	5	6	7	8	9	10
x:	0.85	0.85	0.85	0.85	0.85	0.85	0.85	0.85	0.65	0.65
y:	0.85	0.85	0.85	1.15	1.15	1.15	1.45	1.45	0.85	0.85
z:	0.7	1.1	1.4	0.7	1.1	1.4	0.7	1.1	1.1	1.4
n Injections (2.3nl)	66	33	33	66	33	33	66	33	66	33
Solution (sham)	PBS	PBS	PBS	PBS	PBS	PBS	PBS	PBS	PBS	PBS
Solution (S)	NMDA	PBS	PBS	PBS	PBS	PBS	PBS	PBS	PBS	PBS
Solution (M)	NMDA	PBS	PBS	PBS	PBS	PBS	NMDA	PBS	PBS	PBS
Solution (L)	PBS	PBS	NMDA	NMDA	NMDA	NMDA	NMDA	NMDA	PBS	PBS
Solution (XL)	NMDA	NMDA	NMDA	NMDA	NMDA	NMDA	NMDA	NMDA	NMDA	NMDA

Table 7.4.: Injection sites. Table shows injection sites for each lesion group used in the experiment. For each coordinate (1-10) the x/y/z positions of injection are shown. x position refers to mm away from bregma in the rostro-caudal axis (positive values indicate more rostral positions). y position refers to mm away from bregma in the medio-lateral axis (positive values indicate more lateral position). z position refers to depth from the surface of the brain (positive values indicate deeper penetration into the brain. For each injection site, a number of 2.3nl injections were made, given by the n injections row. For each injection site, the solution injected is shown depending on the desired lesion extent (sham, S, M, L, XL). PBS was at 1% dilution. NMDA solution was 10mg/ml dissolved in 1% PBS.

returned to the AutonoMouse home cage.

7.5. MicroCT imaging

In some cases, the brains of mice in the experimental cohort were imaged using x-ray CT imaging to determine the extent of OB disruption induced by the lesion / sham surgery. The CT imaging method was based on a previously described protocol (Saito and Murase, 2012).

Mice were deeply anaesthetised with ketamine/xylazine solution via intraperitoneal injection (Vetalar/Rompun; 80mg/kg / 10mg/kg) and sacrificed by transcardial perfusion using 1% PBS clearant and 7.5% paraformaldehyde (PFA) perfusative (diluted with 1% PBS). The head was separated from the body and left to soak in a 40ml container containing 20ml Iodinated PFA solution (150mg/ml iodine – (*Niopam 340, Bracco, Milan, Italy*) diluted in 7.5% PFA).

After a minimum of 15 days soaking at 4ºC the heads were transferred to custom made holders with attachments for placement in a microCT scanner (*SkyScan 1172, Bruker, Kontich, Belgium*). A scan of the olfactory bulb area was made using 70kV x-ray source power with an aluminium and copper filter at pixel resolution of 8.6μm. Ring artefacts were reduced by introduction of random movement into the head rotation during the scan. Coronal image sections were reconstructed from the scan using the SkyScan NRECON software.

7.5.1. MicroCT Lesion Quantification

To define intact OB volume size after microCT imaging, a manual segmentation approach was used. The CT stack for a given mouse was loaded using Imaris (*Bitplane, Belfast, UK*). Image stacks were reconstructed coronal sections through the mouse head. To define skull volume, images were segmented by manually tracing the skull perimeter for each image slice, beginning at bregma and ending where OB tissue was no longer visible. This resulted in a sequence of 2D skull perimeter definitions which were reconstructed into a 3D volume using Imaris. The same procedure was repeated for OB tissue using the start and end

points of the skull volume tracing. Finally, if any internal damage in OB tissue was observed in the stack, this was traced using the same method. The result of this procedure was 3 volumes for the skull, intact OB and internal OB damage. Relative OB volume was then defined as (OB volume - OB damage volume) / skull volume. All segmentations were performed by a single tracer, who was blinded to the identity and NMDA injection volume of the mice.

7.6. Experiment maintenance

The installed odours in the olfactometer were replaced every 3-4 days. Fresh odour dilutions were made and the odour vials containing the odours were replaced. Following odour replacement or any change of odour positions, 100-200 'dummy' trials were performed in which air was pushed through each odour position in turn to purge any contamination from the previously installed odour bottles.

8. Odour signal recording

8.1. Overview

For odour signal recording, there were two primary aims. 1) That we should be able to record from two odours individually and simultaneously within a mixed plume, in order to determine the extent of temporal correlation between two odours and 2) that we should be able to record odour signals with sufficient temporal bandwidth to investigate temporal features of their concentration fluctuation. Generally, we were able to achieve both of these aims by using photo-ionisation detectors (PID) (*200B miniPID, Aurora Scientific*, *Aurora ON, Canada*).

8.2. Dual-energy photo-ionisation detection

8.2.1. Principle

PIDs cannot resolve individual odours in a mixture as their output is the sum of all ionised molecules drawn across the sensor, regardless of identity. To be able to record from two odours simultaneously we took advantage of the fact that a PID can only record from odours with ionisation energies lower than the energy of its ultraviolet (UV) bulb. For certain combinations of odours and installed bulbs, we could therefore use 2 PIDs recording simultaneously to extract the individual signals of the odours.

We installed one PID with a 10.6eV bulb (high energy) and another with an 8.4eV bulb (low energy). The potentiometer in the low energy PID controller was adjusted to allow for robust detection of signals in the PID. With these energy ranges we could then record from two odours with these conditions:

- Odour 1 has ionisation energy lower than 10.6eV but greater than 8.4eV (e.g. ethyl butyrate - 9.5eV). This is termed the high energy odour and can only be detected by the high energy PID.

- Odour 2 has ionisation energy lower than 8.4eV (e.g. α-terpinene - 7.9eV). This is termed the low energy odour and can be detected simultaneously by both PIDs.

Under these conditions, in a simultaneous recording from these two odours mixed together in air, the high energy PID will capture the sum of both odours (as both odours have ionisation energy lower than 10.6eV). The low energy PID will only capture the low energy odour. In principle, therefore, the individual odour signal for the low energy odour is the readout from the low energy PID, and the individual high energy odour signal is the readout of the high energy PID minus the low energy PID signal. The procedure for extracting the individual odour signals from simultaneous high / low energy recording is termed 'decomposition' (see figure 15.1).

8.2.2. Decomposition procedure

In principle, the high energy odour signal can be extracted from the high energy PID output by simply subtracting the low energy PID signal. This assumes, however, that the low energy odour will be recorded at the same amplitude in both PIDs. In practice this is not the case as the high energy PID will ionise molecules more readily and the low energy odour will therefore show up with higher amplitude in the high energy odour signal. To account for this, a scaling factor is calculated by making several recordings from the low energy odour alone and fitting a linear transformation that maps the signal in the low energy PID to the high energy PID signal. This linear transformation is then applied to all low energy PID signals in mixed odour recordings to scale the signal amplitude to the same range as recorded in the high energy PID. The subtraction of the scaled low energy signal will then leave only the high energy odour contribution.

8.3. Recording apparatus

Odour plume recordings were made with two PIDs spaced close together (10cm), with the inlet needles connected via a 3-way connector and tubing. Therefore, the two PIDs drew in air from the same point in space, which will be termed the PID inlet. The two PIDs were held with adjustable lab stands and adjusted such that the PID inlet was 4cm above the ground. A digitally controlled fan (*2214F/2TDH0, ebm-past, Chelmsford, UK*) was placed 440cm away from the PID inlet, oriented such it could push air directly towards the inlet. During a recording, the fan was set to maximum speed such that it pushed approximately 552 cf/m (cubic feet per minute) of air towards the PID inlet. A 25x25x25cm Thermocol box was placed 200cm downwind of the fan to act as an obstacle to air movement, breaking up any laminar air flow and ensuring air movement was turbulent once it reached the PID inlet. The odour sources were ceramic dishes filled with 6ml of the desired odour. Odour release was via a custom built Arduino robot that used a stepper motor to raise and lower a covering dish over the odour source dish. This robot could be remotely and automatically controlled with digital commands from a PC.

8.4. Recording conditions

8.4.1. Low energy only

For low energy only recordings, the low-energy odour (α-terpinene) was placed 40cm (radial distance) away from the PID inlet, and either 25cm left or 25cm right of the midline (the midline in this context is the line between the PID inlet and the centre of the fan). For each set of recordings, the odour source was alternated between left and right positioning relative to the midline an equal number of times to remove any signal effects from positioning in the air stream. The purpose of this recording condition was to generate data to calculate the linear transformation from the low energy signal to the high energy signal as detailed in subsection 8.2.2.

8.4.2. Mixture

In the mixture recording, the two odours (ethyl-butyrate, α-terpinene) were mixed together in equal parts and positioned in the same way as the low energy odour in low energy only recordings. The purpose of this recording condition was to determine how the temporal structure of individual odours in a plume behaved when the odours emanated from the same source.

8.4.3. Separated

In the separated recording, the two odours were individually placed in their own dish. Both odours were placed 40cm (radial distance) away from the PID inlet. One odour was placed 25cm left of the midline, and one was placed 25cm right of the midline (or vica-versa, each condition used equal number of times over several recordings) such that the sources themselves were 50cm apart. The purpose of this recording condition was to determine how the temporal structure of individual odours in a plume behaved when the odours emanated from separated sources but were still free to mix in air.

9. Temporal olfactometer

9.1. Overview

To determine the extent to which animals are capable of perceiving temporal features in naturally occurring odour signals, it was necessary to be able to replicate those features reliably in a controlled laboratory setting. To this end we developed an olfactometer capable of releasing odour and altering odour concentration at high temporal bandwidth.

9.2. Construction

The temporal olfactometer was based on a modular design of four separate odour channels (see figure 16.1), and consisted of an odour manifold for odour storage, a valve manifold for control of odour release and hardware for controlling and directing air flow through the system.

The odour manifold was a 12.2x3.2x1.5cm stainless steel block with 4 milled circular indentations (1cm radius). Within each of these indentations was a threaded through-hole for installation of an input flow controller (*AS1211F-M5-04, SMC, Tokyo, Japan*) and an output filter (*INMX0350000A, The Lee Company, Westbrook CT, USA*). For each inset, the cap of a 15ml glass vial (*27160-U, Sigma-Aldrich*, *St. Louis MO, USA*) with the centre removed was pushed in and sealed with epoxy resin (*Araldite Rapid, Hunstman Advanced Materials, Basel, Switzerland*). This meant that glass vials could be screwed in and out of the insets. After installation of the inset thread, the flow controllers and filters were installed on each inset position. Each position where a vial could be installed is henceforth referred to as an 'odour position'.

4 very-high-speed (VHS) valves (*INKX0514750A, The Lee Company, Westbrook CT, USA*) were installed in a 4-position manifold (*INMA0601340B, The Lee Company, Westbrook CT, USA*) with standard mounting ports (*IKTX0322170A, The Lee Company, Westbrook CT, USA*). Each valve was connected to a corresponding odour position in the odour manifold with a 10cm tubing (*TUTC3216905L, The Lee Company, Westbrook CT, USA*). Each valve was controlled by digital commands via a custom-made spike-and-hold driver. Each digital pulse delivered to the spike-and-hold driver delivered a 0.5ms 24V pulse to the valve (to open it) followed by a 3.3V holding pulse lasting the rest of the duration of the digital pulse. This spike-and-hold input allowed for fast cycling of the valve without switching between 0 and 24V at high frequencies and overheating the valve. Each valve was controlled by an individual spike-and-hold driver. Up to 4 drivers could be controlled and powered with a custom-made PSU consisting of a 24V power input and a linear regulator to split the voltages into a 24V and 3.3V line, as well as control inputs taking digital signal input and routing it to the appropriate valve.

To generate air flow through the olfactometer, a pressurised air source was connected to a filter (*AME250C-F02, SMC, Tokyo, Japan*) and demister (*AMF250C-F02, SMC, Tokyo, Japan*) and then split into two separate lines, the input line and carrier line. Both lines were then connected to a pressure regulator (*AR20-F01BG-8, SMC, Tokyo, Japan*) and flow controller (*FR2A13BVBN, Brooks Instrument, Hatfield PA, USA*). The main line was then connected to the input of the valve manifold. The input line was split into 4 separate lines and connected to the input flow controllers (set to 0.25L/min) on each odour position of the odour manifold. The output of the valve manifold was fitted with MINSTAC tubing (*TUTC3216905L, The Lee Company, Westbrook CT, USA*). Where the design was scaled up (e.g. to include 8 odour positions) the valve manifold outputs were connected and consolidated to a single output with 3-way connectors (*TMMA3203950Z, The Lee Company, Westbrook CT, USA*)

9.3. PulseBoy

Pulse profiles for calibration and stimulus production were generated with custom Python software: PulseBoy. PulseBoy is a graphical user interface (GUI) for defining pulse parameters across multiple valves and converting these pulses to digital inputs for the valve spike-and-hold drivers. User-defined modules are used to define pulse parameters and internal logic for conversion to digital signals. Each valve can be assigned its own module such that valves can be individually driven with flexible pulse profiles.

10. Correlation discrimination experiment

10.1. Overview

In this experiment, we aimed to probe whether mice could perceive a particular temporal feature of naturally occurring odour signals: temporal correlations between odour signals. In particular we aimed to investigate this question with the simplest possible case: whether mice could discriminate perfectly correlated from perfectly anti-correlated odour stimuli.

10.2. Odour delivery

Odours were delivered with an 8-position temporal olfactometer (as described in chapter 9). The 8-position odour manifold was installed with 15 ml odour 1 at 1/5 dilution with mineral oil in 3 positions; 15 ml odour 2 at 1/5 dilution with mineral oil in 2 positions; and 15 ml mineral oil in 3 positions. The mineral oil positions are henceforth referred to as 'blank'.

10.3. Task and trial structure

10.3.1. General structure

All tasks followed a standard go/no-go training paradigm. Animals were presented with two odours presented in either a correlated pattern or an anti-correlated pat-

tern (see figure 17.1). For roughly half of all animals, the correlated pattern was S+ (rewarded) and the anti-correlated pattern was S- (unrewarded); in the other half of the group this reward valence was reversed. All stimuli were 2s long. A water reward could be gained by licking such that licking was detected for at least 10% of the stimulus time during an S+ presentation. Licking for the same amount of time during S- presentation resulted in a timeout interval of 7s. In all other response cases the inter-trial interval was 3s and no water reward was delivered.

10.3.2. Stimulus structure

All anti-correlated and correlated stimuli on each trial followed a common pattern in their construction. Generally, wherever an odour position was inactivated a blank position was activated to compensate for flow change. Stimuli were designed such that there were no consistent differences in the amount of odour or flow released during the stimulus between correlated and anti-correlated stimuli. The detailed algorithm for stimulus generation is as follows.

1. Choose whether the stimulus will be correlated or anti-correlated.
2. A set of 1-2 positions each for odour 1 and odour 2 and 2-3 positions for blank are randomly chosen from a pre-defined subset of 6 of the 8 total positions. For example, a valid combination could be odour 1 at position 1, 2; odour 2 at position 5; and blank at position 3, 7. An example combination is shown in figure 17.1d.
3. Create a guide pulse at the desired frequency (e.g. 2Hz pulse with 50% duty) for all positions that follows the chosen stimulus structure. An example guide pulse is shown in figure 17.1c.
4. The relative contributions of each position to the total stimulus are randomly generated. At each time point in the stimulus, only two position types should be active (e.g. odour 1 and blank for an anti-correlated stimulus) so the maximum contribution for any position type is 50% of the total release amount. Where two positions have been chosen for a position type, their relative contributions should add to 50%.
5. The guide pulses are pulse-width modulated according to the relative contributions of each position. PWM is at 500Hz with some added jitter in the

duty to avoid strong tone generation and to introduce some noise to the total released odour.

10.3.3. Task structure

Mice in the correlation discrimination task underwent a number of behavioural tasks to probe various aspects of correlation discrimination. The structure of these tasks is here summarised.

10.3.3.1. Correlation discrimination - static frequency

In this task, animals were trained on correlation discrimination in which the stimulus frequency was the same on every trial. 50% of trials were generated following the algorithm in subsection 10.3.2. 50% were produced with a slight modification to the algorithm: in step 2 only 1 odour position was chosen for each odour type, and 2 positions were chosen for blank.

10.3.3.2. Correlation discrimination - random frequency

This task was the same as the static frequency task, but task frequency was randomised from trial to trial in a range between 2-81 Hz. The choice of frequency was with weighted probability divided into 3 frequency bands. E.g. this task could be arranged such that 2-20Hz would be chosen with probability P = 0.6, 21-40Hz with P = 0.3 and 41-81Hz P = 0.1. Within each of these frequency bands, the choice of individual task frequency was based on a uniform distribution.

10.3.3.3. Control valve additions

Control valve additions could be automatically added to the static frequency and random frequency tasks. These tasks produced their stimuli based on a subset of 6 valves, control valves could be added automatically after a set period of trials to force the algorithm to produce stimuli from all 8 valves (see figure 17.1e, control).

10.3.3.4. Switch controls

In switch controls, the experiment was halted and the positions of all valves and odour positions were shuffled in the olfactometer (see figure 17.1e, switch control). The software definitions for valve positions were remapped to account for the change and the experiment was restarted.

10.3.3.5. Onset disruption

Onset disruption stimulus sequences were generated in the same way as static frequency correlation discrimination tasks, but around 10% of the trials were disrupted such that the first stimulus pulse had the opposite structure to the rest of the stimulus. E.g. a correlated stimulus with onset disruption would display anti-correlated properties for the first pulse (see figure 17.7a).

10.3.3.6. Low vs. High

This task was similar to the random frequency task, but trial frequency was picked from 1 of 2 values: a low-value (2Hz) and a high-value, which was the highest frequency at which a particular animal still performed above chance in the random frequency task (defined as performance vs. frequency intercept at 0.6).

10.3.4. Group structure

The correlation discrimination experiment was performed in 2 separate experimental cohorts (group 1, n = 14; group 2, n = 25). Each cohort was organised into several subgroups which performed slight variations of the behavioural tasks in terms of reward valence and valves utilised, but with the same underlying task aim. Half of the animals in each subgroup were trained on correlated stimuli as the S+ rewarded condition, with the other half trained on anti-correlated as rewarded. Animals were further subdivided into groups which were trained on different subsets of valves as standard in the 8-channel olfactometer (table 10.1). In group 2, an additional subgroup was created in which the valve map was scrambled, as an ongoing control against animals learning extraneous variables in the task.

Valve position	1	2	3	4	5	6	7	8
Installed odour	O1	O1	B	O1	O2	O2	B	B
Front-valves	O1	O1	B	O1 (C)	O2	O2	B	B (C)
Back-valves	O1	O1 (C)	B (C)	O1	O2	O2	B	B
Front-valves, full scramble	O1	O2	B	O1 (C)	O2	B	O1	B (C)
Back-valves, full scramble	O1 (C)	O2	B	O1	O2	B (C)	O1	B
Front-valves, partial scramble	O1	O2	B	O1 (C)	O1	O2	B	B (C)
Back-valves, partial scramble	O2	O1 (C)	B (C)	O1	O2	O1	B	B

Table 10.1.: Valve subgroup mapping. For each valve position (1-8 top row) the associated installed odour in the olfactometer is displayed (O1: odour 1, O2: odour 2, B: blank). In the rows below, the valve map for different animal subgroups is shown. The valve map is the information given to the control software regarding odour positions in the olfactometer such that it can build stimuli from the correct odour profiles. For example, if the installed odour at position 1 is O1, and the valve map at position 1 also specifies O1 (e.g. for front-valves row), the mapping is correct and O1 stimuli will be appropriately delivered. If the installed odour at position 1 is O1 but the valve map at position 1 specifies O2 (e.g. for back-valves, sham - partial scramble), the mapping is scrambled and the software will inappropriately deliver O1 stimuli when O2 stimuli should be delivered. In the valve map, where 'C' is specified, the software will only use these valve positions during control trials.

Subgroup	1	2	3	4	5	6
n Group 1	3	4	3	4	0	0
n Group 2	5	5	5	5	3	2

Table 10.2.: Group assignments. For each subgroup, the number of animals assigned within each cohort is shown. Subgroups were 1) Correlated rewarded, front-valves; 2) Correlated rewarded, back-valves; 3) Anti-correlated rewarded, front-valves; 4) Anti-correlated rewarded, back-valves; 5) Correlated rewarded, front-valves scrambled; 6) Anti-correlated rewarded, back-valves scrambled.

10.3.5. Training schedules

Task (Group 1)	Odours / Hz	Task Type
1	EB vs. AA / 2Hz	Static
2	EB vs. AA / 2Hz	Static + control
3	EB vs. AA / 12Hz	Static + control
4	EB vs. AA / 12Hz	Static + switch + control
5	EB vs. AA / <=16Hz	Random weighted
6	EB vs. AA / <=81Hz	Random weighted
7	EB vs. AA / <=81Hz	Random weighted

Table 10.3.: Training schedules (group 1). The sequence (numbered) of behavioural tasks for cohort 1 in the correlation study is shown (n = 14). The task type according to subsection 10.3.3 is shown for each, as well as the odour pair and correlation frequency used. The terms 'random weighted' and 'random uniform' refer respectively to random tasks in which the choice of frequency from trial-to-trial was weighted; vs. random tasks in which any frequency was equally likely to be chosen. Where tasks are indicated as 'static + switch + control', animals were performing a task in which switch controls had been introduced, with control valve additions also added alter in the task. Some non-standard tasks were present for some groups. In this group, 1 animal underwent a sequence of tasks after task 4, where it was trained on a static frequency with controls at multiple frequencies in sequence (16Hz, 20Hz, 25Hz, 30Hz, 50Hz).

Task (Group 2)	Odours / Hz	Task Type
1	EB vs. AA	GNG
2	EB vs. AA / 2Hz	Static
3	EB vs. AA / 2Hz	Static + control
4	EB vs. AA / <= 16Hz	Random weighted
5	EB vs. AA / <=40Hz	Random weighted
6	EB vs. AA / <=50Hz	Random weighted
7	EB vs. AA / <=81Hz	Random weighted
8	EB vs. AA / <=81Hz	Random weighted
9	EB vs. AA / <=81Hz	Random uniform
10	EB vs. AA / Individual Hz	Static + control
11	EB vs. AA / Individual Hz	Static + switch + control
12	EB vs. AA / Individual Hz	Low vs. high
13	EB vs. AA / Individual Hz	Onset disrupt
14	CN vs. ACP / 2Hz	Static + control
15	CN vs. ACP / 10Hz	Static + control
16	2H vs. 2P / 2Hz	Static + control

Table 10.4.: Training schedules (group 2). As in table 10.3 for cohort 2 (n = 24). This group's 1st task was a non-temporal go/no-go discrimination between the two odours presented statically as 2s square pulses.

11. 2-photon imaging

11.1. Overview

To determine how correlation information is encoded in the early olfactory system, we employed 2-photon imaging of fluorescence responses in M/TC projection neurons in the olfactory bulb while stimulating with correlated and anti-correlated odour stimuli.

11.2. Recording procedure

Prior to surgery all utilised surfaces and apparatus were sterilised with 1% trigene. 16-20 week old mice (Tbet-cre crossed with GCaMP6f reporter line, Otazu et al., 2015) were anaesthetised using a mixture of fentanyl/midazolam/medetomidine (0.05mg/kg, 5mg/kg, 0.5mg/kg respectively). Depth of anaesthesia was monitored throughout the procedure by testing the toe-pinch reflex. The fur over the skull and at the base of the neck was shaved away and the skin cleaned with 1% clorhexydene scrub. Mice were then placed on a thermoregulator (*DC Temp. Controller, FHC, ME USA*) heat pad controlled by a temperature probe inserted rectally. While on the heat pad, the head of the animal was held in place with a set of ear bars. The scalp was incised and pulled away from the skull with four arterial clamps at each corner of the incision. A custom head-fixation implant was attached to the base of the skull with medical superglue (*Vetbond, 3M, Maplewood MN, USA*) such that its most anterior point rested approximately 0.5mm posterior to the bregma line. Dental cement (*Paladur, Heraues Kulzer GmBH, Hanau, Germany; Simplex Rapid Liquid, Associated Dental Products Ltd., Swindon, UK*) was then applied around the edges of the implant to ensure firm adhesion to the skull.

A craniotomy over the olfactory bulb (2x2mm) was made with a dental drill (*Success 40, Osada, Tokyo, Japan*) and then immersed in artificial cerebrospinal fluid (ACSF) (NaCl (125mM), KCl (5mM), HEPES (10mM), pH adjusted to 7.4 with NaOH, $MgSO_4.7H_2O$ (2mM), $CaCl_2.2H_2O$ (2mM), Glucose (10mM)) before removing the skull with forceps. The dura was then peeled back using fine forceps. A layer of low-melt agarose (2%) was applied over the exposed brain surface before placing a glass window cut from a cover slip over the craniotomy. The edges of the window were then glued with medical superglue (*Vetbond, 3M, Maplewood MN, USA*) to the skull.

Following surgery, mice were placed in a custom head-fixation apparatus and transferred to a 2-photon microscope rig along with the heat pad. The microscope (*Scientifica Multiphoton VivoScope*, *Scientifica, Uckfield, UK*) was coupled with a MaiTai Deep See laser (*Spectra Physics, Santa Clara, CA*) tuned to 940nm (50mW average power on the sample) for imaging. Images (512 x 512 pixels) were acquired with a resonant scanner at a frame rate of 30Hz using 16x 0.8 NA water-immersion objective (*Nikon*, *Tokyo, Japan*). The output of a 4-channel temporal olfactometer (see chapter 16) was adjusted to approximately 1cm away from the ipsilateral nostril to the imaging window, and a flow sensor (*SensorTechnics FBAM200DU, Puchheim, Germany*) was placed to the contralateral nostril for continuous respiration recording.

11.3. Stimulus protocol

Stimuli were generated from mixtures of physically mixed monomolecular odorants in order to ensure a high probability of finding odour responsive cells in the dorsal OB. Mixtures diluted in mineral oil at the ratio of 1:5. Odour A: ethyl butyrate + 2-hexanone, odour B: isopentyl acetate + eucalyptol. The mixtures were installed into the 4-channel olfactometer (15ml per vial) along with two blank positions (15ml mineral oil). 6 stimulus conditions were used:

1. Odour 1 only: 1s presentation of odour 1 only at 2Hz (50% duty)
2. Odour 2 only: 1s presentation of odour 2 only at 2Hz (50% duty)
3. Correlated-1: 1s correlated presentation of odour 1 / 2 at 1 of 4 frequencies

(2Hz, 12Hz, 20Hz, 40Hz) (50% duty). The first pulse was from the blank positions.

4. Correlated-2: same as correlated-1 but with the first pulse from the odour positions
5. Anti-correlated-1: 1s anti-correlated presentation of odour 1 / 2 at 1 of 4 frequencies (50% duty). The first pulse was from odour 1.
6. Anti-correlated-2: same as anti-correlated-1 but with the first pulse from odour 2.

For all stimuli, odour valve offsets were compensated by opening a corresponding blank position valve to ensure no global flow changes occurred over the course of the stimulus. Stimulus conditions 1 and 2 were repeated 5 times each. Stimuli 3-6 were repeated 12 times each for each of the 4 frequencies used. Stimuli were generated in PulseBoy and randomly interleaved over the course of the experiment.

11.4. Analysis

Initial analysis was performed with custom scripts in Fiji. Regions of interest (ROIs) around cell somata were manually selected and calcium transients (dF/F) were extracted and exported for further analysis in MATLAB. The mean background signal in an imaging experiment was determined as the 3% of lowest fluorescence values in a maximum projection of raw images (8000 frames). Raw signals were defined as an ROIs fluorescence time course with the mean background signal subtracted. f0 was defined as the median value of raw signals 3 seconds before odour stimulation. dF/F was then calculated as (raw signal - f0) / f0). All traces were aligned to the first inhalation after odour onset. Calcium response integrals were calculated in a 5s window from odour onset.

Odour responsive cells were classified as those which produced mean response integrals greater or less than mean + 1SD of pre-stimulus fluorescence during single odour stimulation. Classification of temporal sensitivity was according to a bootstrapping method. Data for each frequency was randomly split into two groups regardless of correlation structure and the difference in mean between the

two groups was calculated over 1000 iterations of the random grouping, to produce a chance-level distribution of group difference (bootstrap distribution). The mean difference between the true correlated vs. anti-correlated data was then calculated. If this mean difference was outside 2 SDs of the bootstrap distribution the cell was classified as temporally sensitive.

To analyse how well odour responses predicted stimulus correlation on a trial-to-trial basis we generated linear discriminant classifiers from the data set and analysed their prediction accuracy. For each classifier, we performed 50% hold-out validation, splitting the data randomly into a training set and test set with equal numbers of samples. We then performed linear discriminant analysis on the training data set to determine the best linear boundary between correlated vs. anti-correlated data. Classifier performance was then validated on the test data set. To determine the effect of number of ROIs used on classifier performance, we iteratively trained multiple classifiers on random subsets of ROIs with increasing numbers of ROIs within each set. For each ROI subset size, 1000 classifiers were trained and the mean +/- SD of their performance accuracy was calculated.

Part III.

Results

12. Aims

12.1. Overview

As outlined in chapter 4, the primary aims of this thesis are:

1. To generate physical evidence that naturally occurring odour plumes exhibit a rich temporal structure, and that temporal correlations in this structure are associated with the degree to which odour sources are mixed (odour objects) or separated - to the extent that they can be used to efficiently perform olfactory scene segmentation.
2. To show that these temporal correlations are perceptible in mice and can be used to inform behaviour, thereby determining whether animals can potentially use temporal correlations to perform odour scene segmentation.
3. To identify the neuronal representation of these temporal features in the circuit of the olfactory bulb and understand how temporal features are encoded.

12.2. Automated behavioural training

To evaluate whether animals are capable of perceiving temporal correlations a large stimulus space must be explored to produce a meaningful result. This is because temporal correlations can exist between odours at e.g. different frequencies and different overall amplitudes. Exploring this stimulus space, as well as implementing proper controls in behavioural experiments, was predicted to be a laborious and time-consuming task with current behavioural training methods and apparatuses. Therefore, in chapter 13 a method for high-throughput

automated training is described, which aims to allow for behavioural training and analysis of multiple mice simultaneously. This method also aims to achieve robust behavioural training without the use of water restriction, and with minimal external stressors placed on the experimental subjects.

12.3. Methods for recording natural odour plume data

A key requirement for realising the experimental aims of this thesis is the capability of recording concentration changes of individual odours simultaneously. This is necessary to determine the temporal correlations in the fluctuations within odour plumes. Current recording methods for (airborne) odour signals are unable to meet this requirement at the temporal bandwidth expected to be informative. We therefore introduce a new method for odour signal recording in section 15.2 that aims to allow for dual recording of two odours simultaneously.

12.4. Methods for reproducing natural odour plume statistics

Another key requirement for realising the experimental aims is the ability to translate recordings performed from natural odour plumes into stimuli that can be reliably reproduced in the lab. At the time of writing, there is no readily available hardware for generation of these kinds of stimuli (though see Szyszka et al., 2012, 2014) and we therefore describe the development and characterisation of an olfactometer to produce temporally structured stimuli in chapter 16.

13. Automated behaviour as a tool for neuroscience

13.1. Overview

Behavioural analysis is a powerful and crucial technique in many neuroscience experiments. However, many commonly used behavioural techniques are laborious, time-consuming and require significant experimenter intervention (Bodyak and Slotnick, 1999, Abraham et al., 2004, Rinberg et al., 2006). These techniques may also have limitations on the number of animals that can be trained simultaneously (Bussey et al., 2008, Stirman et al., 2016, Francis and Kanold, 2017). Furthermore, many behavioural paradigms call for water restriction in order to motivate animals to complete a task. This can both induce stress on the experimental animal, and create an unpredictable motivational state throughout the experiment as the animal becomes progressively less motivated as it gains water rewards (Cai et al., 2006, Bekkevold et al., 2013). The effect of the presence of an experimenter during behavioural experiments must also be considered. Manual handling can induce significant changes in stress levels in mouse subjects (Meaney et al., 1996, Nunez et al., 1996, Balcombe et al., 2004, Meijer et al., 2007), and there is evidence to suggest that the mere presence of an experimenter (as well as even their gender) can induce variable levels of stress in mice (Sorge et al., 2014). We aimed, therefore, to develop a system capable of automatically training multiple mice simultaneously in one of the most ubiquitous behavioural assays: operant conditioning. Some key design goals of the system were that it should run without an experimenter present; that it should not rely on significant water deprivation; and that it should generate large volumes of useful behavioural data from large cohorts of animals.

13.2. AutonoMouse

In AutonoMouse (Figure 13.1), cohorts of up to 25 mice are housed within a common home cage. The home cage contains various forms of environmental enrichment including bedding, chew-blocks, shelters and running wheels. Food is also available *ad libitum.* To gain water, mice housed in the system must enter an upper chamber containing the behavioural staging area. Entrance into this area triggers an infra-red beam detector linked to a door-close mechanism, isolating the animal in the behavioural area and preventing other animals in the system from interfering with the behaving animal. Once in the behavioural staging area the animal is free to trigger the initiation of a behavioural trial. A port at one end of the staging area contains an infra-red beam sensor that, when occluded by the animal, triggers the control software to initiate RFID decoding - via the RFID coil also present in the port. This allows the software to detect which animal has entered the behavioural area. Sequences of behavioural trials and their parameters are defined before the start of the experiment with the control software. These sequences can be made specific for certain animals based on their implanted RFID codes. Animals are free to initiate as many trials as they wish once they have entered the staging area. The trials delivered to the animals are assigned a particular valence (e.g. rewarded / unrewarded) such that successful completion will deliver a small water reward. Therefore, by continuously performing behavioural trials, animals can gain their daily water intake[1]. AutonoMouse can, therefore, house multiple animals simultaneously, provide them with their basic daily living requirements and motivate them to initiate and complete experimenter-defined

[1] In general, trial sequences are generated according to a standard go/no-go discrimination structure (though other trial sequences can be easily implemented). Roughly half the trials in any set of consecutive trials are assigned as rewarded, and half unrewarded and each of these conditions is paired with some discriminable stimulus (the sequence of rewarded and unrewarded is randomised). The aim is to condition animals to respond to the rewarded stimulus by licking a lick sensor (which also provides water rewards) and withholding licking on the unrewarded stimulus (to avoid a timeout punishment: an extra waiting time of a few seconds until the next trial is delivered. In this structure, even if animals cannot discriminate between the two stimuli, they can still obtain as much water as if they could - it will simply take them longer to obtain the same volume (due to the timeouts from licking on unrewarded trials). Note also that the amount of water reward can be manually adjusted for each individual animal by the experimenter, or automatically adjusted according to the daily trials performed by each animal. This can have the effect of adjusting the number of trials performed daily by each animal (see figure 13.5). This can be useful in some experimental manipulations, e.g. in designing an experiment such that all animals perform the same number of trials per day.

sequences of behavioural trials in a high throughput manner and with minimal experimenter presence or intervention.

13.3. Consistency and reliability of training in AutonoMouse

13.3.1. AutonoMouse gives high volumes of behavioural data

Once acclimatised to the system, mice in AutonoMouse will readily perform hundreds of trials per day (Figure 13.2a). We analysed performance for mice performing a series of olfactory discrimination, go/no-go trials. For a total of 29 animals performing over several months, the total number of trials collected was 479,828. This amount of operant conditioning trials within this space of time far exceeds the amount of data that can be collected with manual methods. Mice housed in the system tended to perform the task in stretches of consecutive trials, with half of all performed trials coming from continuous stretches of more than 39 trials (Figure 13.2b). There was a weak but significant correlation between the number of trials performed in a continuous stretch and the performance within that set of trials (Figure 13.2b, inset, Pearson correlation coefficient R = 0.3348, p = 5.5402×10^{-40}). This can be interpreted in a number of ways. One interpretation is that animals that are generally accurate in the behavioural task tend to perform more trials than animals that have not sufficiently learned the task. Another interpretation is that performance tends to increase over continuous stretches of trials, and increases sufficiently that long stretches of trials will inevitably have higher mean performance scores, regardless of the initial behavioural ability of the animal. Animals with higher average performance across all experiments tended to perform more trials per day (Figure 13.2c, Pearson correlation coefficient R = 0.5032, p = 0.0054), but there was no statistically significant relationship between average performance and mean of consecutive trial lengths for each animal (Figure 13.2d, Pearson correlation coefficient R = -0.0787, p = 0.6847). Therefore, the observation that performance is generally higher in longer stretches of consecutive trials (Figure 13.2b, inset) is best interpreted as evidence that performance tends to increase over long consecutive trial stretches - since better performing

animals do not necessarily tend to perform longer stretches of trials than poorly performing animals.

To determine whether the cohort size trained in AutonoMouse had an effect on behaviour, the average trials per day for several separate mouse cohorts was analysed against the size of the cohort (figure 13.4). There was a small but significant negative correlation between group size and average trials per day. This could be taken as evidence that the upper end of cohort size tested (24) was too great to allow animals to effectively gain their daily water intake. For a standard water delivery amount of 15μl, animals in the system would need to perform around 300 trials per day (to achieve standard mouse daily water intake between 3-5ml). This is close to the number of trials performed by animals in the system (figure 13.2a). For continually performing animals in a group of 24 with 9s long trials (standard time amount for AutonoMouse), this would mean that >300 trials could easily be performed by each mouse in the span of a day (300 trials x 24 animals x 9 seconds = 64,8000 seconds = 18 hours). Therefore, the observation that animals in larger cohort sizes tend to perform fewer trials may be a as a result of having to 'queue' for access to the behaviour port. In large cohort sizes, there is a higher probability of an animal trying to enter the behavioural area while it is occupied by another animal. This may result in some fraction of daily trials being abandoned when the behaviour port is blocked by another animal. Also note, however, that the mean daily trials for the group of 24 animals in figure 13.4 is still at a level where they can comfortable gain their required daily water intake (>300). As expected from the fact that a greater amount of time is needed for a group to perform their daily trials for larger cohorts, the distribution of time where animals perform trials is flatter for large cohorts (figure 13.4b). For animals in a cohort of 9, most trials are performed during the dark phase whereas for a cohort of 24, trials are performed roughly equally by the group throughout the day. This suggests that since in large cohorts animals are more likely to find the behaviour port occupied, they compensate by performing trials later. This therefore spreads out the distribution of times that trials are performed at.

13.3.2. Performance accuracy is stable throughout training

AutonoMouse contains an internal day-night cycle system to maintain the circadian rhythm of animals housed inside. Mice are crepuscular animals and behaved as such under the artificial day-night of AutonoMouse with number of trials performed per hour ramping up as the cycle approached the dark phase; and reaching a peak during this phase. Mice in the system tended to follow this pattern regardless of the total number of trials they performed per day, and analysis of fraction of trials performed at all hours of the cycle across animals revealed a typical day-night activity pattern (Figure 13.3a, b) with a significantly greater fraction of trials performed in the night phase (21:00 - 09:00) than the day phase (fraction trials night: 0.6296 +/- 0.0739, fraction trials day: 0.3704 +/- 0.0739, t-test t = 14.8493, p = 1.6167×10^{-43}, df = 694). Crucially, mice in AutonoMouse were not more or less accurate in the behavioural task at different hours of the day, despite the cycle of total activity across the day. Fraction of trials performed correctly per hour was not significantly correlated with the fraction of trials performed in that hour (Figure 13.3v, Pearson correlation coefficient R = -0.0312, p = 0.4117). Furthermore, the average performance accuracy per hour across all animals showed no significant differences between times (Figure 13.3d, 1-way ANOVA, $F_{(23, 671)}$ = 0.29, p = 0.9996).

13.3.3. Mice are motivated but not water restricted

A key feature of AutonoMouse is that mice are motivated to perform behavioural trials - to gain all water intake - but not water restricted as they are free to perform trials whenever they wish. This point was demonstrated by adjusting the amount of water given as a reward per correctly performed trial on different experimental days (figure 13.5a). Increasing the water reward per trial decreased the amount of trials performed per day, even though animals were clearly capable of performing more trials, as evidenced by their performance before the water reward level was increased. This suggests that mice in the system are free to perform the requisite amount of trials required to gain their required daily water intake [2]. Furthermore,

[2] It should be noted that the proportional relationship between water reward and daily trials performed (figure 13.5a) was not preserved for lower amounts of water reward (75% level, 9μl).

the recorded daily weight of the mice was significantly positively correlated with the number of trials performed on the same day (figure 13.5b, Pearson correlation coefficient R = 0.4129, p = 1.05×10^{-31}). This suggests that animals were capable of regulating their own metabolic demands through completion of behavioural trials while housed in the system.

13.3.4. Mice maintain a normal level of weight increase

To demonstrate that mice housed in AutonoMouse have the same health status as animals housed in more standard laboratory conditions, the weights over time of 3 groups of mice housed under different conditions (singly housed, colony housed, AutonoMouse housed) were recorded for several months (figure 13.6). In the days prior to transfer of the AutonoMouse group into the system, all mice gained weight at a comparable rate (1-way ANOVA weights from P22-P30, $F_{(2, 429)}$, p = 0.0816). At P30, mice in the AutonoMouse cohort were rehoused from colony housing to the AutonoMouse system. Body weight for this group dropped significantly below animals in the other 2 groups on the day immediately following the transfer (1-way ANOVA P31, $F_{(2, 45)}$, p = 1.8×10^{-9}), but grew at a comparable rate to the other groups in the following months (1-way ANOVA weight differential P32-P115, $F_{(2, 3981)}$, p = 0.9303). Although mice in AutonoMouse were therefore consistently of lower weight compared to animals housed in more standard caging, their steady weight gain suggests normal development. The disparity in weight likely results from the fact that animals housed in AutonoMouse developed in a larger space with more environmental enrichment (including running wheels) compared to the other groups (Maesako et al., 2012, Slater and Cao, 2015).

13.4. Summary

The design of AutonoMouse solves a number of issues that present with common behavioural training methods in neuroscience. Primarily, AutonoMouse greatly in-

At this level, mice were expected to perform ~133% normalised trials according to the 1/x relationship, but their actual trial volume was closer to the level observed with 100% water reward (12µl). This suggests that a certain amount of water reward is necessary for proper motivation of animals to complete behavioural tasks.

creases the throughput of experimental data that can be achieved by a researcher by allowing for simultaneous training of a cohort of mice continuously over relatively long periods of time. The automated nature of this system also means that training can occur without an experimenter present, which is likely to decrease stress levels in the experimental animals and improve the reliability of behavioural results (see section 13.1). Animals housed in the system are free to gain water rewards at any time, but can only gain these rewards through completing behavioural tasks. This design means that animals in the system are motivated to complete assigned behavioural tasks, but the only water-restriction that occurs is that which is self-imposed. This is in contrast to the normal method of water-restriction in which water is withheld for some set period of time prior to the start of a behavioural experiment. The advantage of the AutonoMouse design is, therefore, that water restriction and motivational state are controlled by the animals themselves. Importantly, this means that the level of water-restriction severity in AutonoMouse will often be less than in manual water-restriction experiments, and there will be fewer physiological abnormalities (e.g. dehydration) underlying the collected data. The self-initiation of trials in AutonoMouse also means that behavioural data is generally only collected when animals are motivated to complete the current behavioural task.

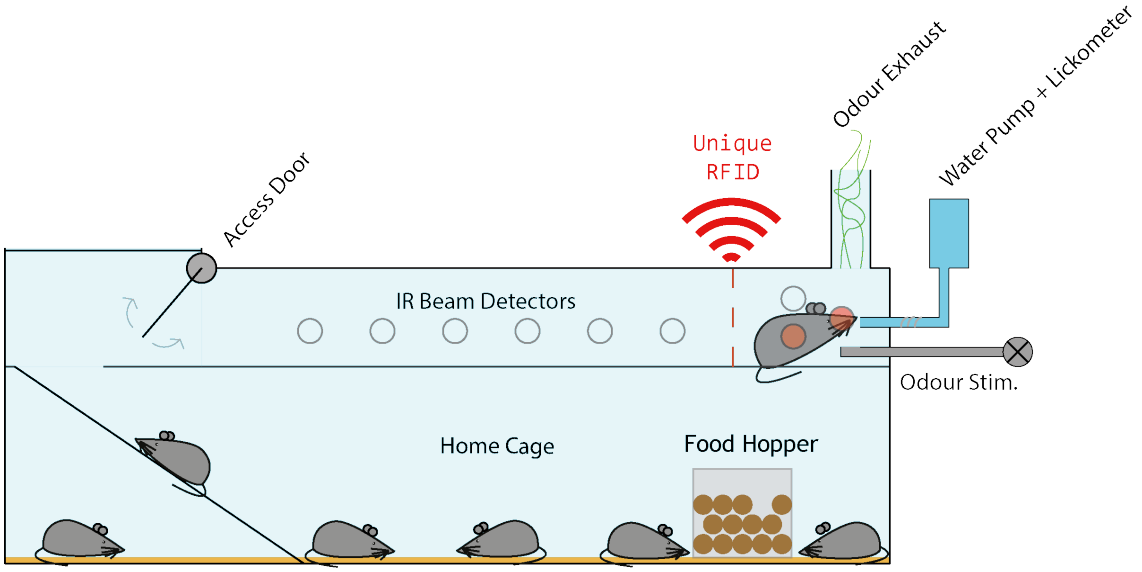

Figure 13.1.: AutonoMouse schematic. Mice are group-housed in a common home cage (lower chamber) where they have access to food, environmental enrichment and social interaction. Each mouse housed in the system undergoes an RFID tag implant surgery prior to the start of the experiment. To gain access to water, mice must use a ramp to enter the upper chamber. As they move through the upper chamber towards the behaviour port (top right area) a series of IR beam detectors are triggered as the animal's body blocks the IR beam path. This triggers closure of an access door behind the animal ensuring that only one animal can enter the behavioural port at a time. A final set of IR beams is linked to initiation of the start of a trial - once these sensors are triggered the RFID coil in the behaviour port registers the RFID of the animal currently in the behaviour port and determines the next trial scheduled for the animal to do. In the schematic shown, the system is setup for olfactory go/no-go discrimination and the behaviour port contains an odour stimulus delivery port (see e.g. figure 14.3) and an exhaust line for removal of odours between trials. Correct performance of a trial releases a small water reward and animals are free to perform as many trials as they wish once they have entered the behaviour port.

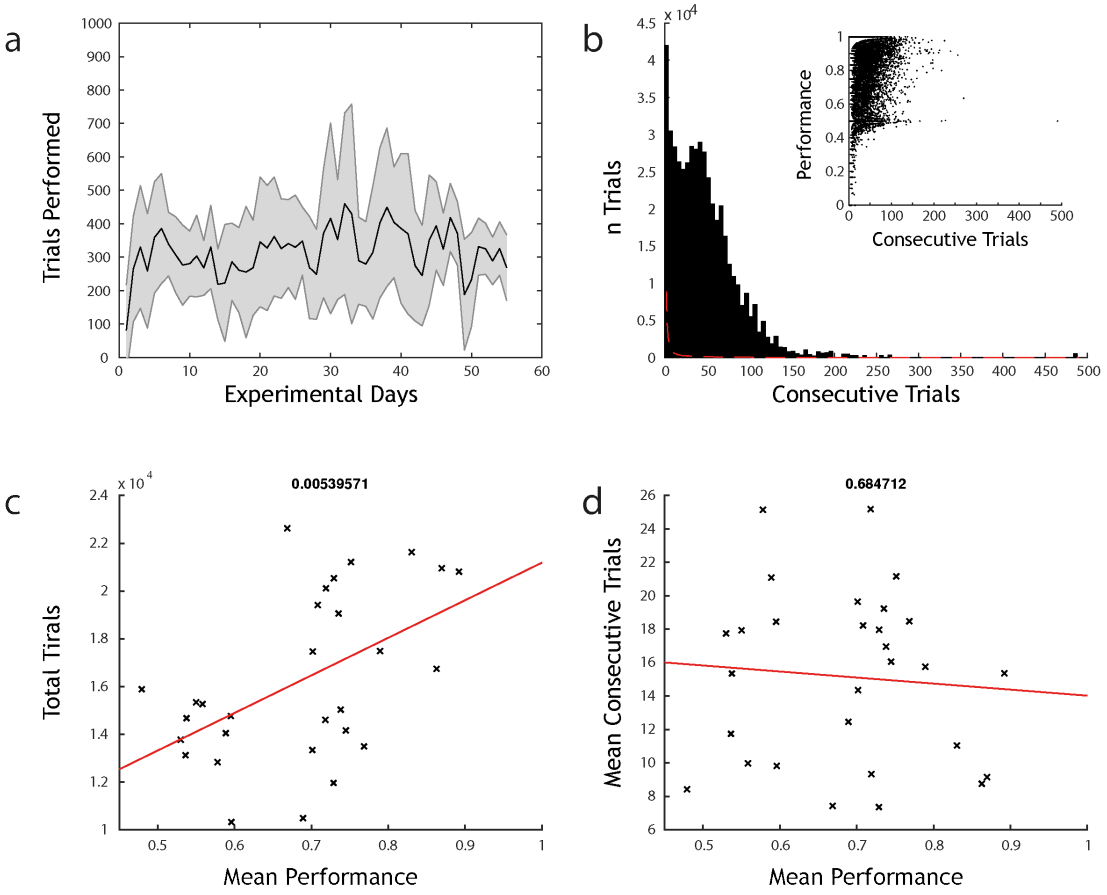

Figure 13.2.: AutonoMouse gives high volumes of reliable behavioural data. a) Number of trials performed per day by animals housed in AutonoMouse (n = 29, mean +/- std, total trials = 479,828). b) Number of trials that are performed in a continuous sequence of trials of a given length (consecutive trials, mean = 48). Consecutive trials are sets of trials performed by the same animal, where each trial precedes the next by <= 20 seconds. Red dashed line: probability of n consecutive trials occurring. Inset: performance in each set of consecutive trials plotted against the number of trials within the set. Performance is positively correlated with the number of trials in the set of consecutive trials.

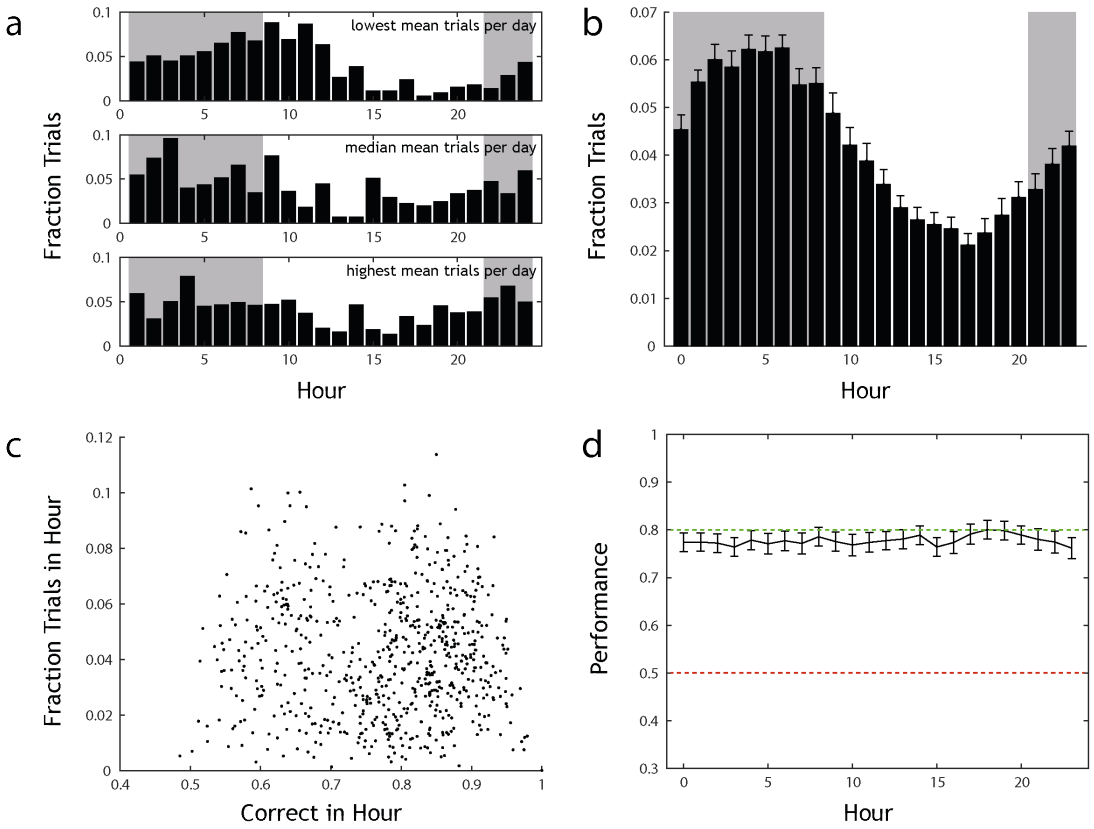

Figure 13.3.: Performance relative to day-night cycle. a) Fraction of trials performed in each hour of the day for the data set presented in figure 13.2. Three representative animals are shown, top: the animal that performed the lowest mean trials per day, middle: the animal that performed the median mean amount of trials per day, bottom: the animal that performed the most mean trials per day. b) Mean fraction trials performed each hour for all animals (mean +/- sem). Animals begin to perform more trials as the dark phase approaches (21.00-09.00) and perform the largest fraction of trials in this phase. c) For each animal, the overall fraction of trials performed in each hour is plotted against the average accuracy in that hour. There is no appreciable correlation between these variables (R = -0.0312, p = 0.4117) suggesting that phase of day/night cycle does not affect performance accuracy in AutonoMouse. d) Average performance accuracy in each hour of the day is plotted, averaged over all animals (mean +/- sem). There is no significant difference between average performance at each hour, supporting the finding in c) that phase of day/night cycle has no systemic effect on performance accuracy in AutonoMouse, and that data from different phases of the cycle can be meaningfully compared and/or grouped.

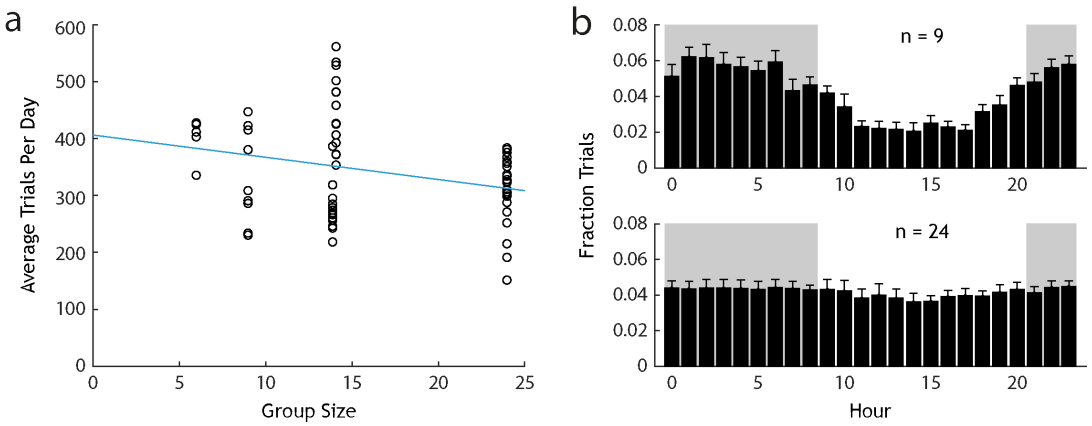

Figure 13.4.: Differences in performance for AutonoMouse cohort sizes. a) Average trials per day for each animal plotted against the group size (number of animals) in which the animal performed. There is a significant negative correlation between group size and daily trials performed for each animal Pearson correlation coefficient R = -0.2884, p = 0.0179. b) Fraction of trials performed each hour analysed as in figure 13.3 for a cohort of n = 9 mice (top) and n = 24 mice (bottom).

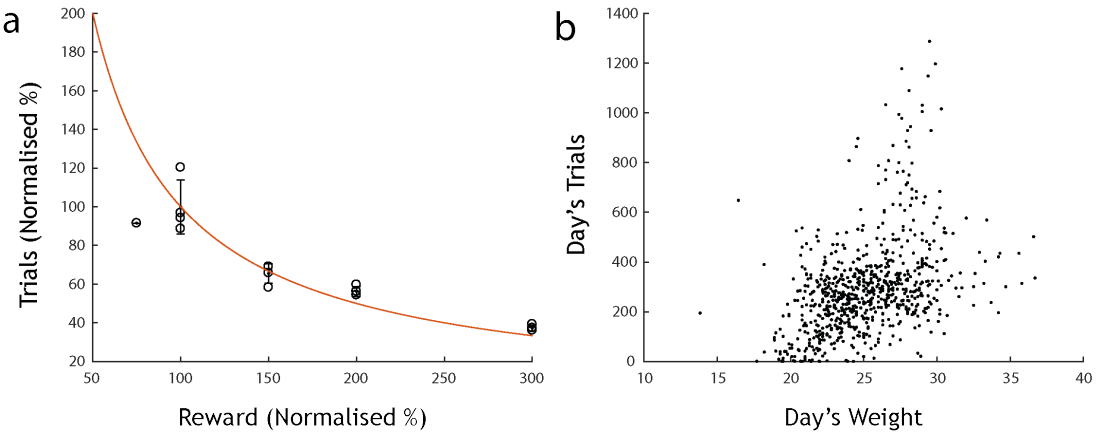

Figure 13.5.: Mice are motivated but not water restricted. a) Normalised number of trials performed is plotted against the amount of reward delivered on each correct trial (n = 4 mice, 100% reward = 12μl). Mice perform fewer trials with larger reward volumes (roughly according to the 1/x line: red line), even though they are capable of performing more trials (as evidenced by n trials performed at 100% reward volume). This suggests they perform as many trials as required to gain their daily water intake. b) For each animal (n = 29), number of trials performed in a day is plotted against the recorded animal weight for that day. There is a strong positive correlation between weight and number of trials performed, suggesting that animals are capable of regulating their own metabolic demands within AutonoMouse.

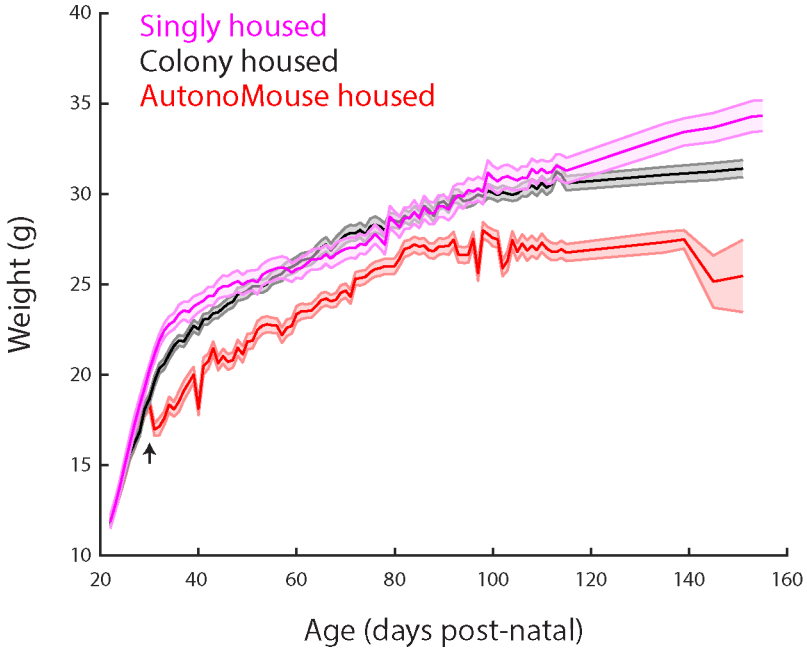

Figure 13.6.: Mice maintain a normal level of weight increase. Mean +/- sem weights over time of 3 seperate mouse cohorts housed under different conditions. Magenta: mice housed alone in single cages (n = 8), not performing behavioural tasks; black: mice housed together in a group cage (n = 20), not performing behavioural tasks; red: mice housed in AutonoMouse (n = 20), performing a standard olfactory discrimination AutonoMouse experiment. AutonoMouse mice are transferred to the system at P31 (black arrow).

14. Investigation of olfactory bulb redundancy with AutonoMouse

14.1. Overview

As introduced in section 13.1, the limitations of standard behavioural training methods can impose a bottleneck on experimental data. This bottleneck can impede systemic analysis of subtle behavioural phenotypes, for example by limiting the extent to which parameter space can be employed. One case of this kind of limitation is in discussion of the function and mechanism of the early mammalian olfactory system where an ongoing discussion on the topic of odour coding and discrimination regards the extent to which the odour identity code is redundant, given the level of overlap in affinity for different odours across OSNs and their associated glomeruli. Results of lesioning experiments (e.g. Lu and Slotnick, 1998, McBride and Slotnick, 2006, Slotnick, 2007) in the mouse olfactory bulb and from knockout mice with OSN axon guidance defects (Knott et al., 2012) have been interpreted as evidence that relatively large disruptions to the olfactory bulb leave a great deal of olfactory function intact (Laurent, 1999, Wilson and Mainen, 2006). By contrast, other studies that challenge the early olfactory system report conflicting results (Johnson and Leon, 2007), for example that major disruptions cause deficiencies in odour recognition and discrimination, whilst minor disruptions largely affect recognition (Bracey et al., 2013). One explanation for these apparently divergent lines of evidence is that the parameter space of both olfactory system disruption and olfactory behaviour are not sufficiently explored. A systematic approach is required to resolve this in which graded disruptions to the olfactory system are performed in conjunction with olfactory tasks of varying complexity.

To address these issues we applied AutonoMouse to perform systematic lesions of the olfactory bulb of varying size and analyse odour discrimination and recognition performance across a wide variety of tasks and odours. An additional aim of this experiment was to validate the use of AutonoMouse as a tool for behavioural experiments, confirming that the quality of behavioural data gathered was comparable to that produced with more standard manual behavioural testing methods.

14.2. Quality of learning during olfactory discrimination

Due to the automated nature of AutonoMouse, it is not required for an experimenter to be present during behavioural experiments to monitor progress. This is certainly an advantage in terms of throughput of experiments and alleviating stress on experimental subjects; but the argument could be made that there may be a detriment to performance accuracy without constant experimenter observation and intervention, e.g. in the case of poorly performing animals. Therefore, we first sought to confirm that speed and accuracy of learning in AutonoMouse in standard operant conditioning tasks was comparable to more standard methods. Similar to conditioning experiments with a more manual component (Abraham et al., 2004), mice rapidly learned to discriminate between two odours in the AutonoMouse system (Figure 14.1). After 7 days of habituation and pre-training, the first odour pair was learned in 1-2 days (Figure 14.1a1, b, performance >80% correct) or 54-398 trials. The second, subsequent odour pair was learned in approximately half the time / number of trials (Figure 14.1a2, b, 20-246 trials). Recognition of the initially learned odour was virtually instantaneous (Figure 14.1a3, b, 20-46 trials). We asked whether there was an appreciable difference in the learning quality of different animals housed in the system, based on the observation that learning rates in the initial stages of various odour tasks were variable across animals. We first analysed the number of trials of learning needed for animals to reach a criterion level of discrimination to determine whether this was a constant feature for individual animals across different olfactory tasks. Over three tasks - initial odour pair learning, novel odour pair learning and a binary mixture discrimination (Figure 14.2a1, b1, c1) – there was no appreciable correlation in

trials to criterion (Pearson correlation coefficient), suggesting that although animals varied in their learning rates, they were not necessarily consistently poor or exemplary in their ability to reach criterion level over all tasks.

For each task we defined a group of 'fast' and 'slow' learners based on their performance within the first 200 trials of the task (Figure 14.2a2, b2, c2), where slow animals were those performing at less than the mean performance in this task period. These groups were defined separately for each task given the above finding that rate of learning was not consistent across tasks. Although performance in the slow group was significantly worse than the fast group in the initial stages of each task, final discrimination performance was comparable between the groups (Figure 14.2a3, b3, c4); and the maximum discrimination accuracy was indistinguishable between fast and slow learners (Figure 14.2a4, b4, c4). This reveals another advantage of AutonoMouse: that the rapid, automated acquisition of trials in the system allows for a greater fraction of experimental animals to reach behavioural criterion, even if they are initially poor performers.

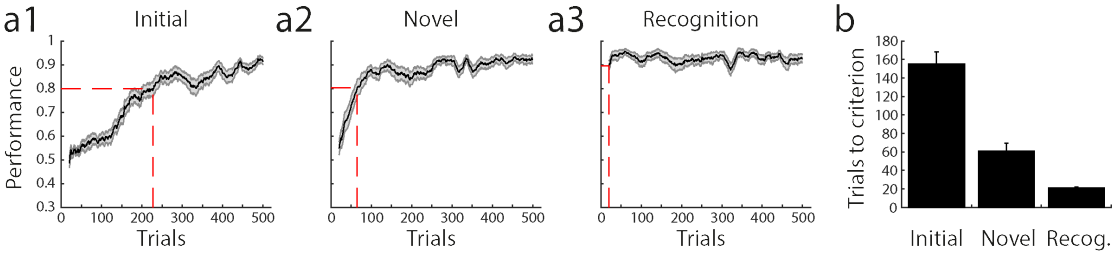

Figure 14.1.: Quality of learning during olfactory discrimination in AutonoMouse. a1) Learning curve for animals performing the initial encountered odour pair discrimination (n = 29, mean +/- sem). Performance is calculated in a 20 trial sliding window. a2) Same as in a1) but for a novel odour pair discrimination (n = 29). a3) Same as in a1) but for a previously learned odour pair (n = 29). b) Analysis of number of trials needed to reach criterion (0.8) over the animals and tasks shown in a1), a2), a3). Bars indicate average trials to criterion, error bars are sem.

14.3. Odour delivery

As AutonoMouse is designed to run continuously for months at a time, for olfactory discrimination experiments it is necessary that it uses a highly stable ol-

factometer with reliable signal output and low levels of contamination. We constructed an airflow dilution olfactometer with multiple separate odourised channels (Figure 14.3a). Odours were released into a central carrier air stream via solenoid valves. Mass flow controllers were used to control the amount of odour released into the carrier stream, allowing for control of the odour intensity of the generated stimuli (Figure 14.4c). A high flow air stream was released into the carrier channel in between stimuli to clean any remaining odour from the olfactometer before the next stimulus presentation. The olfactometer reliably generated square-pulse odour stimuli with rapid rise times (Figure 14.4a, rise from baseline to 90% of maximum in 20 ms). Contamination between odour channels was minimal and only release of odourised channels produced any appreciable odour signal (Figure 14.4b). The air flow dilution method with adjustment of input flow was sufficient to reliably produce desired odour stimuli intensities. Reduction in flow was linearly related to the resulting odour signal amplitude (Figure 14.4c).

A key consideration for any olfactometer is that only the odour stimulus provides salient behavioural information for animals to learn. Extraneous variables such as valve opening noise or changes in pressure/flow must not be informative of the reward condition of the stimulus. We tested whether extraneous variables other than odour identity affected learning in the GNG task by training animals on a subset of the available odour channels, then introducing new odour channels after several hundred trials had been completed. If animals were learning information not associated with the odour (e.g. valve noise) then introduction of new odour channels would significantly reduce their performance accuracy. This was not the case, however, and performance was indistinguishable before and after introduction of new odour channels (Figure 14.5a, b, c; paired t-test pre vs. post performance, initial: $t = 0.4858$, $p = 0.6337$, $df = 16$; novel: $t = 0.3639$, $p = 0.7207$, $df = 16$; familiar: $t = 0.7493$, $p = 0.4645$, $df = 16$), suggesting animals were indeed learning odour stimulus information alone. Furthermore, completely removing odour information by blocking odour release reduced GNG performance to chance levels (Figure 14.5d, t-test final odour diversion performance vs. chance $t = -0.9363$, $p = 0.3801$, $df = 8$), again showing that the odour stimulus was the primary information used to complete the task.

14.4. Excitotoxic lesioning of the olfactory bulb

To induce olfactory bulb lesions (as introduced in section 14.1) we utilised an excitotoxic chemical lesioning method involving injection of NMDA solution into the bulb. After animals had been trained on a series of olfactory tasks to establish baseline performance, varying concentrations of NMDA were injected into the olfactory bulb to produce graded lesion severity in different experimental groups (figure 14.6). A sham group was also generated in which the same volume of PBS solution was injected with no NMDA. To confirm that these injections indeed produced lesioning of the olfactory bulb we perfused experimental animals with an iodinated PFA solution (see Methods section 7.5) and imaged the intact head and skull with CT imaging. This allowed for imaging of olfactory bulb volume changes relative to the skull size of the animal and avoided potential damage to the brain tissue associated with removal for slice histology. Coronal image sections were reconstructed from the CT image stack to inspect OB disruption. In the sham group (figure 14.6, left column) olfactory bulb tissue appeared largely intact (homogeneous colour region within skull boundary) throughout the stack and at the injection site (~1mm posterior to bregma, middle image). For lesion groups (S, M, L, XL, XXL) some degree of bulb tissue reduction was observed, indicated by reduction in size of lighter regions (dark regions correspond to bone / CSF) within the skull boundary.

To quantify the effects of injected NMDA on olfactory bulb damage, the skull and bulb regions of injected animals were manually traced (figure 14.7) in the olfactory bulb region from reconstructed CT slices. Skull volume was included such that it was possible to define intact bulb relative to the size of the animal, allowing for fair comparison between different mice at different ages / weights. There was a strong correlation between injected NMDA and relative OB volume, showing that injection of NMDA did indeed produce graded lesions according to NMDA amount (figure 14.8).

14.5. Extreme lesions induce anosmia

To investigate lesion-induced anosmia we trained 8 mice with extensive OB lesions (2125ng NMDA, XXL in figure 14.6) and 6 control animals (sham, same volume 1% PBS injection) on a battery of odour discrimination tasks. Both cohorts readily acquired various odour discrimination tasks before lesion surgery (figure 14.9, tasks before dotted black line). Sham injected mice reliably recognized previously learned odours (Figure 14.9) and quickly learned odour detection tasks. Lesion group performance was significantly reduced for recognition after NMDA OB lesion surgery and was at no stage distinguishable from chance performance (t-test final task performance level vs. chance level, CN vs. EU: t = -1.2287, p = 0.2589, df = 7; EB vs. AA: t = 0.2513, p = 0.8088, df = 7). This deficit originated from an inability to process odour stimuli, rather than from reduced ability to perform GNG tasks in general, as lesioned animals were still able to perform auditory discrimination tasks at comparable levels to control animals (t-test final performance level sham group vs. lesion group, Audio1 (0.3kHz vs. 3kHz): t = 0.2292, p = 0.8226, df = 12; Audio 2 (5kHz vs. 10kHz): t = 1.2998, p = 0.2181, df = 12) but were incapable of even discriminating odour from clean air (Figure 14.9: S+ detection / S- detection, t-test final performance level vs. chance, S+ detection: t = -0.0968, p = 0.9256, df = 7; S- detection: t = -1.0037, p = 0.3490, df = 7). Thus, near-complete lesioning of both OB hemispheres indeed resulted in anosmia to odour stimuli, completely preventing odour detection, discrimination and recognition.

A range of olfactory tasks and odours were used to probe lesion induced-deficits in performance accuracy. It is presumed that certain tasks (e.g. recognition of a previously learned odour pair) should be less behaviourally demanding than others (e.g. binary mixture discrimination). To determine the gradation of behavioural demands, performance data were pooled across all odours used for all pre-lesion tasks and sham injected animals (Figure 14.10). Sorting this information by task identity (e.g. familiar odour pair, novel odour pair etc.) revealed a grouping of task types according to a performance score defined as performance in the first 100 trials in a 20 trial bin sliding window (Figure 14.10f). As expected, performance for a familiar odour pair was consistently higher than for other tasks while novel odour pairs and non-trigeminal odour pair tasks showed significantly lower perfor-

mance (ANOVA with Tukey-Kramer correction for multiple comparisons, $F_{(4, 114)}$ = 65.13, p = 1.4566x10^{-28}) than for a familiar odour pair. Performance was statistically indistinguishable between novel and NTS tasks. Both tested binary mixture discrimination tasks – standard mixture and non-trigeminal mixture – showed the lowest performance score, significantly lower than both the familiar odour task and the novel/NTS task.

14.6. Varying lesion size results in graded performance across olfactory tasks

We next asked what odour discrimination capability remained in animals with less extensive lesions than those used to produce anosmia. Animals with smaller lesions (303.6-607.2ng NMDA) readily learned to discriminate a novel odour pair (Figure 14.11a1). Both asymptotic performance as well as learning rate were indistinguishable from sham injected animals (Figure 14.11a2, a3). Animals with larger lesions (1214-1669.8ng NMDA) also showed above chance performance (Figure 14.11a1) but attained criterion level performance at a slower rate. Final performance was marginally less than the sham and small lesion groups though statistically indistinguishable (Figure 14.11a3). Although all lesion groups (except anosmic) were capable of performing simple binary discriminations of odours, when groups were presented with an odour pair learned prior to lesion induction (Figure 14.11d), a more subtle phenotype was observed. Performance was generally similar to the novel odour case with the small lesion group reaching comparable accuracy to sham animals and the large lesion group reaching consistent above-chance performance (Figure 14.11d1). In the early stages of the task, however, a clear reduction in performance for the small lesion groups relative to sham was present (Figure 14.11d1, d3). This difference was significant relative to sham animals in the first 10 trials of the task but quickly increased within the first 20 trials of the task. This suggests that, for a relatively small OB lesions, the ability to quickly learn a new odour pair discrimination is largely unaffected but recognition of a previously learned pair is significantly diminished. Mice were also asked to perform an additional simple binary odour discrimination in which the odours were non-trigeminal activating (Figure 14.11b1) (Doty

et al., 1978, Cometto-Muñiz et al., 2005, Chen and Halpern, 2008). As with the other simple discrimination tasks, there was little difference between the lesion groups relative to sham after a sufficient learning period (Figure 14.11b2, b3). However, in contrast to the case of a trigeminal activating odour discrimination (Figure 14.11a) the learning rate in the small lesion group was significantly impaired compared to sham. The largest difference between groups was observed for non-trigeminal mixture discrimination (Figure 14.11c). In this case, both lesion groups performed significantly worse than controls for several hundreds of trials (Figure 14.11c3). In particular, the small lesion group showed a marked reduction in performance compared to sham. Given that for simple non-trigeminal discrimination this group in many periods exceeded sham performance, this suggests that the additional complexity of mixture discrimination poses a significant challenge for even a mildly impaired olfactory bulb.

14.7. Lesion results summary

These results indicate that damaged OB can cope relatively easily with simple odour discrimination tasks and that tasks of this nature are not sufficient to reveal the phenotype change associated with this damage. By looking in more detail at odour pair recognition, and ability in the case of increasing task demands such as mixture discrimination, significant impairments can be observed with even relatively mild OB damage. A novel odour discrimination task was used to determine baseline discrimination ability in the lesion groups (figure 14.11a1-3) as performance in this task did not depend on prior experience with an odour set. In the novel discrimination task all lesion grops were capable of above-chance performance (though for the large lesion group task acquisition was slower) demonstrating that even relatively large lesions do not destroy the ability of the OB to encode separate odorants differently. To then address the redundancy of this odour code, the groups were tested with a familiar odour pair, learned prior to lesion induction (figure 14.11d1-d3). Performance even in the early stages of this task (10 trials) was well above chance for the sham group, as expected given that they had learnt this discrimination previously and did not have damaged olfactory bulb. All other lesion groups performed poorly in the initial stages of the task, and

then regained performance over time. This is consistent with a hypothesis that animals with OB damage are capable of performing simple odour discriminations (as shown by the novel task) but that individual odours are encoded and recalled with a relatively non-redundant OB map since even minor damage to the OB resulted in poor performance in discriminating the familiar odour pair, presumably since the representation of these specific odours was degraded under lesions, changing their perceptual quality and effectively making the task a novel odour pair discrimination from the point of view of lesioned animals.

A further hypothesis is that these simple odour discriminations are possible in lesioned animals since odours can also activate the trigeminus and not just the olfactory bulb. Therefore, even if OB function was completely destroyed by lesions, odours could still be recognised by differential activation of the trigeminal system. Two pieces of evidence here argue against this hypothesis. First: massive lesions of the OB resulted in total anosmia (figure 14.9) showing at least that not all odour pairs can be discriminated by differential trigeminal activation. Second: animals were subjected to an odour discrimination task that used only non-trigeminal odours (figure 14.11b1-3) and performance here was similar to the novel odour task. If it were true that lesioned animals could only perform odour discrimination using trigeminal activation, then no above-chance discrimination performance should have been observed in this task. Mice also underwent a binary mixture discrimination task (figure 14.11c1-3) to determine the effect of greater task complexity on post-lesion performance. Where there was no significant difference between performance levels in the novel odour task, in the discrimination task the large lesion group's performance was significantly impaired, showing that OB damage affects how well animals can perform more demanding olfactory tasks as well as how individual odours are represented in the OB.

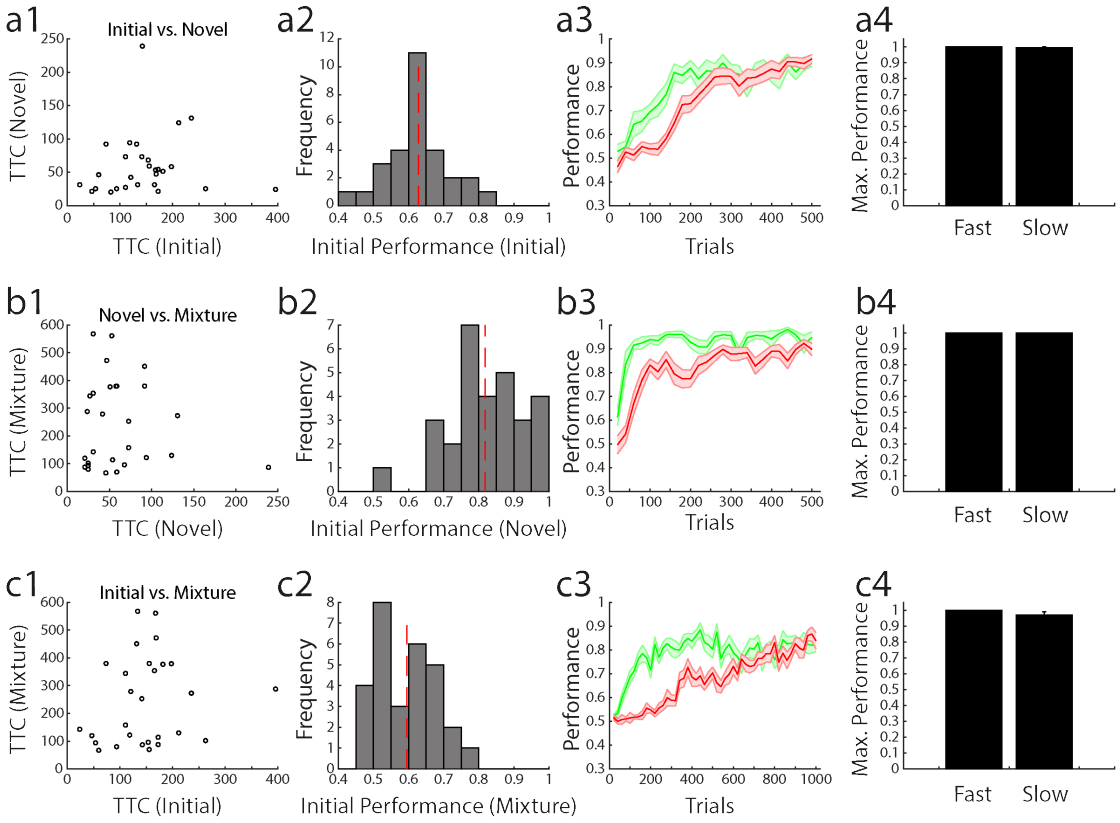

Figure 14.2.: Fast vs. slow learning in AutonoMouse. a1) For each animal, trials needed to reach criterion (TTC) for a novel odour pair is plotted against the trials to criterion on the initial odour pair discrimination. a2) Histogram of performance levels reached by animals in the first 200 trials of the initial odour pair discrimination. Dashed red line indicates mean performance. a3) Learning curves for animals, separated by whether their performance level was greater than the mean performance (fast, green) or lower than the mean performance (slow, red) in the first 200 trials of the initial odour pair discrimination (mean +/- sem). a4) Maximum performance levels reached for animals in the fast and slow groups (mean +/- sem). b1) As in a1) but with trials to criterion in mixture discrimination (n = 29) vs. trials to criterion in novel odour pair discrimination. b2) As in a2) but for novel odour pair discrimination. b3) as in a3) but for novel odour pair discrimination. b4) As in a4) but for novel odour pair discrimination. c1) As in a1) but with trials to criterion in mixture discrimination vs. trials to criterion in initial odour pair discrimination. c2) As in a2) but for mixture discrimination. c3) as in a3) but for mixture discrimination. c4) As in a4) but for mixture discrimination.

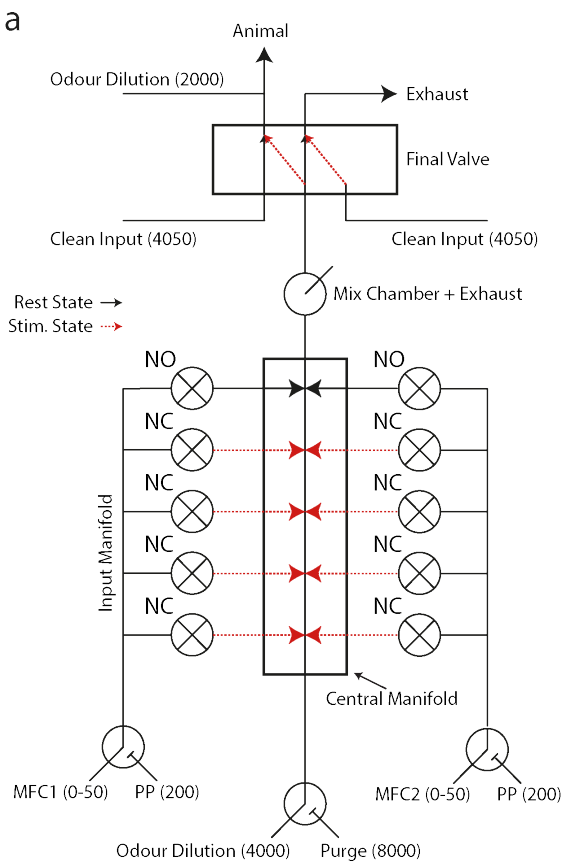

Figure 14.3.: Odour delivery. a) Schematic of the olfactometer used in the lesion phenotype experiment. Numerical values shown indicate supplied air flow in cubic centimetres per minute. Black / red lines indicate resting state (between trials) and odour delivery state air pathways respectively. A central manifold is supplied with air from two lines, the active line can be chosen with a 3-way solenoid. Two input manifolds are used to supply odourised air to the central manifold to be carried to the output. The input manifolds consist of two normally open 2-way solenoids (NO) which maintain non-odourised airflow in between odour stimulus generation. When odour is delivered, a subset of normally closed (NC) 2-way solenoids are opened to provide desired odour input; while the NO valves are inactivated. The input manifolds are supplied with two air lines, a 'pre-pulse' flow line (PP) and a variable mass-flow controlled line (MFC). During stimulus presentation, the PP line is utilised first to build up pressure in the input manifolds, followed by the MFC line adjusted to control desired air-dilution and resulting concentration. The output of the central manifold outputs to a glass mixing chamber, which allows the output odourised air to homogenise briefly, before being released by the final valve: a 5-way solenoid. The final valve switches between a constant output clean air stream with the manifold output sent to exhaust when no odour stimulus is being presented, and the output of the central manifold during odour presentation.

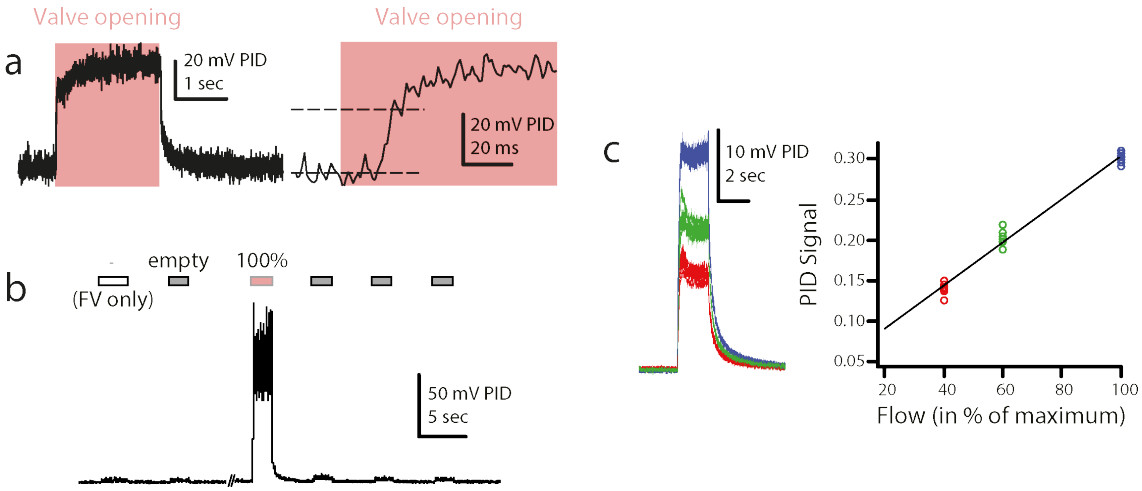

Figure 14.4.: Odour delivery characterisation. a) Example PID recorded odour trace from the olfactometer schematised in figure 14.3. Left: entire recorded pulse, right: at higher temporal resolution to show fast rise time of odour signal. b) Example recording from the olfactometer switching between final valve only (FV only), empty (non-odourised) input and odourised input (100%, red). Odour signal is negligible during empty valve and final valve activation, suggesting minimal contamination between input lines. c) Output odour concentration can be reliably controlled by airflow dilution. Left: 10 example odour pulses during maximum MFC input (blue), 60% MFC input (green) and 40% MFC input (red). right: summary of PID recorded odour signal in the three conditions. PID signal is linearly related to the amount of MFC flow in the input line.

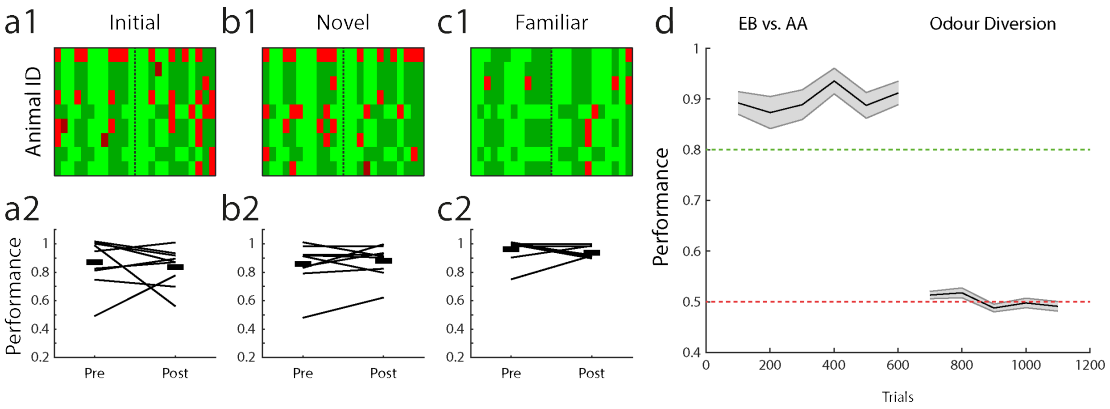

Figure 14.5.: Olfactometer controls. a1) Map of trial performance before and after introduction of an extra valve set into the odour stimulus production, during the first odour pair discrimination learnt by this set of animals (n = 9). Each row corresponds to an animal, with each column in the row corresponding to a trial (pre-switch n = 12, post-switch n=12). The vertical dashed line indicates the point at which new valves were introduced. Light green: hit, dark green: correct rejection, light red: false alarm, dark red: miss. a2) Summary of data shown in a1 showing mean performance before and after for each animal in the group (connecting black line, start and end values jittered for ease of visualisation). Thick black lines indicate mean of the group pre- and post- new valve introduction. b1), b2), c1), c2) Same analysis as in a1, a2 but for novel and familiar odour pair discrimination respectively. d) Performance across the same group of animals in a standard odour pair discrimination (EB vs. AA) followed by diversion of the odour stream in the olfactometer final valve (mean +/- sem). Performance analysed in 100 trial bins for each animal.

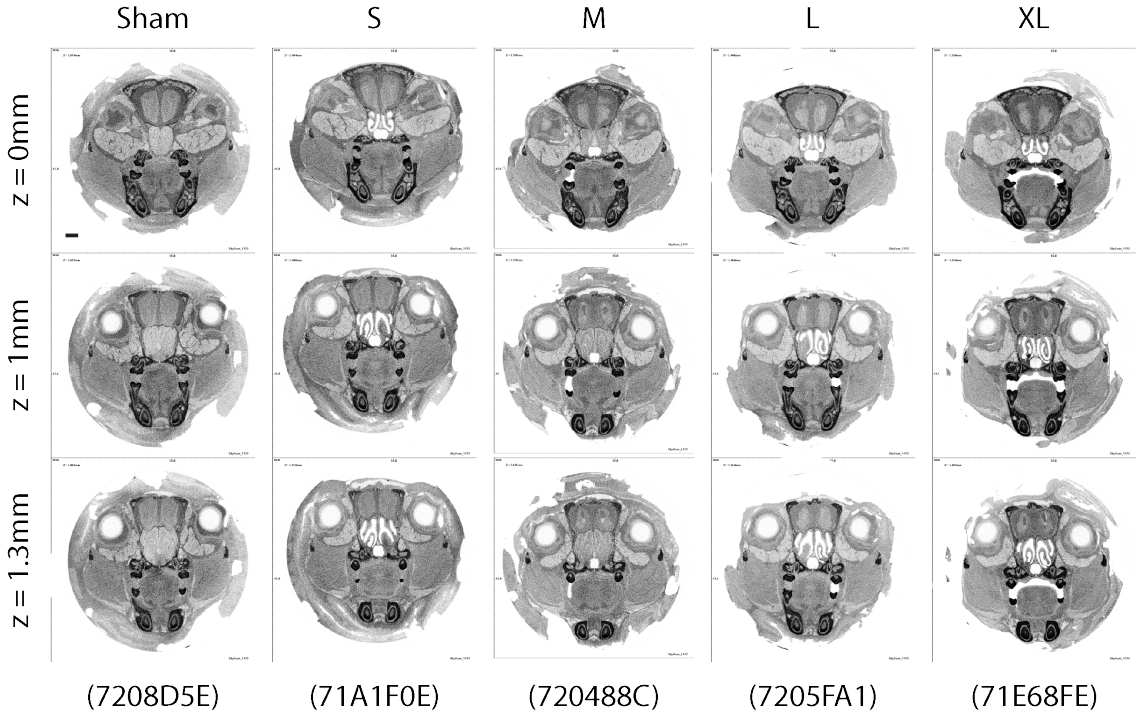

Figure 14.6.: Excitotoxic olfactory bulb lesions. CT images from mice injected with varying amounts of NMDA into the olfactory bulb (Sham: 0ng, S: 303.6ng, M: 607.2ng L: 1214ng, XL: 1669.8ng). Images are reconstructed coronal sections from a whole mouse head, starting at 0mm from bregma, to 1-1.3mm anterior from bregma (roughly the olfactory bulb injection site). Images are inverted such that darker regions correspond to more x-ray absorbent areas (e.g. skull, teeth, soft tissue absent areas where contrast agent has pooled). Bottom row: codes in brackets indicate RFID of animal used as representative example of group. Scale bar: 1mm.

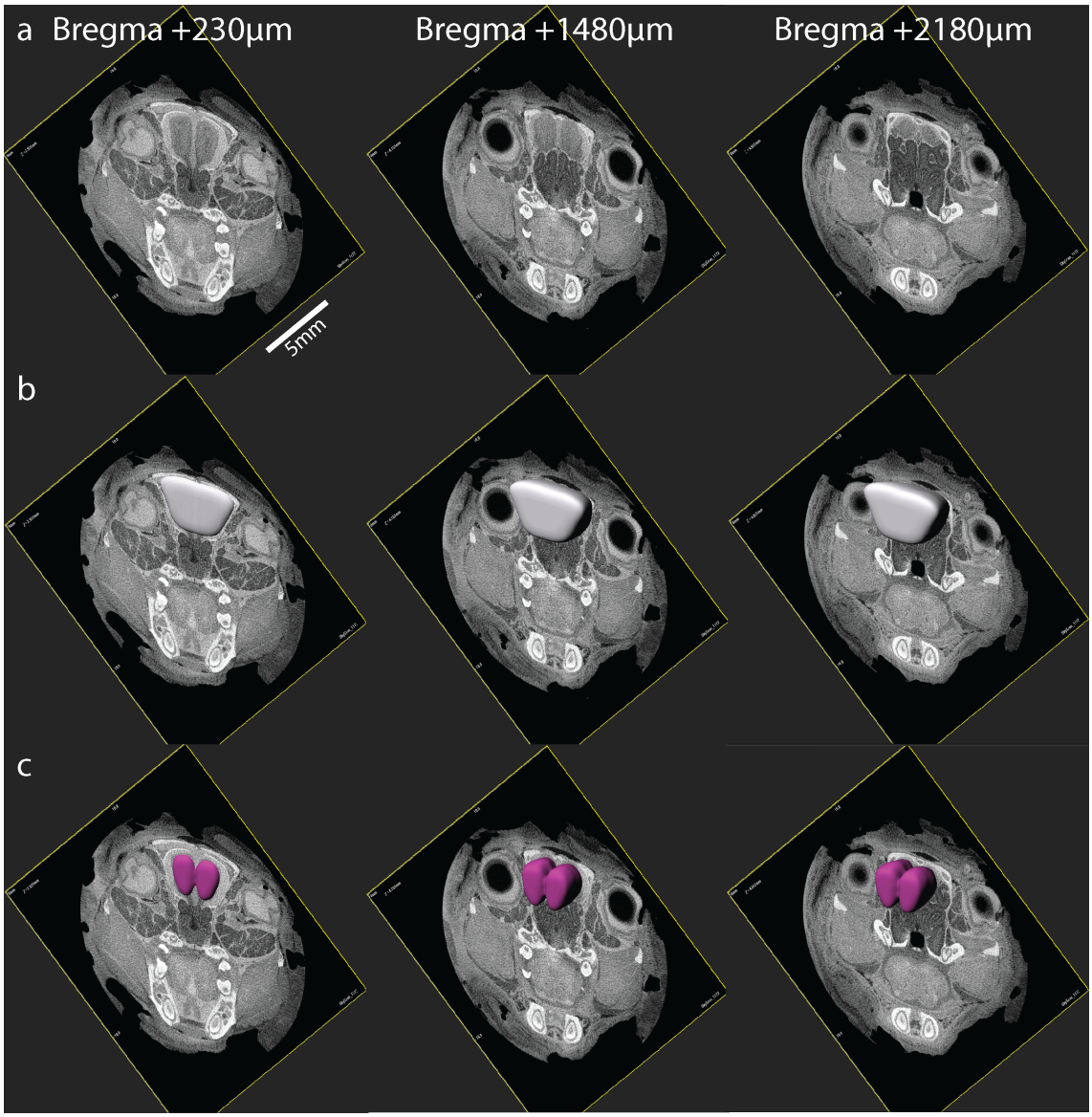

Figure 14.7.: Lesion quantification procedure. Example of the procedure used to characterise intact bulb volumes from CT images relative to skull volume. a) Row of images shows example reconstructed coronal CT slices in rostral to caudal direction (left to right) in the olfactory bulb region caudal to bregma. b) Same example images as in a) after skull volume has been manually defined by tracing outline in the stack of slices. Grey volume shows reconstructed skull volume around the bulb. c) Same images as in a) after bulbar volume has been defined manually. Pink volume is reconstructed bulbar volume.

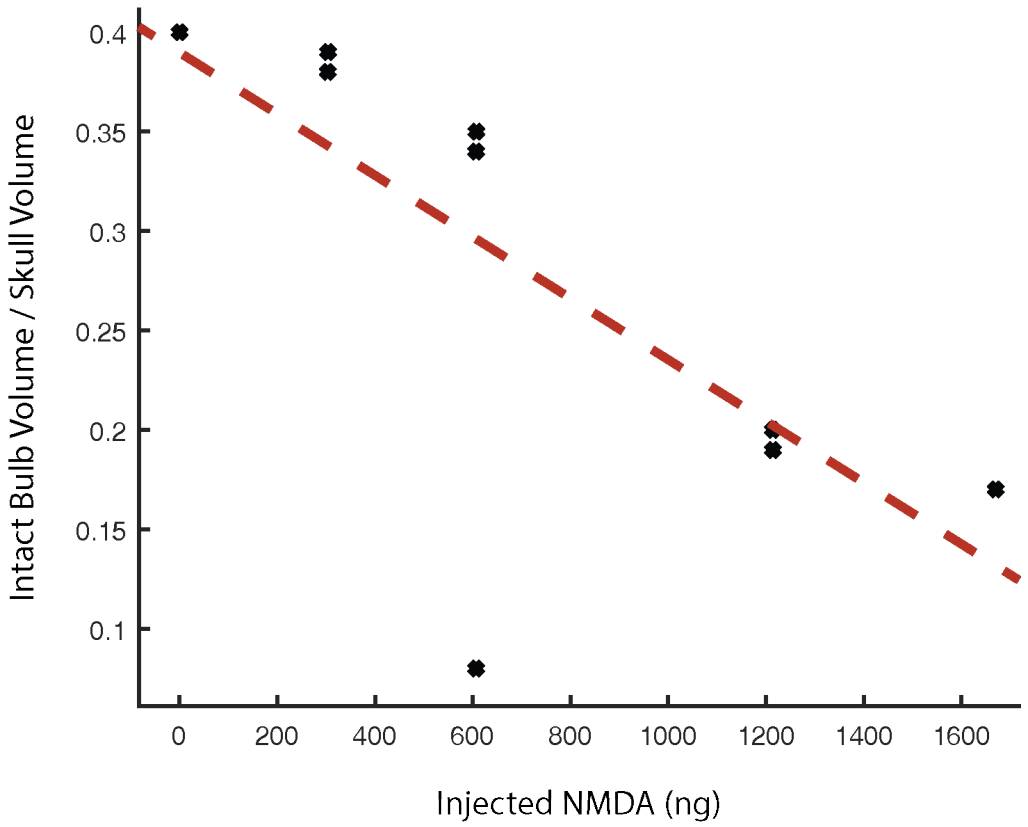

Figure 14.8.: Lesion quantification. After manually defining intact bulb volume and skull volume, bulb volume relative to skull volume is plotted against injected NMDA for 9 CT imaged mice. There is a significant negative correlation between relative bulbar volume and injected NMDA (Pearson correlation coefficient R = -0.7005, p = 0.0356), showing that larger volumes of injected NMDA have a graded, progressive effect on olfactory bulb damage.

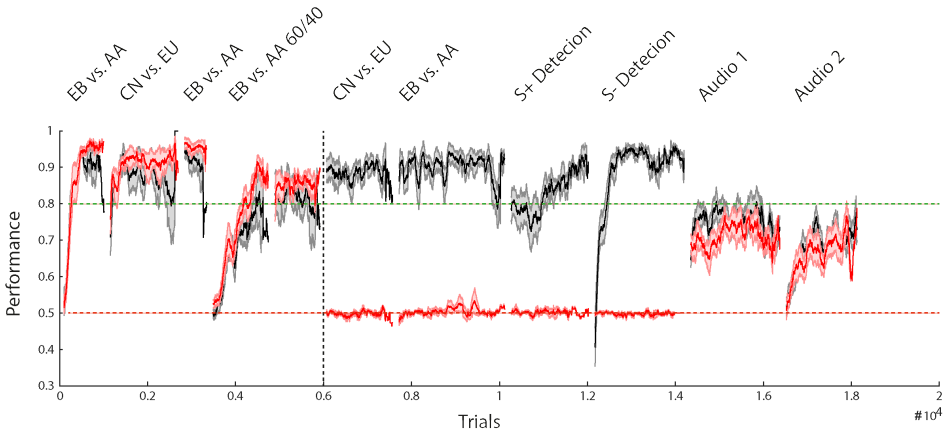

Figure 14.9.: Anosmia induced by extreme lesions. Performance (mean +/- sem) over several olfactory tasks for control animals (black, n = 6) and lesion animals (red, n = 8). Performance is calculated in a 100 trial sliding window. Performance is comparable between the two groups prior to lesion/sham injection (dotted vertical black line). After this point, lesion group performance is not significantly greater than chance for all olfactory tasks. Performance is comparable during auditory discrimination tasks, suggesting the lesion deficit is olfactory specific. EB vs. AA: ethyl butyrate vs. isopentyl acetate, CN vs. EU: eucalyptol vs. eugenol, EB vs. AA 60/40: mixture discrimination of 60:40 ratio ethyl butyrate:amyl acetate vs. 40:60 ratio. S+ detection: ethyl butyrate (S+) vs. clean air (S-). S- detection: clean air (S+) vs. ethyl butyrate (S-). Audio 1: 0.3 vs. 3kHz tone. Audio 2: 5 vs. 10kHz tone.

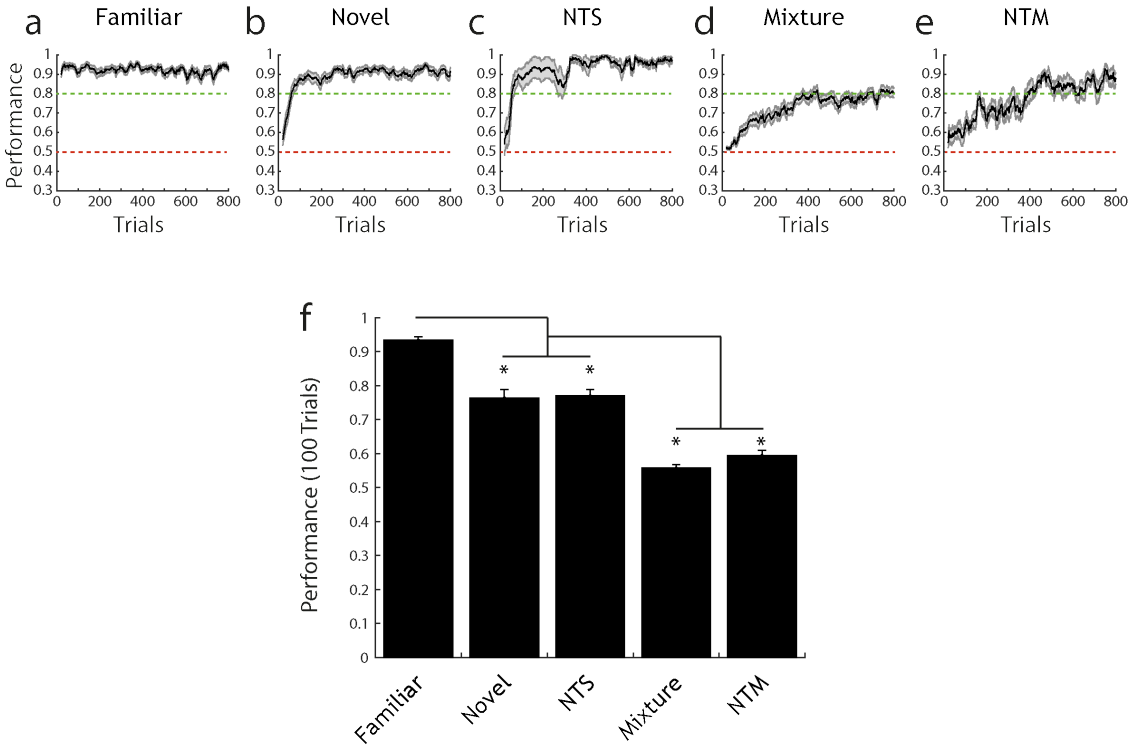

Figure 14.10.: Progressive task difficulty. Pre- lesion/sham performance for both groups tested in figure 14.9 analysed according to task identity. All performance is shown calculated over a 20 trial sliding window (mean +/- sem). a) Performance in a familiar task where animals are performing discrimination on a previously learnt odour pair (n = 38). b) Performance on a novel task in which the odour pair has not been previously encountered (n = 32). c) Performance on a non-trigeminal simple task, in which the odour pair has not been encountered and both odours are non-trigeminally activating (n = 9). d) Performance on a mixture task in which animals are asked to discriminate between simultaneously presented odours in the ratio 60:40 vs. 40:60 (n = 31). e) Performance on a non-trigeminal mixture task, same as in d) but both odours are non-trigeminally activating (n = 9). f) Performance in the first 100 trials (calculated over 20 trial sliding window) on each task type. Novel and NTS tasks showed significantly lower performance than the familiar task, mixture and NTM task showed significantly lower performance compared to novel, NTS and familiar.

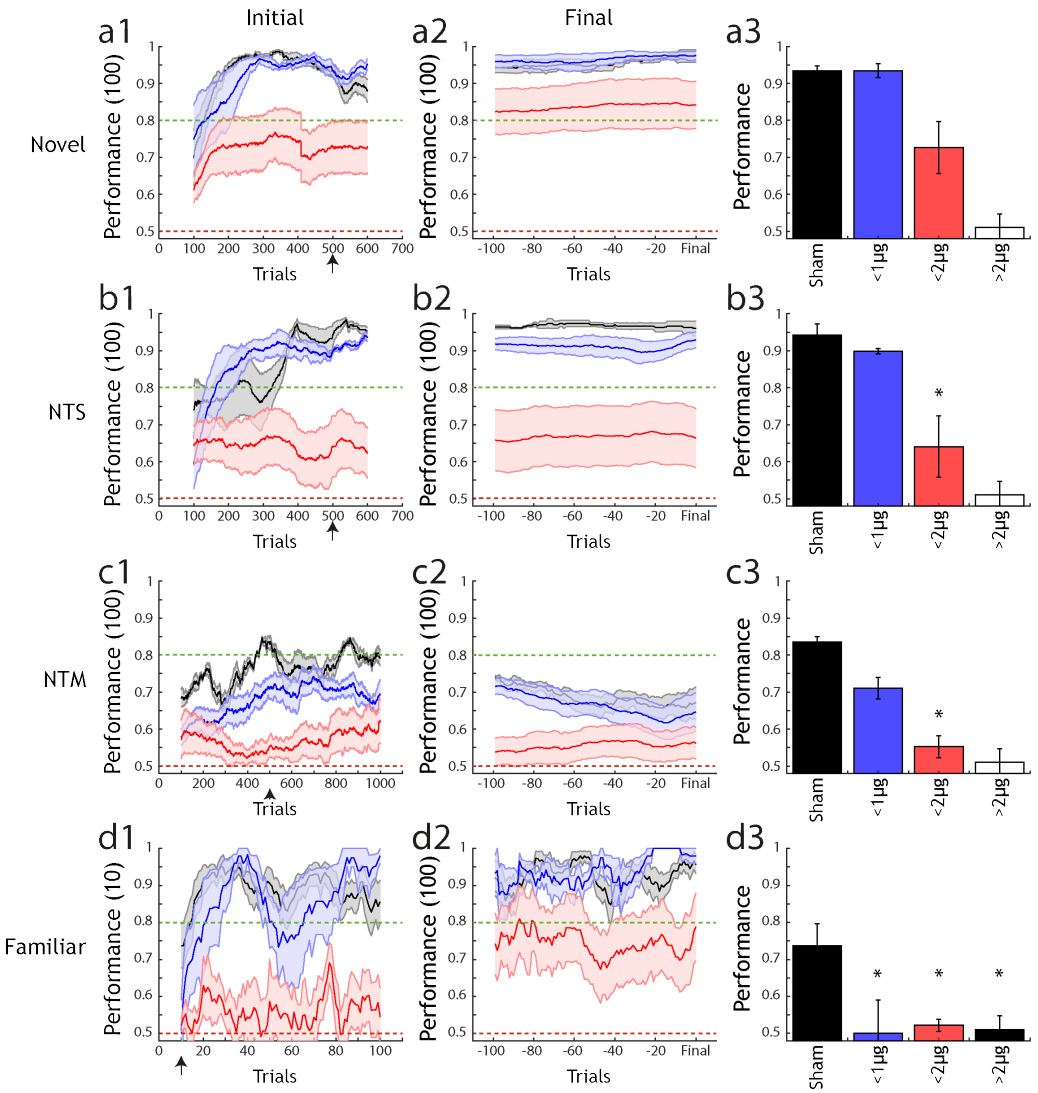

Figure 14.11.: Varying lesion size. Analysis of performance across lesion groups and type of olfactory task. a1) Performance of 3 lesion size groups (sham: black, <1000ng NMDA: blue, <2000ng NMDA: red) in a novel odour discrimination task (mean +/- sem). Performance is calculated in a sliding bin of 100 trials. a2) Final performance in the same groups as a1), performance is calculated for each animal with a sliding window of 100 trials from 100 trials before (x-axis: -100) up to the final trial performed (x-axis: Final). a3) Average performance (mean +/- sem) for each group after the number of trials indicated by the black arrow on the x-axis in a1). Final unfilled bar indicates performance for the anosmic group on data gathered for the familiar odour task d3). As this group does not perform above chance for any odour task it is assumed the group performance will be close to 0.5 for all tasks. * indicates significantly different performance compared to sham within same task under 1-way ANOVA with Tukey-Kramer correction for multiple comparisons (adjusted significance level of $p < 0.05$). b1)-3), c1)-3) and d1)-3) are as in a1)-3) but for a non-trigeminal simple task, non-trigeminal mixture task and familiar task respectively. In d1)-3) performance is calculated in a 10 trial sliding window as the crucial metric for a familiar task is performance in the first few trials, where animals must rely on recognition of the previously learned pair rather than learning ($F_{(3, 24)}= 4.96$, $p = 0.0081$).

15. Physical features of temporal dynamics in olfaction

15.1. Overview

The studies presented in chapter 3 propose that olfactory scenes contain a rich temporal structure due to the transmission of odours by turbulent air movement. In particular, it is suggested that temporal concentration dynamics found in naturally occurring odour plumes can be used to infer information about the odour source origin. In theory, the proximity of individual odour component sources to each other can be inferred from temporal correlations in their individual concentration fluctuations over time within a mixed plume. We aimed to prove that both of these signal features are present in naturally occurring odour plumes with direct physical measurements of odour concentration fluctuations.

15.2. Dual energy photo-ionisation detection

Temporal correlations between odours detected in a plume can, in theory, be used to determine whether these odours originate from the same source, or from different positions in space (see chapter 3). In other words, temporal correlations in odour concentration could be used to determine which odours in a plume belong to particular perceptual objects in the environment. To examine whether this is truly the case in natural odour scenes, we would need to be able to measure concentration changes in two odours independently and simultaneously with high temporal bandwidth. The best candidate for this kind of measurement is the

photo-ionisation detection approach due to its high temporal bandwidth. Unfortunately, photo-ionisation detection cannot resolve the individual odour components that make up its detected output. This is because the detector has no means of discriminating between the volatile chemicals that it draws over its UV bulb and sensor, the output is simply a measure of the current change induced by all ionised molecules.

To overcome this issue and be able to record the odour signals from multiple odours independently and simultaneously we developed a method termed dual energy photo-ionisation detection. With this method we take advantage of a limitation of photo-ionisation detectors; namely that the UV lamps used to ionise the odour molecules drawn over their sensors will only produce an appreciable output signal when the ionisation energy of the odour molecule is lower than the eV of the UV lamp. By using separate PIDs installed with UV lamps of different lamp energies and using these sensors to record from a common point in space, we can begin to dissect out the odour components likely to have contributed to the overall signal recorded by all sensors. Consider the example given in figure 15.1: two detectors are used with different UV bulb energies, a high energy detector with a 10.6 eV UV bulb and a low energy detector with a 8.4 eV UV bulb. Two odours are then chosen for the recording based on their ionisation energies, such that one odour is detectable by both sensors (has ionisation energy lower than the low energy detector's UV bulb eV) and the other is detectable by only the high energy detector (has ionisation energy greater than low energy UV bulb eV but less than high energy bulb eV) (Figure 15.1a). When recording signals simultaneously from the two odours with this configuration, the output of the low energy detector will reflect signals from the low energy odour only. The output of the high energy detector will be the summed signal from both odours. Therefore, the individual odour signals can be resolved by subtraction. The low energy odour signal is the output of the low energy detector and the high energy odour is the output of the low energy detector subtracted from the output of the high energy detector.

The difference in bulb energies between the two detectors means that the same signal recorded with both detectors will have different amplitudes in the sensor outputs (Figure 15.2a3). Therefore, before individual odour signals can be extracted from a dual-energy recording, a calibration step is needed to determine the mapping of one sensor onto the other. This is achieved by recording simul-

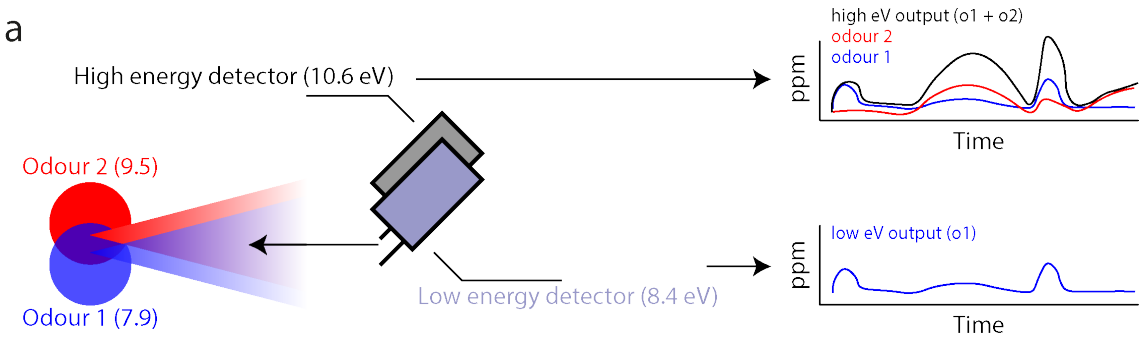

Figure 15.1.: Dual-energy photo-ionisation detection. a) Schematic of the dual-energy photoionisation method. Two odours are recorded simultaneously by two PIDs with different bulb eVs. The odours are chosen such that one odour (odour 2, 9.5 eV) has an ionisation energy greater than the low energy PID bulb, but less than the high energy PID bulb. The other odour (odour 1, 7.9 eV) is chosen such that its ionisation energy is lower than both PID bulbs. The result is that the low energy PID can only record from odour 1 (right bottom trace), whereas the high energy PID records the sum of both odours (right top trace, black).

taneously from only the low energy odour. A linear transformation can then be calculated that maps the low energy signal onto the high energy signal (Figure 15.2a3, inset). This means that the amplitudes of both signals are in a range where subtraction produces a meaningful result.

The result of the decomposition process is exemplified in figure 15.2. Where only the low energy odour was recorded (odour 1), the decomposition process results in significant periods of activity for odour 1 (15.2b3). Odour 2 activity is relatively flat, suggesting the process correctly determined that odour 2 was not present in the original raw signal. Where both odours were recorded simultaneously (either physically mixed together or separated in space), the decomposition process reveals simultaneously occurring bouts of increased concentration for both odours in the mixture case (Figure 15.2b1); and periods where only one of the odours was detected - absent the other - when the odour sources were separated (Figure 15.2b2).

15.3. Temporal correlation structure predicts odour source spatial separation

A primary prediction of the studies presented in section 3.2.2 is that odour sources close together in space will produce odour plumes with high levels of temporal correlation in their concentration fluctuations. As odour sources are separated this correlation should decrease and, therefore, detection of temporal correlations is a potential mechanism by which odour objects can be identified in the environment. To investigate this experimentally we constructed an experimental apparatus in which wind direction, speed and turbulence generation could be controlled; and in which the release of odour into the air stream could be automated (see Methods chapter 9). Using the method outlined in section 15.2 we recorded the evolution of odour signals from two odour sources in the apparatus, either mixed together or separated.

Visual inspection of the odour signals revealed that concentration fluctuations in the odour plumes tended to be correlated when their sources were mixed (figure 15.3a, mixed sources). When the odour sources were separated, this correlation was degraded (figure 15.3a, separated sources). This phenomenon was observed over multiple recordings, and correlation coefficient between the odour signals was overall significantly higher for the mixed source condition than the separate sources condition (Figure 15.3b). The low energy odour only condition was included as a control to determine what fraction of the calculated correlation could be accounted for simply by errors in the signal decomposition method in the subtraction step. The correlation coefficient in this case was significantly lower than for mixed sources, suggesting the high correlation coefficient observed here was not due to errors in the method used to extract the individual odour signals.

Although certain factors in this experimental setup were controlled (e.g. air direction and speed), the odour signals were still generated by air movement and governed by turbulence. Therefore, the amount of odour detected on each trial was random and not under experimental control. It can be assumed that there will be some relationship between the calculated correlation in a recording and the total amount of odour detected (in the extreme case, if no odour is detected in either channel then correlation coefficient will be close to zero, as the only detected

fluctuation will be noise). We therefore asked to what degree the correlation coefficient results depended on the amount of odour recorded from trial-to-trial (Figure 15.3c) and, importantly, whether significantly different amounts of odour were recorded between the 3 experimental conditions and could account for the overall differences in correlation (Figure 15.3d). In the case of mixed sources, correlation on each trial was significantly related to the amount of each odour recorded (odour integral) (Figure 15.3c, left column). In the separated case, a negative correlation between odour integral and signal correlation was observed for the low energy odour (Figure 15.3c, top middle). Although there was a positive correlation between signal correlation and odour integral in the mixture case, this could not account for the higher signal correlation observed in the mixture condition, as odour integral was significantly higher for the separated odour condition. Some degree of non-zero correlation was observed in the low energy odour only recordings (Figure 15.3b, c), likely due to the subtraction step in the odour extraction method[1]. This observation, however, could not account for the differences between signal correlation in the mixed / separated sources conditions as signal correlation was generally much larger than the maximum correlation observed in the low energy odour condition; and the variance in the separated sources condition was lower than in the low energy condition, with the mean centered around 0. Analysis of odour integrals for the low energy odour condition showed that estimated high energy odour levels were not significantly different from 0, which suggests that the odour extraction process accurately captured the dynamics of both odours (Figure 15.3d).

In summary, the dual energy photo-ionisation method provided a means by which

[1]The relationship between the low energy and low energy odour signals in the dual energy method is not completely linear (see e.g. figure 15.1b3, inset). non linearities likely arise from differences in rise times and decay constants in the detection of different odours, as well as differences in signal recording arising from the use of two different bulb energies. Therefore, although the process of linearly scaling and subtracting the low energy signal is largely appropriate for decomposing individual odour signals, there exists the possibility of producing a small subtraction error. A subtraction error occurs where the linear relationship between the two signals does not exactly describe the mapping from one to the other in a particular time window and the low energy signal is either scaled too high or too low. The result of this is that during the subtraction step the high energy signal may be reduced by too great an amount (resulting in negative signal values that are correlated with the low energy signal) or too little an amount (not completely removing the contribution of the low energy signal to the high energy signal resulting in residual correlation not related to the fluctuations of the individual odour signals).

to record from two odours individually and simultaneously while they travelled in turbulence generated plumes. Analysis of the concentration fluctuations between the two odours revealed that source separation can be extremely accurately predicted based on temporal correlations in the odour signals.

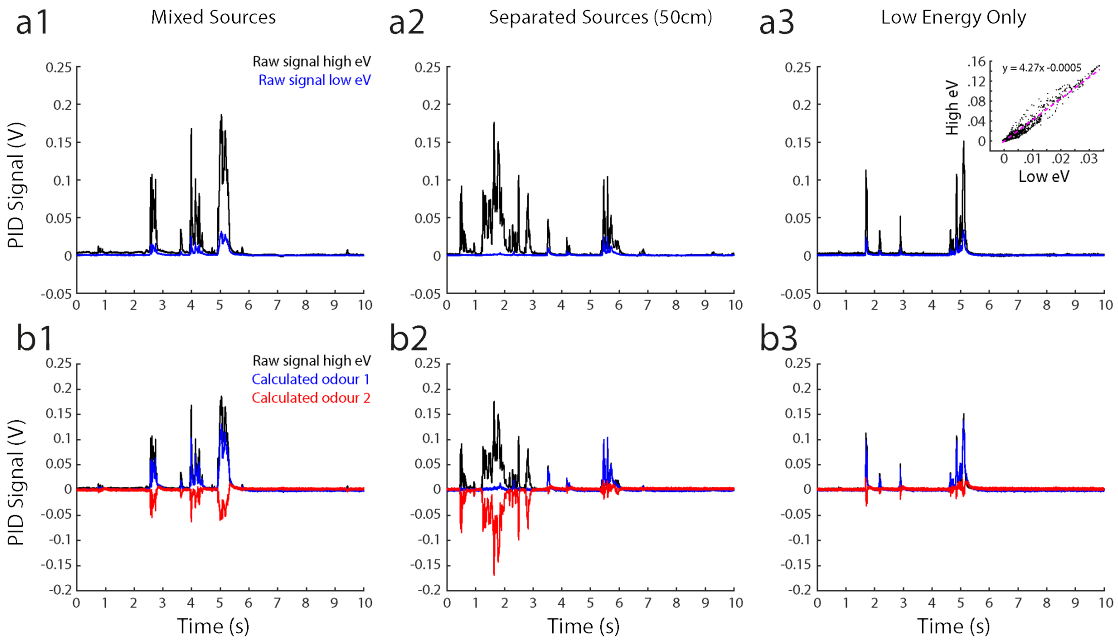

Figure 15.2.: Dual-energy photo-ionisation detection example. a1) Example simultaneous recording with the method shown in figure 15.1 with a physical mixture of odours ethyl butyrate (high energy) and α-terpinene (low energy), blue trace shows output of low energy PID, black trace from high energy PID. a2) same as a1) but recorded from the same odours physically separated by 50cm. a3) same recording method but recording from low energy odour only. Inset: scatter plot of low energy signal vs. high energy signal for all time points (down sampled by a factor of 10). Magenta dotted line and equation indicates linear fit for this recording. b1) Same recording as a1) with decomposition process applied. Black line: original high energy recording, blue line: original low energy recording scaled according to a3) linear fit (estimated true odour 1 values), red line: estimated true odour 2 values (high energy - scaled low energy). b2) Same process but applied to recording from separate sources in a2). b3) Same process but applied to low energy odour only recording in a3).

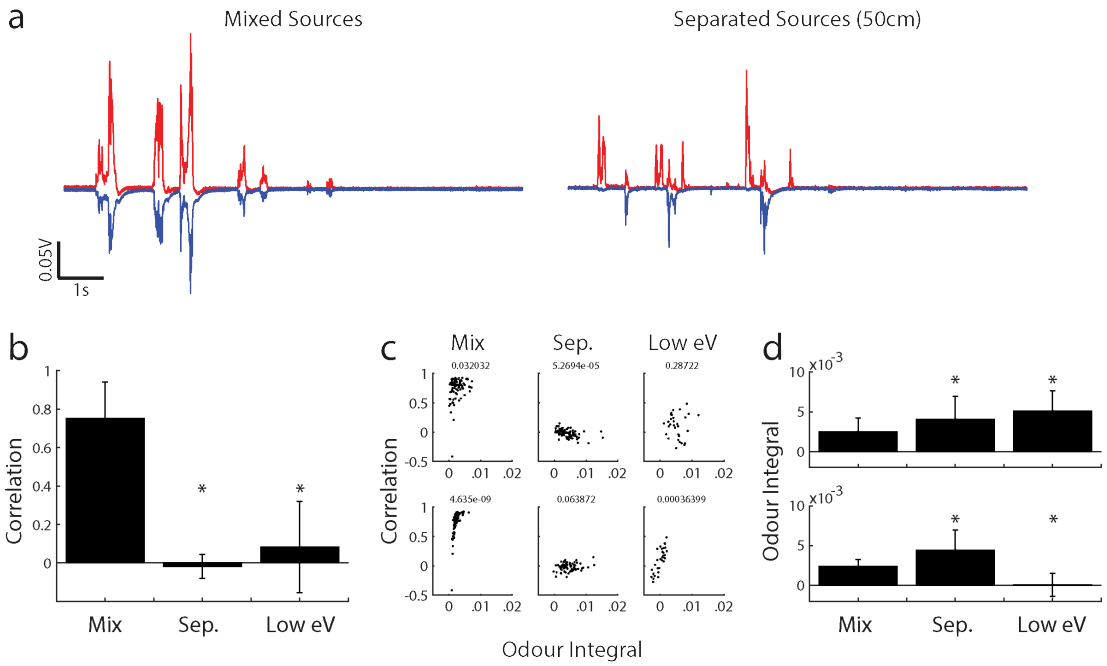

Figure 15.3.: Temporal correlation structure predicts odour source spatial separation. a) Example traces recorded from two odours: ethyl butyrate (high energy, red), α-terpinene (low energy, blue) using dual energy method. Scale bar (lower left) shows odour amplitude and time scale. The plumes were recorded from the two odours physically mixed (mixed sources) or separated by 50 cm (separated sources). b) The average correlation (mean +/- std) was calculated over all recordings for mixed sources (n = 88), separated sources (n = 77) and recordings in which only the low energy odour was present (n = 32). c) Relationship between amount of odour signal detected (odour integral) and resulting correlation for each recording in the mixed sources (left column), separated sources (middle column) and low energy odour only conditions (right column). Top row: relationship for low energy odour integral, bottom row: relationship for high energy odour. d) Average odour integral (mean +/- std) for low energy (top row) and high energy (bottom row) odours for each recording condition.

16. Reproduction of naturally occurring odour signals

16.1. Overview

In chapter 15 we show that temporal features of naturally generated odour signals contain potential behaviourally salient information. However, as these signals were generated via air turbulence we had limited control over the recorded features and could not reliably replicate them in a controlled setting. To determine 1) whether odour signal temporal features are used in animal behaviour and 2) which of these features contain the most significant information it was necessary to design and construct an odour delivery device that could reliably - and with sufficient temporal bandwidth - produce odour signals with experimenter defined parameters.

16.2. Olfactometer design

The general design of the olfactometer is schematised in figure 16.1. This design offered a number of advantages over standard olfactometer designs. Firstly, the odour delivery itself was controlled by high-speed valves with open cycles greater than 1 kHz. This allowed both for fast pulsing of odours, as well as pulse-width modulation of the valve opening in order to fine-tune the amount of odour released over a given period. This is in contrast to many standard olfactometers which use air dilution and computer controlled mass flow controllers to achieve concentration changes. By designing the concentration adjustment / odour release part of the olfactometer to be controlled at the level of the valve we were able to reduce the

total air volume of the system and achieve a more temporally responsive output. The manifold based design also meant that the system could be easily scaled and expanded.

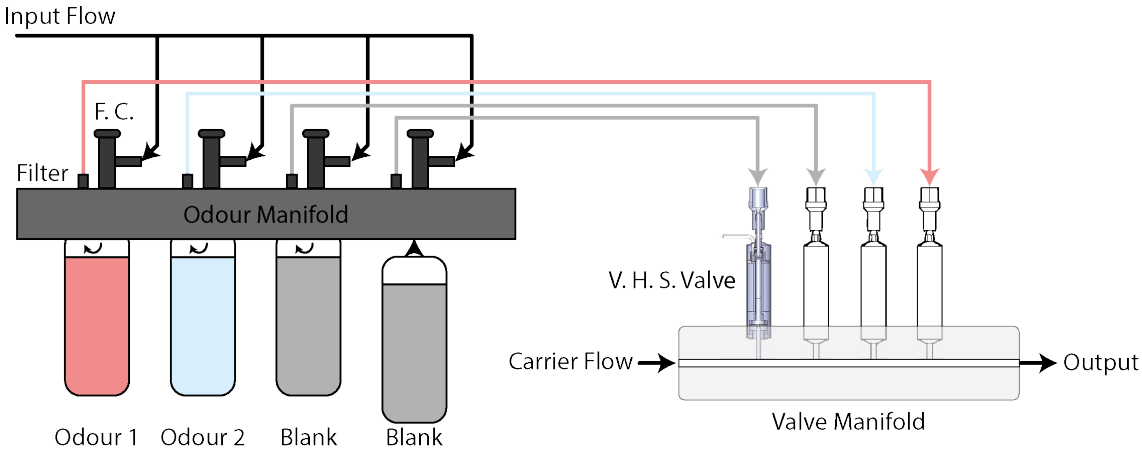

Figure 16.1.: Olfactometer design. The high temporal bandwidth olfactometer consists primarily of an odour manifold for odourising a set of air flow lines; and a valve manifold for fast, reliable release of odours into the output air stream. The odour manifold is a stainless steel block with 4 screw sockets for odour vials. The screw socket design means that odour vials can be quickly installed or removed, without having to unattach tubing or other pneumatic connections. Each socket on the manifold contains an internal thread for screwing in vials, an input flow controller (F. C.) for fine-tuning the amount of flow released into the vial, and a filter for ensuring no particulates from the vial can be released to the valve manifold. A common input flow is connected to the flow controllers on the manifold to provide separate air flow and pressure to each odour position. Each odour position is individually connected to a corresponding valve in the valve manifold, which controls release of the odour into the constant carrier flow. Each valve can be controlled individually by a spike-and-hold valve driver and associated control software.

16.3. Olfactometer characterisation

16.3.1. Signal fidelity and pulse frequency

To determine the temporal bandwidth of the temporal olfactometer we analysed frequency/response properties of odour signals under a number of different fre-

quency and pulse duty conditions with different odours. Odour pulses with almost perfect signal fidelity could be created at frequencies up to 50 Hz (Figure 16.2a). Increasing the pulse duty of an odour pulse train tended to reduce signal fidelity (Figure 16.2b, c), especially at high frequencies. This effect on the temporal profile of odour signals is likely due to adsorption of odour molecules to air tubing and the inner walls of the manifold which results in a signal delay: the odour signal does not immediately return to baseline as some odour molecules will continue to deadsorb from the manifold materials once the valve is switched off. The effect of the delay is more prominent at high frequencies and pulse duties as under these conditions there is less time between one pulse finishing and the next one starting. This effect on signal fidelity was observed for all odours tested, with some variety depending on the odour used (Figure 16.2c). This variability likely arises from the different adsorption properties of the different odours.

16.3.2. Control of output concentration with pulse width modulation

In the simplest operation of the olfactometer, odour is released over a given stimulation period by opening the valve and holding it open for the desired length of time. Due to the high-speed cycle time of the valves, however, odour release could be pulse width modulated. During this mode of operation, the valve was cycled at a high frequency (normally around an order of magnitude higher than the major frequency used to produce the main pulse temporal profile). The duty period of this high frequency pulse could then be varied to control odour release over the stimulation period, as schematised in figure 16.3a. We examined the effect of pulse width modulation on released odour with a set of 4 odours (Figure 16.3b). Pulse width modulation duty of odour release was linearly related to the resulting amount of detected odour.

16.3.3. Generation of random concentration step changes

The results in figure 16.3 originated from experiments in which odour amplitude was recorded during PWM at a constant duty level and confirmed that PWM could

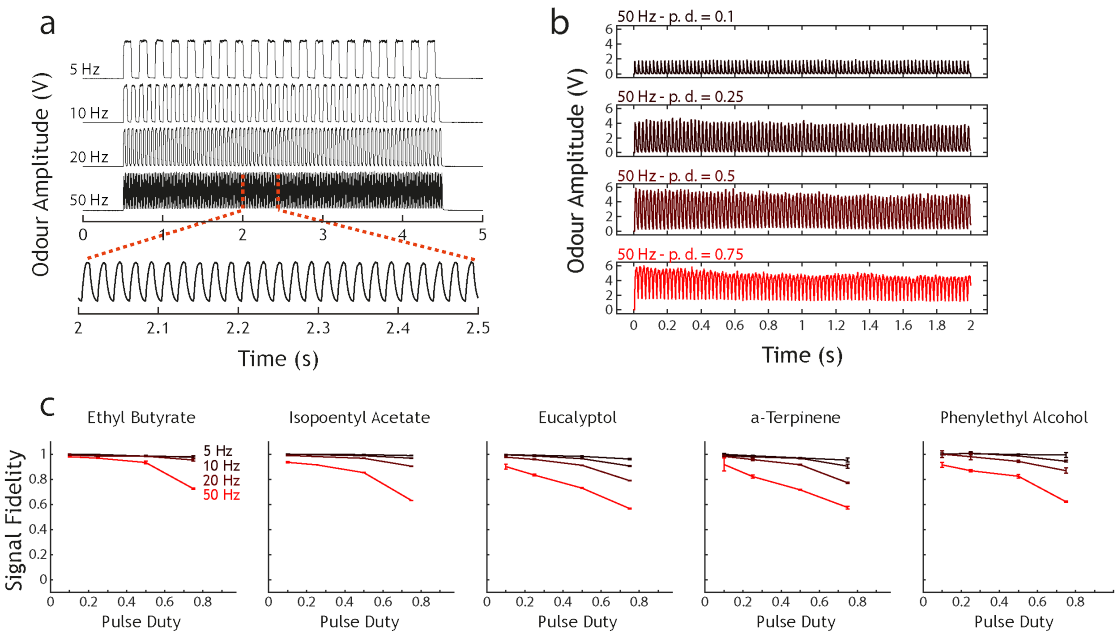

Figure 16.2.: Analysis of signal fidelity and pulse frequency capabilities. a) Representative odour signals produced by opening the valve at 5-50 Hz with 0.5 pulse duty (ethyl butyrate). The 50 Hz pulse train is expanded (bottom panel) to show the reliable fluctuation created by the valve manifold. b) Representative examples of adjusting the pulse duty during valve opening. 4 examples of valve opening at 50 Hz for 2s are shown. As the pulse duty is increased, the amplitude of the signal increases (valve is open for a longer period of time) but the signal fidelity begins to decrease. c) Calculated signal fidelities for several different odours pulsed at a set of different frequencies and pulse duties. Each error bar indicates mean +/ sem of signal fidelity for the given odour at a particular combination of frequency and pulse duty (over 3 repeats).

be used to reliably control the amount of odour release. We next asked whether odour release was still tightly controlled by PWM when the PWM duty was continuously varied over time. Over several repetitions of a sequence of random PWM values, varied at 20Hz, odour signal temporal profile was extremely consistent (Figure 16.4a, b). At several different frequencies of random PWM change, resulting odour amplitude was linearly related to the PWM duty (Figure 16.4c, Pearson correlation coefficient 10Hz cc = 0.99, $p = 4.99 \times 10^{-44}$; 20Hz cc = 0.99, $p = 8.0126 \times 10^{-45}$). At higher frequencies (50Hz), there was still a linear relationship between PWM duty and odour amplitude on average (Pearson correlation coefficient cc = 0.99, $p = 1.853 \times 10^{-45}$), but the variance of odour amplitude values

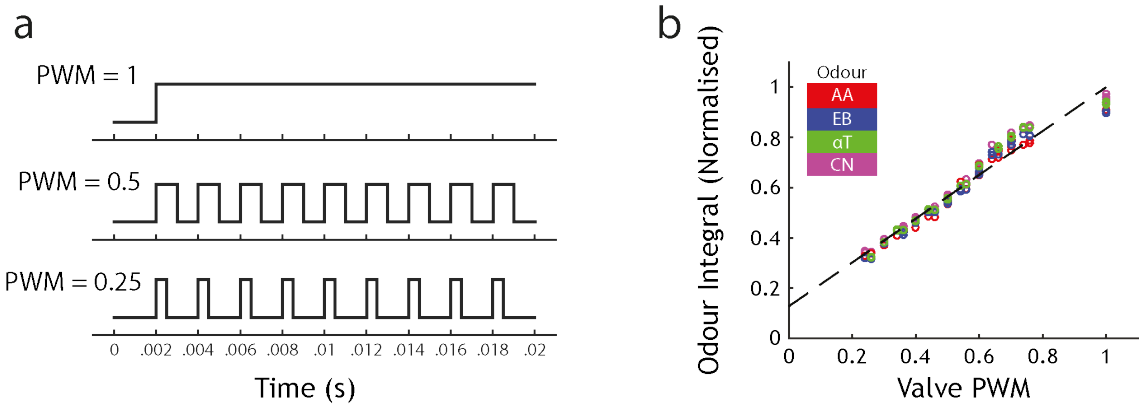

Figure 16.3.: Pulse width modulation control. a) Schematic of the pulse-width modulation (PWM) method. For any period of odour release, the maximum amount of odour release is achieved by holding the valve consistently open (top). The amount of odour released can be reduced by cycling the valve at a high frequency (here 500 Hz) with a different level of pulse-width modulation. For example, the amount of odour release can be halved with 0.5 PWM (middle, each 500 Hz pulse lasts 1 ms) and halved again with 0.25 PWM (bottom, each 500 Hz pulse lasts 0.5ms). b) Valve PWM reliably controls the amount of odour released. Odours were released over a 2s period with different pulse width modulation duties at 500 Hz and recorded with a PID (n = 3 repeats each condition). The resulting released odour amount is normalised to the maximum release (PWM = 1) to account for the intrinsic different signal amplitudes in PID recordings for different odours. Black dashed line: linear fit over all trials.

increased relative to other frequencies (mean standard deviation across PWM 10Hz = 0.1053, 20Hz = 0.1203; 50Hz = 0.2179). This is likely due to the fact that during concentration step changes, odour amplitude cannot instantly change value because of the odour signal decay and rise times (i.e. steps between concentration are not independent in time). As PWM change frequency increases, this component of the signal has more effect on the odour amplitude as more step changes occur in a shorter period of time, so the length of the rise and decay times form a greater fraction of the time spent on each step.

16.3.4. Reproduction of recorded odour plumes

The valve PWM method allowed for virtually arbitrary control over odour temporal profile (up to a certain frequency) within a certain amplitude range. We used

this feature to replicate odour signals from naturally occurring odour plumes (Figure 16.5). This was achieved by mapping odour signal amplitudes from recorded plume data to PWM duties (figure 16.3), converting a time series of amplitudes to a time series of PWM duties. These duties could then be used as the input to an odour valve to reproduce the original signal (figure 16.5a). For 10 separate odour plume recordings, replicated amplitude matched closely with the original signal amplitude (figure 16.5b), although at higher plume signal amplitudes, the replicated amplitude saturated out. The correlation between the original signal and the replicated signal was extremely high for all plume recordings tested (figure 16.5c).

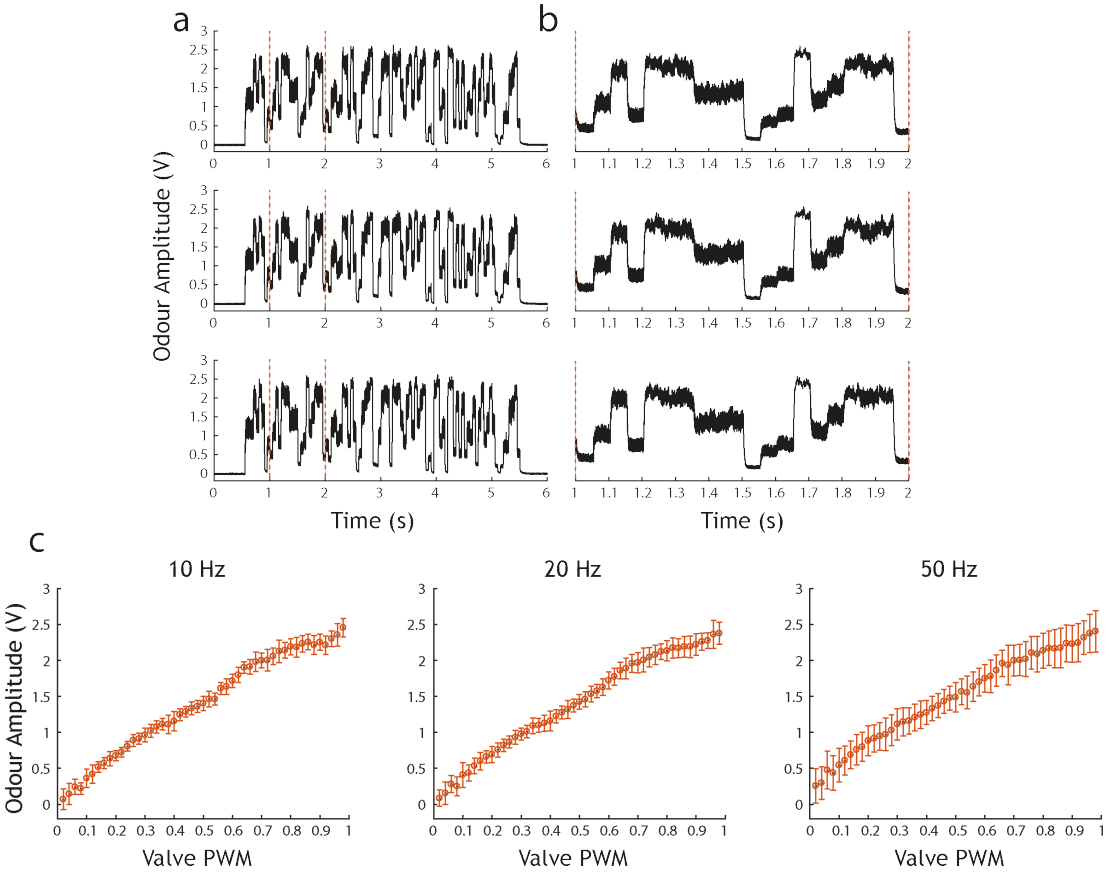

Figure 16.4.: Concentration step changes. a) 3 repetitions (top left to bottom left) of a sequence of random pulse width modulations, changing at 20Hz. b) The same 3 repetitions as a) plotted in higher temporal resolution, over the specified time window (red-dashed lines). b) Relationship between recorded odour amplitude and valve PWM over 50s of continuous random step change. This experiment was repeated with the step change occurring at 3 different frequencies (10Hz, 20Hz, 50Hz).

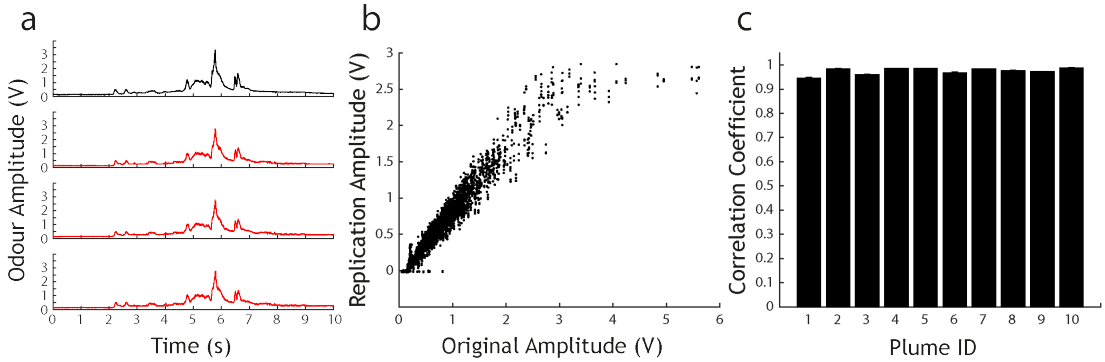

Figure 16.5.: Reproduction of recorded odour plumes. a) Top (black): an example recorded ethyl butyrate plume from an outdoor setting. Bottom (3 red traces), replication of plume using continuously varied PWM. b) For 10 different 10s plumes, replication was performed with the PWM method. Resulting replication amplitude is plotted against the original plume amplitude for all corresponding time points (down sampled by a factor of 500). c) Correlation coefficient (mean +/- std for 3 independent repetitions) between the original recorded plume data and the PWM replication.

17. Perception of temporal features

17.1. Overview

Given the results of chapter 15 it is evident that temporally patterned odour signals in natural plumes contain behaviourally salient information. Which of these features can animals perceive and utilise in behavioural responses? One particularly informative signal component is temporal correlations between odour plumes emanating from sources positioned close together in space (Section 15.3). If an organism could detect both the individual odours in a mixed plume, as well as the temporal correlation structure between these odours; it would be able to determine with high probability whether the odours emanated from the same source or multiple spatially separated sources. This perception could, therefore, be a potential basis for odour scene segmentation and for perceptual 'binding' of odours to a common object.

17.2. Stimulus and experiment design

17.2.1. Stimulus production

To address whether mice can perceive temporal correlations in odour signals, we initially considered the simplest possible case: in which mice display a perceptual difference for odours in perfect synchrony (correlated) or perfect asynchrony (anti-correlated). We conditioned mice to discriminate between these two stimulus cases (rewarded - S+, unrewarded, S-) in a go/no-go behavioural paradigm, using the temporal olfactometer to reliably generate these signals in conjunction with AutonoMouse to train multiple animals simultaneously on this task (17.1a, b).

To ensure that mice truly learnt to discriminate between temporal structure in the odour stimuli during training, a number of controls and stimulus parameters were introduced. To be able to implement these stimulus designs, an 8-channel olfactometer was developed based on the temporal olfactometer design.

The first important control was to ensure that flow changes through the olfactometer initiated by pushing odourised air towards the animal were not a salient signal in learning to discriminate between the task conditions. To achieve this, we ensured that a clean air valve was always actuated after a corresponding odour valve was shut off, such that the change in flow was always compensated for by non-odourised air flow (figure 17.1c). This ensured that flow was static during the stimulus period and was not perceptually different between the two stimulus conditions.

We also utilised the 8-channel olfactometer to ensure that S+ and S- stimuli could be generated dynamically on a trial-by-trial basis. As there were multiple positions for odourised and non-odourised air streams in the olfactometer, the stimulus on each trial could be generated by a random subset of the 8 valve positions (figure 17.1d). As the valve opening could also be pulse-width modulated, the contributions of each valve could be dynamically varied. For example, an odour 1 pulse could be generated by 70% opening from one valve and 30% from another. This meant that it was unlikely that animals would be able to learn subtle differences between the stimulus conditions based on valve actuation noise or some other such extraneous variable as correlation structure was the only engineered constant between S+ / S- stimuli. Further, during training phases all stimuli were produced with a restricted subset of 6 valves. At some pre-determined point during training, the unused extra 2 valves were introduced into the stimulus generation. This served as a control against animals learning some extraneous variable based on the subset of valves being used, stable performance after introduction of the new valves would indicate that only the odour correlation structure was being learned (figure 17.1e, f).

17.2.2. Counterbalanced group assignment

To further ensure that no aspect of the stimulus structure biased performance of experimental animals in any way, all experimental groups trained on the correlation discrimination task were divided into groups which performed slightly different versions of the task. Half of the animals were trained that the rewarded condition was a correlated stimulus, while the other half were trained on anti-correlated as rewarded. Within each of these subgroups, half of the animals were presented with stimuli generated by one subset of 6 valves, and the other half were trained on a complementary subset of 6 valves. The valve subsets were designed such that throughout the experiment, all valves were utilised equally over time. In one experimental cohort, we also defined an additional group of animals that were trained on a scrambled subset of valves (sham). This group was trained on the same stimuli as the other groups, but the mapping between odour valves and desired stimulus was scrambled at the level of the control software (figure 17.1e, f). This meant that all possible extraneous variables were consistent with the other groups, but correlation structure was unpredictable from trial to trial and could not predict reward outcome. These animals were trained simultaneously with other groups and served a number of purposes. Firstly, the performance of the sham group was used as a further control to ensure that no extraneous variables could account for learning in the correlation discrimination task. Above chance performance in theses animals would suggest that the task was solvable without using temporal correlation structure. Second, as the experiments were conducted over a relatively long period of time (months) these animals served as an ongoing control against any malfunction in the AutonoMouse / olfactometer hardware. For example, if the experiment progressed as predicted for several days (above chance learning on the correlation task, chance-level learning in the sham group) and then the sham group performance began to rise above chance level, this would suggest that animals were capable of learning the task but that some issue with the hardware had arisen that meant extraneous variables could also be used in learning. This would serve as an indicator that this data should be discarded and the hardware should be checked.

This experiment was performed with 2 separate cohorts of mice (group 1, n =14; group 2 n = 24; see Methods section 10.3.4 for detailed group assignment and

definition of each group). The choice of group assignment for group 1 was based on performance on a temporal correlation task at 2Hz, with group assignment randomised until there were no significant differences between the groups for performance in the first 1200 trials (1-way ANOVA, F = 1.77, p = 0.2213). For group 2 task assignment was based on a set of experiments in which animals performed a non-temporal discrimination task, and were simply asked to discriminate between two odours (EB vs. AA). The group assignment was randomised until there was no significant difference between the groups in performance in the first 200 trials of this task (1-way ANOVA, $F_{(4, 20)} = 0.2$, p = 0.9344).

17.3. Mice learn to discriminate temporal correlations in odour signals

17.3.1. Performance in correlated vs. anti-correlated experiment

Over several hundreds of trials, mice learned to discriminate between temporal structure in the the correlated vs. anti-correlated experiment. In many cases, learning was robust and stable once above criterion performance was achieved (Figure 17.2a), with significant drops in performance observed only at stimulus frequencies well above natural breathing rate (Figure 17.2a, 50 Hz). To confirm that mice that learnt the task truly used temporal correlation in the odour signals, we analysed the effect on performance during control trials as described in section 17.2.1 (Figure 17.2b, c). Trial performance maps revealed that mice tended to continue performing at comparable pre-control levels after control trials were introduced (Figure 17.2b). We also observed that, in many cases, the first S- trial after control trials were introduced was performed correctly (Figure 17.2b), suggesting that the continued performance accuracy could not be accounted for by random licking during the first set of trials after control introduction. Post-control performance was indistinguishable from pre-control performance at initial low frequency training (Figure 17.2c, top row: 2Hz control (first) paired t-test, t = 0.1004, p = 0.9222, df = 9; 2Hz control (last), t = 0.9055, p = 0.3817, df = 13), as well

as at higher frequencies (Figure 17.2c, bottom left: paired t-test t = 0.7293, p = 0.4825, df = 10) and after the switch control (Figure 17.2c, bottom right: paired t-test t = 0.9178, p = 0.3768, df = 12). Whilst the majority of animals were able to acquire the discrimination task at 2 Hz, performance in the sham group was significantly lower for a partial valve scramble (Figure 17.2d, t-test performance vs. control performance after 600 trials t = 2.2940, p = 0.0279, df = 35; 700 trials t = 2.6791, p = 0.0112, df = 35; 800 trials t = 2.7474, p = 0.0098, df = 32), and was indistinguishable from chance for a complete scramble[1] (Figure 17.2d, full scramble after black arrow trial point, final performance t-test vs. chance t = -0.6163, p = 0.5710, df = 4). Taken together, these results suggest that mice can perceive differences in our correlated and anti-correlated stimuli. Control analysis shows that this perceived difference truly arises from the ability to detect correlation in odour signals.

The results suggested that this correlation discrimination could occur over a relatively wide frequency range. We next asked at what frequency the perceptual limit for correlation discrimination was reached; and how performance in the task changed over a wide range of frequencies up to and including this perceptual limit. To investigate this we repeated the correlation discrimination experiments as before, but pseudo-randomly varied the task frequency from trial-to-trial (see Methods section 10.3.3.2). Average performance in the low frequency bands was still consistently above criterion during the random frequency experiment (figure 17.3b) and showed a roughly monotonic decrease (in the log-scale) as frequency increased and the task presumably became harder. Performance was binned

[1] The difference between a partial scramble and full scramble is described in detail in Methods section 10.3.4. In a partial valve scramble, only the assignment of odour position is scrambled and blank positions are faithfully recorded in the control software. In a full scramble, all positions (both odour and blank) can be scrambled. This is a significant distinction as although odour identity information is degraded in a partial valve scramble, it is relatively trivial to complete the task in this condition. Because blank position identity is not changed in the partial scramble, a correlated stimulus will consist of two random odour pulses being delivered, followed by blank pulses and so on in that sequence. In the anti-correlated case the stimulus will switch between two different sets of random odours. Therefore, the task can be solved in a partial scramble by discriminating between on/off pulses of odour (correlated) and constant odour delivery (anti-correlated). This likely accounts for the above chance performance seen in the control group in figure 17.2d prior to introduction of the full scramble (black arrow), after which performance drops to chance level (the same strategy cannot be used to solve the task in the case of a full valve scramble).

across animals and frequencies (approximately by half-octave[2], intervals: 2, 3, 4, 5, 6:7, 8:10, 11:13, 14:17, 18:22, 23:29, 30:37, 38:48, 49:62, 63:81) and compared to sham group performance to determine in which frequency bands task performance was significantly above chance. Using this approach, we found that mice were able to perform the task significantly above chance up to 49:62 Hz bin (Figure 17.2). We therefore estimate the perceptual limit of correlation discrimination in mice to be 48Hz.

17.3.2. Learning occurs regardless of group assignation

As described in section 17.2.2, mice were assigned to 1 of 5 groups with varying experimental parameters. Apart from the sham group, mice in all groups should have been capable of learning the correlation discrimination task as correlation structure should be the only discriminable feature regardless of reward valence and valve subgroup. Several animals from each subgroup (with the exception of sham) attained >0.8 performance in the discrimination task (Figure 17.4). Some above chance performance was observed in the sham group, however this is likely due to the use of partial valve scrambling in initial trials: performance dropped to chance levels with the introduction of full scramble in later stages (Figure 17.4).

17.3.3. Simulated behavioural performance to extraneous sensory cues

As an additional source of evidence that observed learning in the temporal correlation discrimination task was truly due to perception of temporal profile of the odour stimuli, we took PID (figure 17.5a1, a2, a3) and flow sensor (figure 17.5b1, b2, b3) measurements over 600 correlated and anti-correlated trials. These trials covered a range of frequencies (2Hz, 5Hz, 10Hz, 20Hz and 50Hz) and used both valve subgroups assigned to behaving animals.

PID recorded odour signals showed the expected temporal profile with anti-correlated stimuli stepping between two amplitude values as the two odours were alternated

[2]Note that because animals were trained on discrete frequencies in the random frequency task, binning exactly by half octave is not possible.

(figure 17.5a1, left); and correlated signals (figure 17.5a1, right) showing odour pulses followed by a complete return to baseline (alternating between simultaneous odour pulse and blank pulse). Flow signals also showed the expected temporal profile of a constant square wave over the stimulation period (as odour pulses were always offset with blank pulses to maintain constant flow, see figure 17.1c), for both correlated and anti-correlated stimuli (figure 17.5b1). There was no significant difference between correlated and anti-correlated stimuli in terms of total odour released over all trials (figure 17.5a2, mean correlated odour integral was 1% less than anti-correlated odour integral, t-test t = 0.7173, p = 0.4311, df = 598). There was a small but significant difference in total flow between the two stimulus conditions (figure 17.5b2, mean correlated flow integral was 0.8% greater than anti-correlated flow integral t-test, t = 1.5695, p = 0.011, df = 598).

We asked whether the small differences in odour and flow signal between correlated and anti-correlated conditions could account for discrimination performance of animals in the behavioural task. To this end we simulated behavioural performance by creating a decision model based on either the odour or flow integral data shown in figure 17.5a2, b2. The model was assigned a decision threshold which determined its prediction of whether a trial was correlated or anti-correlated: the model would predict a trial as correlated if the integral for a given trial was above the threshold, and vica-versa for a trial with integral below the threshold. The model was trained with several decision thresholds, covering the entire range of recorded odour / flow integrals in order to determine the optimal threshold. Simulated performance for each model was then calculated as the fraction of trials correctly assigned as correlated / anti-correlated. For both odour integral (figure 17.5a3) and flow integral (figure 17.5b3) models, maximum simulated performance was relatively low (odour integral maximum performance = 0.5267, flow integral maximum performance = 0.5633) and could not account for the high levels of accuracy seen in animals performing the correlated vs. anti-correlated task. These data strongly suggest that animals were truly learning to discriminate temporal structure in the task, and not simply discriminating differences in total odour or flow amount between the stimulus conditions.

17.3.4. Reaction time increases for higher task frequencies

We next asked how mice sample the stimulus during behaviour. In theory, the task can be solved by sampling only the first pulse of the stimulus as in the correlated case the first odourised pulse will be a mixture of the two component odours; whereas in the anti-correlated case the first odourised pulse will consist of either component odour presented in isolation. To determine the level of stimulus integration required to complete the task accurately we analysed reaction time over trials in the randomised frequency experiment, using time to first lick in S+ trials as a proxy for reaction time. In general, task performance appeared to be highly related to reaction time. For example, the three mice with the highest global performance in the randomised frequency experiment showed a gradual increase in reaction time as task frequency increased (Figure 17.6) whereas the three worst performing animals did not change their reaction time (or decreased it) with the same frequency increase.

Indeed, reaction time across a frequency range from the minimum tested (2 Hz) up to beyond the calculated perceptual limit (52 Hz) was strongly correlated with performance across all animals (Figure 17.6), suggesting that a greater amount of stimulus information was sampled by mice in order to complete the task accurately at higher frequencies. As task frequency increased, the slope of the linear relationship between reaction time and performance decreased which suggests that high performance accuracy became less attainable at higher frequencies, but that accuracy levels comparable to lower frequency performance could be achieved by sampling the stimulus for a longer period. Finally, the change in average reaction time between the lowest frequency (2 Hz) and the highest frequency band tested (64-80 Hz) was significantly positively correlated with global performance. This suggests that mice that adopted a strategy of sampling the stimulus for longer before making a discrimination decision tended to perform better in the task, and that increasing reaction time for more perceptually demanding high frequency tasks was required to maintain the same levels of performance achieved in the low frequency trials.

17.3.5. Task accuracy is not based on onset detection

One interpretation of the results so far presented is that animals do not use the full correlation structure of the stimulus to solve the discrimination task. Rather, it is possible that they could use only a short period at the start of the stimulus and perform a form of onset detection to reach high performance accuracy. This is because the first portion of the stimulus will always be a mixture of two odours in the correlated case. In the same time period in an anti-correlated case, only one odour will be detected (figure 17.7). To determine whether this was the case we designed an experiment in which animals were trained in the same way as with the previous correlation discrimination experiments, but stimuli in which the onset was disrupted were randomly presented. These onset disruption stimuli were designed such that their onset took on the opposite correlation structure to the rest of the stimulus (figure 17.7a). For example, for a correlated onset disruption stimulus, the first odour pulse period would be anti-correlated, after which it would change back to a correlated profile.

If mice used only onset detection to solve the discrimination task, their performance should reverse during (i.e. drop to below chance levels) the onset disruption trials; as they would only be utilising the portion of the stimulus that was reversed in correlation structure. If animals use a more significant portion of the stimulus in the task, their performance should drop slightly during onset disruption trials (due to the slightly degraded information in the stimulus) but still remain at comparable levels to performance for the standard stimuli. Performance was degraded during the onset disruption trials (non-probe performance 0.7582 +/- 0.0422, probe performance 0.6776 +/- 0.0646, paired t-test $t = 5.0421$, $p = 9.99 \times 10^{-4}$, $df = 8$), but remained significantly above chance (figure 17.7b, t-test vs. chance $t = 8.2496$, $p = 3.54 \times 10^{-5}$, $df = 8$). This suggests that animals do not use onset detection to perform correlation discrimination, but instead need to integrate information about the global temporal structure of the stimuli.

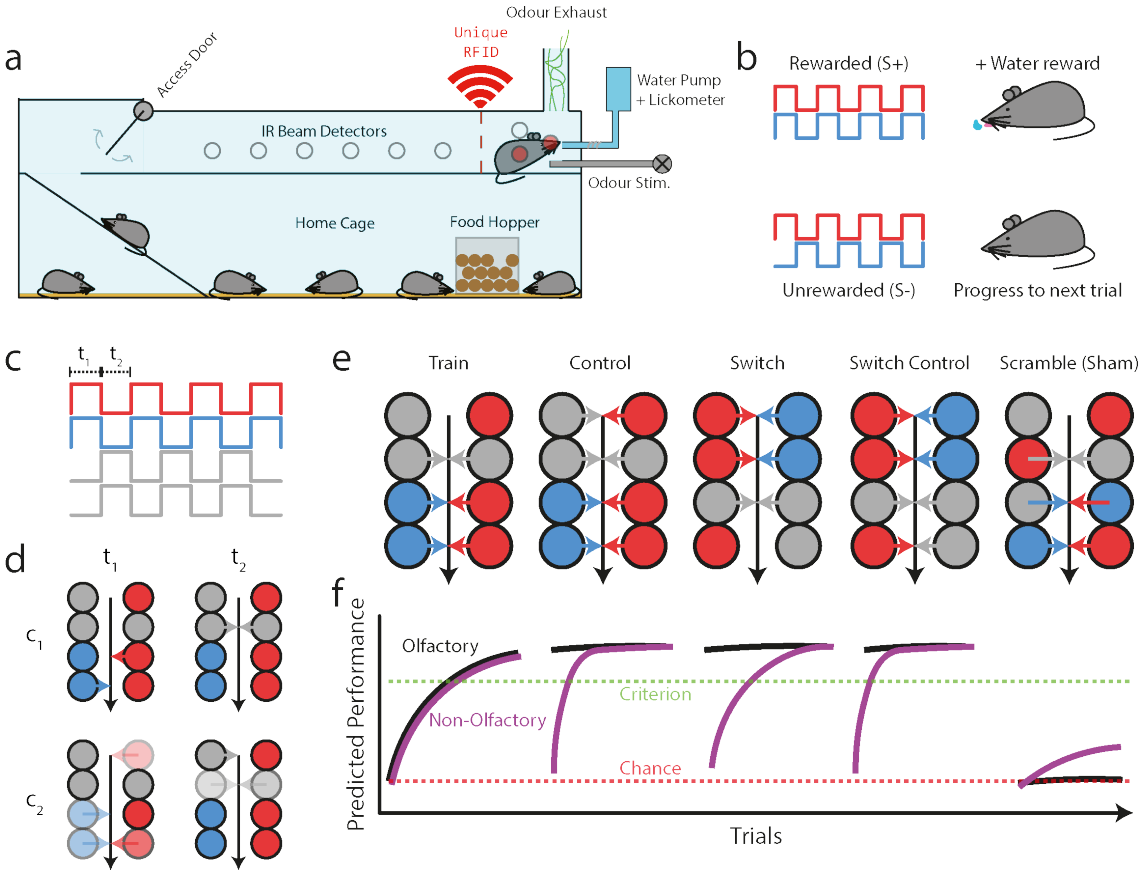

Figure 17.1.: Stimulus and experimental design.a) Schematic of AutonoMouse system used to train the animals. b) General design of the stimuli that animals were asked to discriminate. c) More detailed schematic of stimulus production, odour presentation (blue, red) is always offset by clean air valves at the same flow levels, to ensure that total flow during the stimulus is constant. d) Schematic of the use of valve subsets to produce the desired stimulus. t1 and t2 represent valve openings at the corresponding time points shown in c). c1 and c2 represent two possible configurations that could be used to produce the same resulting stimulus at the two time points. Opacity in the colours represent total concentration contribution to the resulting stimulus at the time point. For example, to produce the dual odour pulse at t1, configuration c1 can be used in which odour 1 (blue) is generated by 50% opening of two valves, with odour 1 (red) produced by 70% / 30% opening of two valves respectively. e) Schematic of the controls used throughout the experiment. Train: a subset of 6 valves is used to produce the stimulus. Control:, two extra valves are introduced. Switch: valves and odour positions are physically switched around on their position on the manifold. Switch control: a new valve control is introduced as with the original train and control conditions. Scramble (sham): odours are arranged in the same configuration as the other conditions, but the software running stimulus production is given a scrambled map of odour placement (represented by arrow colour). f) Predicted learning curves for animals in the case that they truly use olfactory temporal correlations only (black) and in the case that they use extraneous non-olfactory cues also. The learning curves are shown underneath the corresponding experiment/control point shown in e).

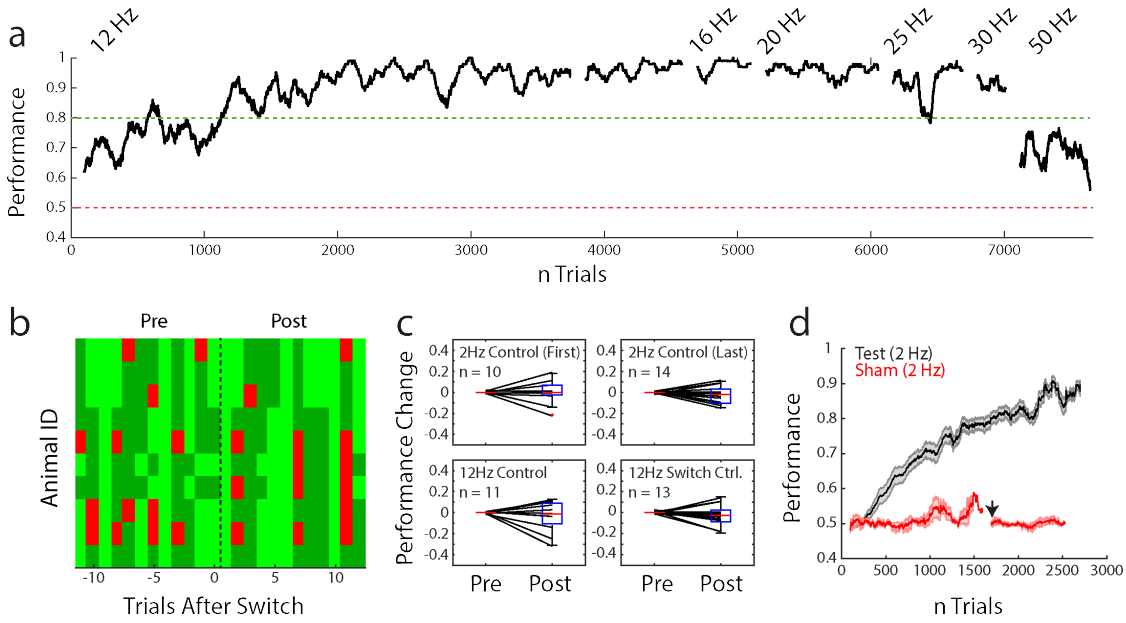

Figure 17.2.: Mice can discriminate odour temporal correlation structure over a range of frequencies. a) Example animal performing the correlation discrimination task at different frequencies. Performance calculated over a 100 trial sliding window. b) Trial map of 10 representative animals before and after introduction of control valves (n = 12 trials pre-, n = 12 trials post- new valve introduction, new valve introduction indicated by black vertical dotted line. Each row corresponds to an animal, each column within the row represents a trial. Light green: correct lick, dark green: correct no lick, light red: false alarm, dark red: miss. c) Summary of mean pre- and post- control performance in 4 control conditions. Pre-control performance normalised to 0, post-control performance indicates change from pre-control level. d) Group learning curves (mean +/- sem, calculated in 100 trial sliding window) for animals performing correlation discrimination at 2Hz (n = 20, black) and animals performing the same task under the scramble control condition (n = 5, red), first under a partial control, then under full control (starting at black arrow).

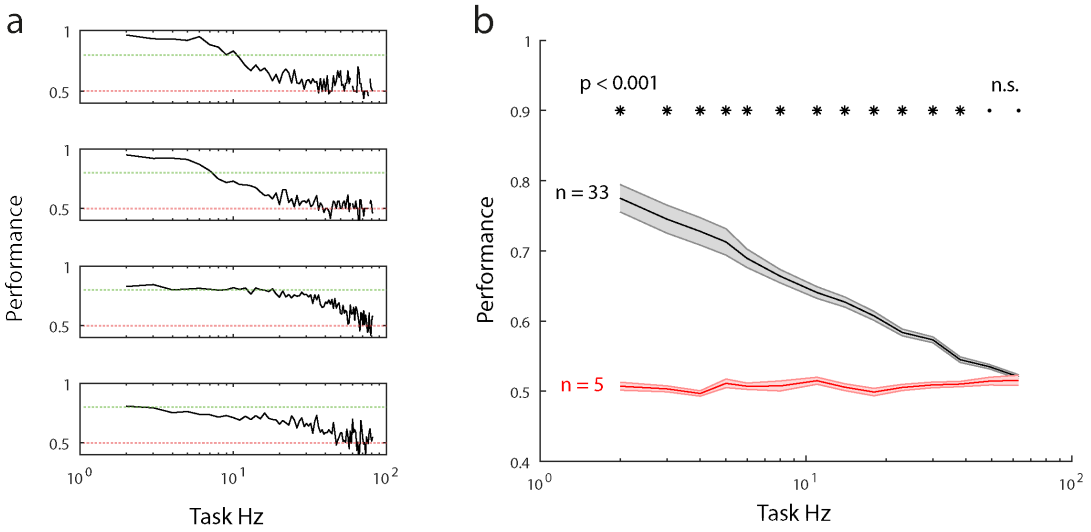

Figure 17.3.: Discrimination of temporal correlation at multiple frequencies. a) Performance of 4 representative animals performing correlation discrimination where task frequency is randomised from trial to trial. Performance binned by frequency of task. b) Group performance in the random frequency experiment (black: standard training, red: full scramble). Performance binned by frequency within approximately a half octave range and across animals within each group. Significantly different performance according to t-test in standard training vs. full scramble indicated by *.

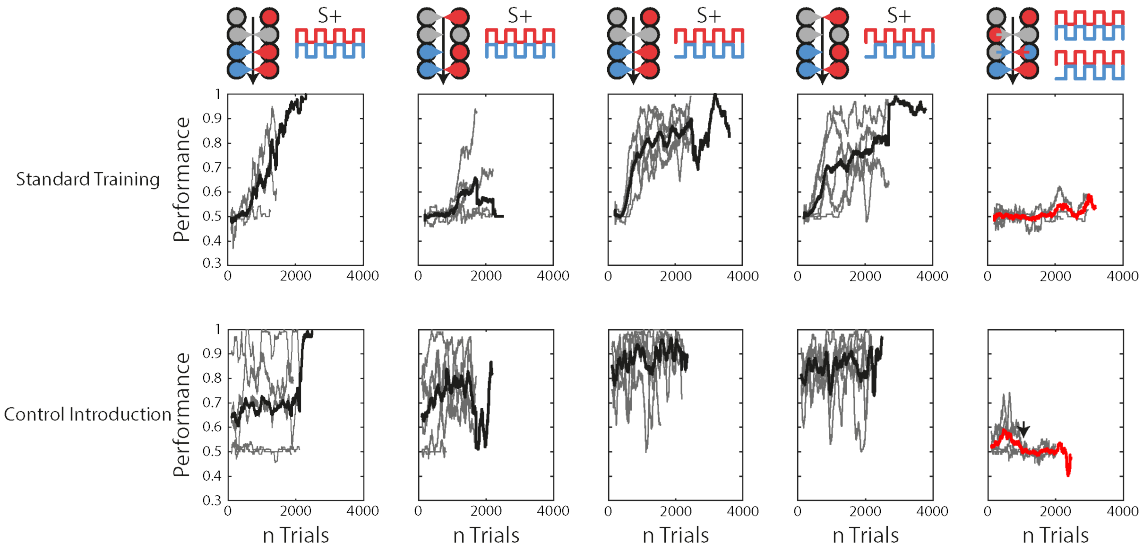

Figure 17.4.: Learning within counterbalanced groups. Individual performance (light grey) and subgroup mean (thick black, thick red for sham group) for each subgroup (n = 5 for each group) used in the correlated vs. anti-correlated discrimination experiment (shown: 2Hz task). Each column corresponds to a particular animal group. Schematics above columns show the subgroup of valves in the 8-channel olfactometer used to produce stimuli in each group and the stimulus profile. Filled circles indicate physical positions of odour/blank within the olfactometer (red: odour 1, blue: odour 2, grey: blank). Arrows indicate control software mapping for the group (e.g. red arrow from red circle at position 1 indicates that software map registers odour 1 inhabiting position 1). Top row: performance in standard training in which no additional valves to the 6-valve subgroup are used during training. Bottom row: performance while new valves are introduced to the subgroup for 12 trials every 300 trials. Bottom right black arrow: trial point at which sham group switched from partially scrambled valve map to fully scrambled valve map.

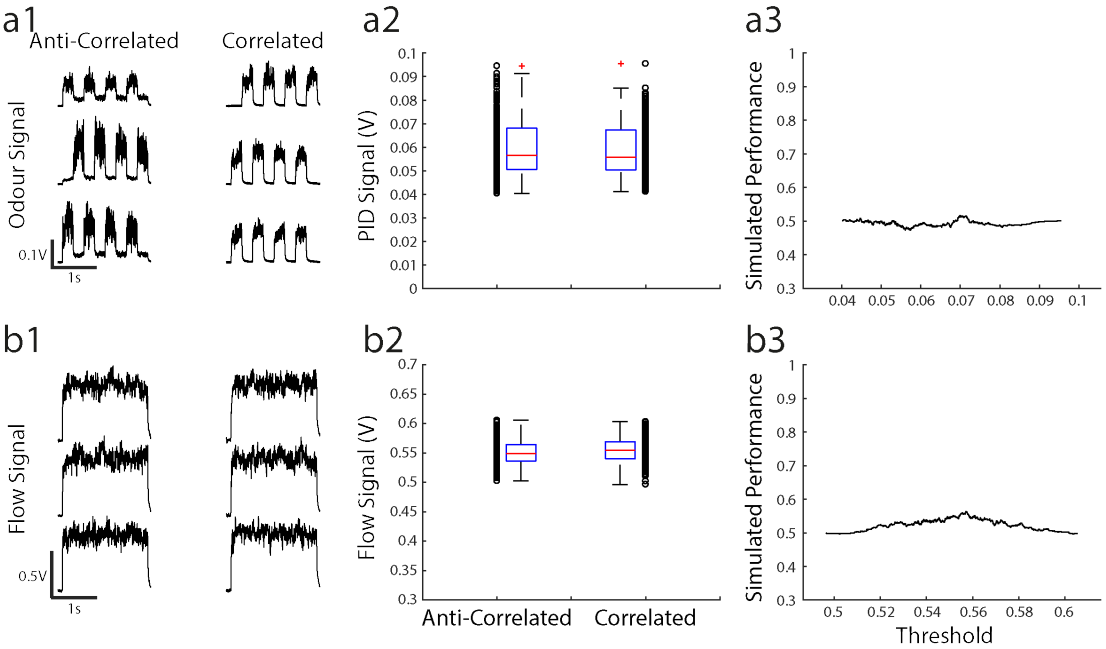

Figure 17.5.: Simulated behavioural performance. a1) Example traces of odour signal (ethyl butyrate, amyl acetate, PID recorded) during anti-correlated trials (left) and correlated trials (right). a2) Mean odour signal for all recorded anti-correlated and correlated stimuli (total anti-correlated: n = 300, total correlated: n = 300. For each stimulus type, 150 trials were generated with valve subgroup 1, 150 with valve subgroup 2 (see figure 17.4). Within each subgroup: 30 trials each at 2Hz, 5Hz, 10Hz, 20Hz, 50Hz). Box plots show median (red line), 25th to 75th percentile (blue box), most extreme points not considered outliers (black dashed line) and outliers (red +). a3) Simulated maximum performance based on differences in mean odour signal. Simulated performance was calculated as the fraction of trials correctly identified as correlated/anti-correlated based on a decision threshold set at some level between the minimum and maximum mean signal. Simulated performance was calculated for multiple decision thresholds, increasing the decision threshold from minimum odour signal to maximum odour signal in steps of 1/5000th of the range between minimum and maximum.

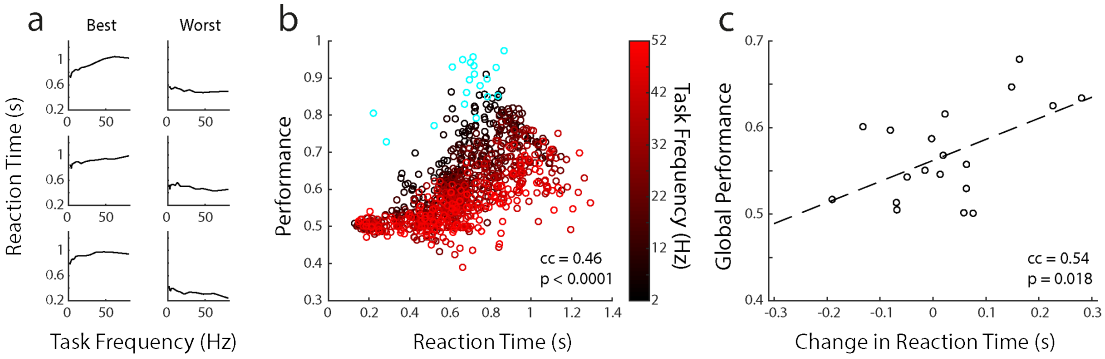

Figure 17.6.: Reaction time scales with performance and task frequency. a) Mean reaction time on S+ trials, binned according to trial frequency. Reaction time over task frequency shown for the 3 best performing animals (left), and the three worst performing (right). Performance is defined as mean performance over all trials in the random frequency task. b) Mean overall performance vs. mean reaction time binned by trial frequency for each animal performing the random frequency task (n = 19). Task frequency colour-coded according to colour map (right). Blue coloured points indicate performance vs. reaction time for the same animals performing a simple odour discrimination task (EB vs. AA). Correlation coefficient (cc) and p-value calculated for random frequency task trials. c) Overall mean performance vs. change in mean reaction time between 2Hz trials and trials in the 64-80Hz frequency band for the random frequency task.

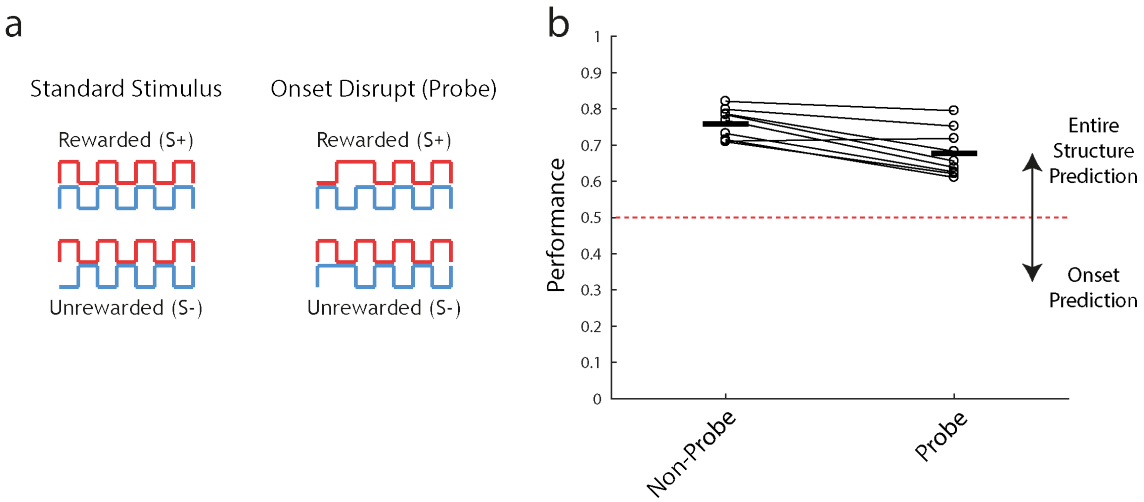

Figure 17.7.: Onset detection. a) Schematic of the onset disruption probe stimuli. Left: structure of standard stimuli in a correlated vs. anti-correlated discrimination. Right: structure of corresponding onset disruption probe trials. For a correlated onset disruption probe (top right) the first few pulses are altered such that the beginning of the stimulus is anti-correlated, and then morphs into a correlated structure. The opposite case is true for an anti-correlated disruption probe trial (bottom right). b) Mean performance for all animals in non-probe trials and in random trials where the onset disruption trials are introduced. Only animals with mean performance > 0.7 in non-probe trials were selected for this analysis (n = 9) Horizontal black bars show the mean performance across animals for each condition.

18. Neural representation of temporal features

18.1. Overview

Given that temporal information exists and represents a potential mechanism for odour scene segmentation and that animals can perceive differences in correlation structure; it seems probable that there is a robust representation of some temporal features of odour signals in the brain. The olfactory bulb is an early information processing centre for olfaction, with its projection cells synapsed onto directly by axons of the sensory neurons in the olfactory epithelium. These projection cells then send signals onto higher olfactory areas and olfactory cortex. The projection cells of the OB were, therefore, identified as a potential candidate for representing incoming temporal information in odour signals.

18.2. 2-photon imaging of projection neurons

2-photon imaging was performed from the dorsal olfactory bulb of anaesthetised mice, whilst simultaneously recording respiration rate with a flow sensor from the contralateral nostril to the imaging hemisphere (figure 18.1a). Odour stimuli were presented to the ipsilateral nostril with a temporal olfactometer (see chapter 16), either as single odours (odour 1: EB + 2H, odour 2: AA + CN), or both odours together with a correlated or anti-correlated temporal pattern, and at different frequencies; as in chapter 17. All fluorescence responses were aligned to the first inhalation after stimulus presentation.

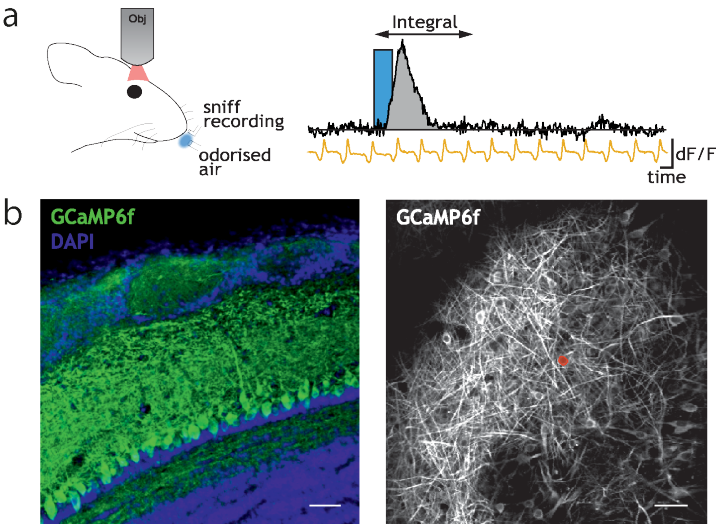

Figure 18.1.: 2-photon imaging. a) Left: Schematic of the recording approach. 2-photon imaging of the dorsal olfactory bulb was performed while delivering correlated or anti-correlated odour stimuli. Respiration rate was simultaneously measured with a flow sensor placed close to the nostril contralateral to the bulb hemisphere being recorded. Right: integral of fluorescence measurements in a 10s window after stimulus onset, including the 1s stimulus, were used for further analysis. The simultaneously recorded respiration rate was used to align all responses to the first inhalation after stimulus onset. b) Left: coronal section, transgenically expressed GCaMP6f (green) in M/TC projection neurons in the Tbet-cre driver line. Right: example dorsal view maximum projection (8000 frames) of fluorescence imaging, red area marked is ROI that generated the response in a). Scale bar: 20μm

We recorded 710 ROIs from putative M/TCs over 6 mice (see Methods chapter 11). Recorded cells displayed heterogeneous responses in their calcium transients to single odour presentations (figure 18.2a). As well as cells that responded preferentially to only 1 odour (either with excitatory or suppressed responses), we observed cells that responded to both odours and cells that were non-responsive. From the 710 recorded ROIs, we identified 360 cells that were significantly responsive to single odour presentations, with largely excitatory responses (figure 18.2b). Aside from non-responsive cells, the most frequent response type was an excitatory response to odour 1 (figure 18.2c) though a variety of other response profiles were observed across the population.

18.3. Temporally sensitive responses

We next investigated whether cells displayed differential response properties to these odours depending on correlation structure. We presented odour 1/2 in either a correlated or anti-correlated manner over several trials and at a range of frequencies (2Hz, 12Hz, 20Hz, 40Hz). Cells were defined as temporally sensitive based on a bootstrapping method comparing mean response integrals to the two stimulus conditions (see Methods section 11.4). Examples of ROIs that passed the bootstrapping criterion for different frequencies are shown in figure 18.3. Of the total 710 ROIs, 515 were found to display significant responses to the correlated / anti-correlated stimuli. Of these responsive ROIs, 59 were found to be temporally sensitive with significant difference in their response integrals to correlated vs. anti-correlated stimuli. Temporally sensitive cells were generally only differentially responsive to correlation structure at a particular frequency (temporally sensitive at 2Hz only: 1.2%, 12Hz: 4.1%, 20Hz: 7.4%, 40Hz: 0.8%).

There was a clear difference in the distributions of response integrals between correlation profiles for temporally sensitive cells, but animals performing the same correlation discrimination (see chapter 17) were readily able to distinguish correlated from anti-correlated stimuli on a trial-to-trial basis. We therefore asked whether the imaged cells in our experiment were also able to distinguish correlation structure in a single trial, rather than over repeated presentations. We therefore generated response vectors from multiple ROIs for each stimulus presentation and trained a linear classifier to distinguish between response vectors for the two correlation conditions. The data set was composed of 24 repetitions each of anti-correlated / correlated at each frequency, resulting in 192 total trials in each experiment for each ROI. We used 50% holdout validation to train each classifier (50% training data, 50% test data).

We first trained the classifier on correlated vs. anti-correlated stimuli at a specific frequency. For single frequencies, classifier accuracy was significantly greater than chance (defined by shuffled data classifier accuracy) and grew as a function of the number of ROIs included (figure 18.4b); both when trained on temporally sensitive cells only and when trained on all ROIs. Training only on temporally sensitive cells, mean classifier accuracy reached 95% of maximum with only 13 cells (figure 18.4b, black), and with 124 cells when trained on all ROIs. Projection of

correlated and anti-correlated response integrals for all ROIs onto the first 3 principal components revealed clear separation in the data, accounting for the high degree of classifier accuracy and the relatively small number of cells needed to reach this accuracy. To ask how well the population of recorded ROIs generalised their ability to discriminate correlation structure, we trained a set of classifiers on all frequencies simultaneously using the same method (figure 18.4d). As with single frequencies, classifier accuracy grew with increasing numbers of ROIs for both temporally sensitive training data and for all ROIs. Classifier accuracy was generally lower than at single frequencies but still significantly above chance, with mean accuracy reaching 95% of maximum with 13 cells when trained on temporally sensitive ROIs only; and with 101 cells over all ROIs. These results suggest that the information necessary to perform correlation discrimination in our experimental cohort (chapter 17) was robustly encoded by relatively small populations of projection cells in the OB. All ROIs were image at depths between 100-300μm from brain surface - therefore it is highly likely that the majority of all imaged cells were tufted, rather than mitral cells given that the mitral cell layer containing the cell bodies is located at 250-300μm on the medio-dorsal bulb.

Presentation of correlated and anti-correlated stimuli was randomised throughout all experiments to ensure that any signal drift over time would not affect the results, however fluorescence responses were highly stable during imaging (figure 18.5). In some cases there were small but significant differences between response integrals in early and late phases of imaging experiments, though there was no consistent decrease in response integral (in some cases response integral was on average higher during the late experiment phase) suggesting that photobleaching / receptor adaptation did not have a major effect on the results presented in figure 18.4.

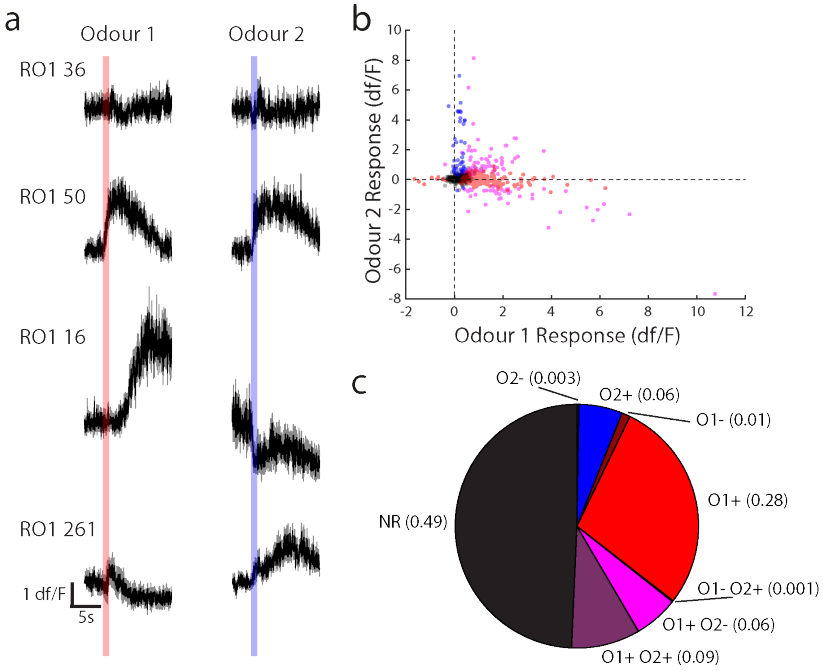

Figure 18.2.: Single odour responses. a) Representative single odour responses from several example ROIs showing the heterogeneity of responses. Responses to odour 1 (EB + 2H, red region indicates stimulus time) and odour 2 (AA + CN, blue region indicates stimulus time) are shown for each ROI averaged over 5 trial repetitions (black line: mean, shading: s.e.m.). b) For all recorded ROIs (710 over 6 mice), the mean response to odour 1 vs. odour 2 is shown. Colour coding indicates whether the ROI was classified as non-responsive (black, no response to either odour), responsive only to odour 1 (red, excitatory or suppressed response to odour 1 only), responsive only to odour 2 (blue, excitatory or suppressed response to odour 2 only) or responsive to both odours (magenta, excitatory or suppressed response to both odours). c) Proportions of ROI response types. Pie chart shows response type (NR: non-responsive, O1: odour 1, O2: odour 2, +/- indicated excitatory or suppressed response respectively) with fraction of all ROIs falling into the category of each response type.

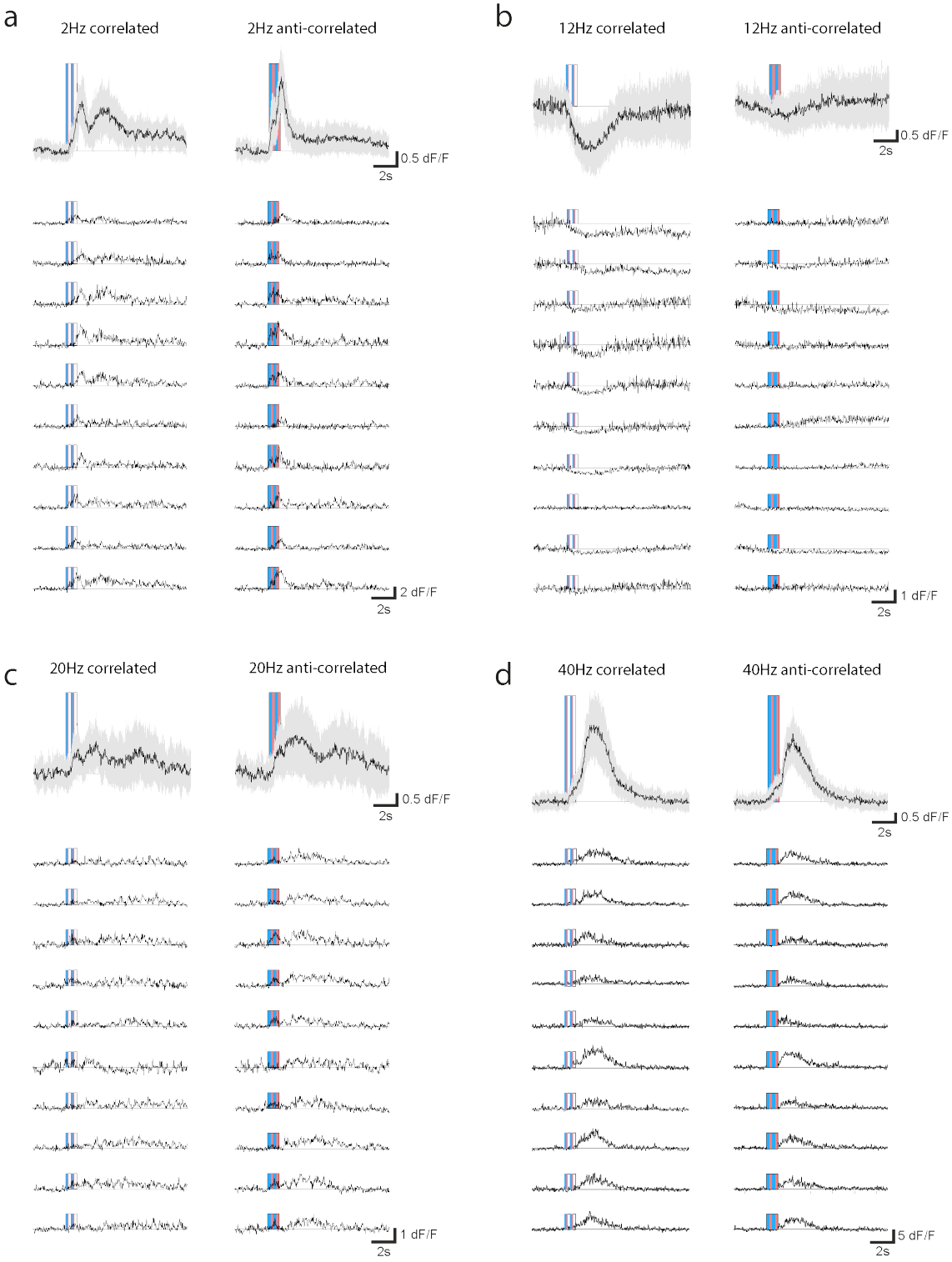

Figure 18.3.: Cell responses to correlated and anti-correlated odour stimuli. a) Top: the average response of an example ROI to correlated and anti-correlated odour stimulation patterns at 2Hz. Black line is mean response, shading is s.e.m. Below: Representative individual trial traces in response to the stimulus types for the same ROI. Red/blue bands indicate stimulation period. b) as in a) for 12Hz patterns. c) as in a) for 20Hz patterns. d) as in a) for 40Hz patterns.

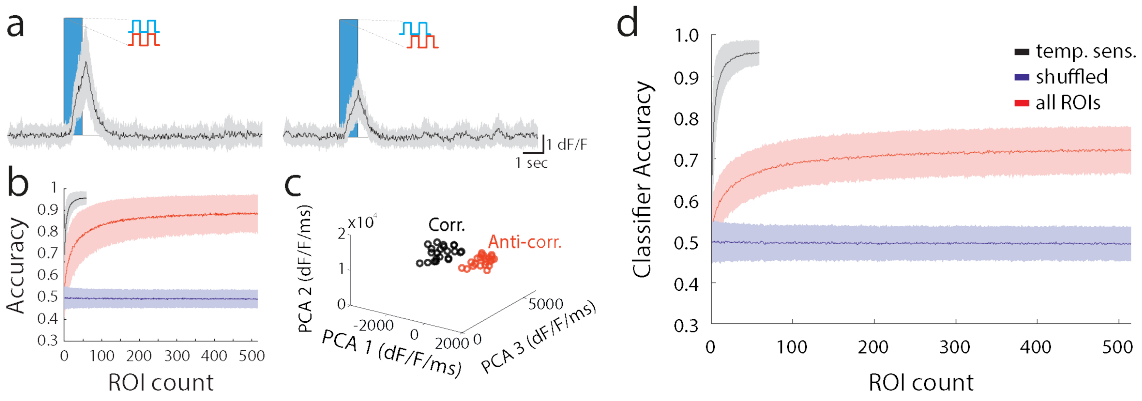

Figure 18.4.: Neural representation of correlation structure. a) Example traces of a cell's response to correlated (left) and anti-correlated (right) stimulation at 20Hz. Traces show mean fluorescence change over 24 trials, with shading indicating standard deviation of responses over time. b) Linear classifier accuracy when trained on 20Hz cell response integrals in discriminating between correlated and anti-correlated stimuli at 20Hz. Performance of the trained classifier is plotted against the number of randomly selected ROIs used in the training set. For each subset of n ROIs, the training was repeated 1000 times and a separate performance level was calculated each time (mean +/- std). Subsets of ROIs used in the training set were collected from only those ROIs identified as temporally sensitive (grey); from all ROIs (red); or from all ROIs with the training labels shuffled (blue, shuffle control). c) Principal component analysis of temporally sensitive ROI responses from b). Response integrals from all ROIs defined as temporally sensitive are shown projected onto the first three principal components. Points in PCA space are colour coded according to whether they were observed during correlated (black) or anti-correlated (red) stimulation. d) Linear classifier accuracy when trained on all correlated vs. anti-correlated stimuli at all frequencies.

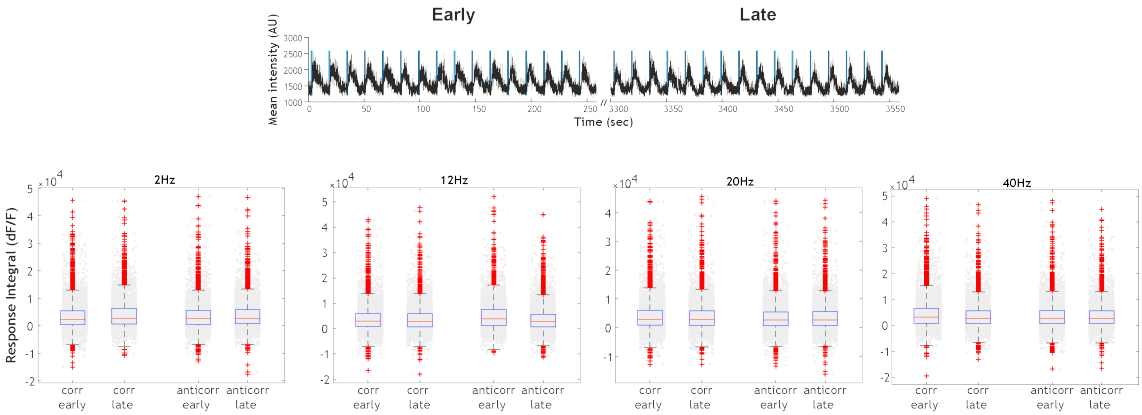

Figure 18.5.: 2-photon imaging signal stability. Top: example responses of an ROI to repeated, randomised stimulations with different odour temporal structures (correlated vs. anti-correlated at 2, 12, 20 or 40Hz) over an entire experiment showing stable responses both in the first 250s of the experiment (left) and last 250s (right). Bottom: summary of response integrals for all ROIs and experiments (n = 4120 ROIs). Response integrals for a 5s window following odour stimulation are shown for both correlated and anti-correlated stimuli at different frequencies either in the first half of the experiment (early) or the last half of the experiment (late). t-test 2Hz corr early vs. late: t = -10,2974, p = 1.434×10^{-24} df = 4119; 2Hz anticorr early vs. late t = -5.1952, p = 2.1444×10^{-7}, df = 4119; 12Hz corr early vs. late t = 1.9252, p = 0.0543, df = 4119; 12Hz anticorr early vs. late t = 22.6098, p = 8.5597×10^{-107}, df = 4119; 20Hz corr early vs. late t = 4.7761, p = 1.8496×10^{-6}, df = 4119; 20Hz anticorr early vs. late t = -0.6946, p = 0.4873, df = 4119; 40Hz corr early vs. late t = 16.8632, p = 9.474×10^{-62} , df = 4119; 40Hz anticorr early vs. late t = 2.1747, p = 0.0297, df = 4119.

Part IV.

Discussion

In this thesis I have aimed to advance understanding of neural circuit function and animal behaviour with an investigation into an aspect of sensory processing that has largely been overlooked in mammalian model systems - the temporal domain of olfaction. It has been been generally supposed that fast temporal features of olfactory stimuli are effectively filtered out in mammalian olfaction, due to the internal structure of the nasal cavity and the fact that odorants must diffuse across a mucous membrane to bind to OSNs. I have, however, shown here that temporal structure exists in natural odour transmission, and that it can be a highly informative and salient signal property for behaviour in mice. I suggest that this finding can be extrapolated to other mammals, since the steps in olfaction that are thought to be temporally filtering are generally common across mammalian species. I conclude that olfaction operates at a significantly higher temporal bandwidth in mammals than previously thought, and that this should be taken into account in future investigations of the olfactory system.

Additionally, I have here introduced a number of novel experimental techniques including high-temporal bandwidth olfactometry; dual-energy photoionisation detection for recording of multiple odours simultaneously; and high-throughput automated operant conditioning for simultaneous phenotype analysis of large cohorts of mice. These techniques have been instrumental in achieving my experimental aims but it is hoped they will continue to be of use in the field. In particular, AutonoMouse presents a general strategy for increasing throughput in behavioural experiments and could be used to increase the efficiency of such experiments in a number of different fields.

19. AutonoMouse

19.1. Conclusions and discussion

AutonoMouse was designed to enable large-scale, systematic behavioural experiments by allowing for fully automated training of multiple animals simultaneously. I show in chapter 13 that this system can train up to 25 animals in a variety of behavioural tasks, producing 1000s of trials per day and motivating animals to perform without imposing severe water restriction. Another key advantage of the system is that behavioural experiments can be conducted with minimal experimenter intervention due to automation of the majority of its functionality. This means that, for mice housed in the system, external stressors such as handling are kept to a minimum. Additionally, relatively little time is needed to monitor ongoing experiments so it is completely feasible to have several systems running in parallel with oversight by a single experimenter, increasing throughput of behaviour studies even more. I show here that olfactory discrimination tasks can be quickly and efficiently trained in mice housed in AutonoMouse. Accuracy levels reported are generally comparable to or well above the >75% criterion levels commonly used in olfactory neuroscience research (Bodyak and Slotnick, 1999, Uchida and Mainen, 2007, Bracey et al., 2013, Resulaj and Rinberg, 2015).

One potential capability of AutonoMouse that has not been utilised in this thesis is the transfer of animals from the system to head-fixed behavioural apparatuses. Head-fixed behaviour is a crucial, powerful technique in sensory neuroscience that allows for neural circuit interrogation simultaneous with quantification of behavioural readout. The main limitation of this technique is that it can be extremely time-consuming to train animals to criterion in a behavioural task in a head-fixed setting (~14 days to criterion per mouse in whisker behaviour: O'Connor et al., 2010; >4 days in olfactory discrimination including habituation: Abraham et al.,

2012). It is also limited in terms of the number of animals that can be trained simultaneously as the electronics for each rig must be repeated for each extra animal trained and training must generally be monitored to ensure no issues occur that might halt learning. A more efficient approach would be to use AutonoMouse to train animals in the intended head-fixed behaviour task first. In this way, a 'stock' of trained animals could be built up through simultaneous training. These animals could then be transferred to a head-fixed setting once they had reliably reached a criterion level, completely circumventing the laborious task of manually training them.

19.2. Future work

In this thesis, the utility of AutonoMouse is presented in a relatively limited context with all animals trained performing some variant of olfactory go/no-go discrimination. The general principle of this system can however be applied to a range of experimental requirements. This gives AutonoMouse some advantage over current RFID based mouse behaviour systems which are generally designed for some specific behavioural task (e.g. IntelliCage, Voikar et al., 2010). The AutonoMouse design is amenable to operant conditioning in any number of sensory modalities. The odour port could be replaced with, for example, a small screen for visual discrimination training - or a speaker for auditory discrimination studies. A second lick port could be easily introduced for 2-alternative forced choice behavioural paradigms rather than go/no-go. Further, there is no reason that the behavioural training implemented should be limited to those that can be installed in a small behaviour port. The access tunnel of AutonoMouse could instead open into a wide-field arena or maze for testing navigational ability. In this situation, the RFID decoder would identify the animal as it passed into the arena and an overhead camera could be triggered to monitor mouse behaviour. A one-way exit tunnel leading from the arena back into the home cage could be installed to ensure a 1-way flow of animals into the arena and that single animals would only ever be present in the behavioural area.

The AutonoMouse design and software also allows for installation of extra sensors with relative ease. In the experiments presented, the sensor profile was rel-

atively limited; being composed of the IR beam detectors, the RFID decoder and the lick sensor. In future experiments, a respiration monitor (such as a pressure sensor or infra-red camera) could be installed to monitor sniffing during olfactory discrimination. Recent technical advances have seen the advent of a number of neurophysiological techniques moving to compact wireless technology platforms, e.g. head-mounted optogenetic stimulation (Wentz et al., 2011, Park et al., 2015) and neural recording (Szuts et al., 2011, Hasegawa et al., 2015). Using these devices in conjunction with the high-throughput nature of AutonoMouse's behavioural data collection would comprise an extremely powerful technique for general neuroscience research.

Health status of the animals in AutonoMouse was monitored primarily with periodic weighing and monitoring of daily water intake (inferred from number of trials performed per day). Aside from cleaning of the system, weighing of the animals was the only manual component of training in AutonoMouse that required direct contact with the animals. This is certainly an area for improvement and future iterations of the system could use a weighing platform under the behaviour port in order to continuously monitor animal weight without experimenter intervention.

20. Lesion study

20.1. Conclusions and discussion

In chapter 14 I utilise AutonoMouse to perform a systematic study of the effect of excitotoxic lesions in the OB on olfactory discrimination performance across a wide range of odours and task contexts. This study was conducted in response to a conflict in the literature regarding aspects of the redundancy of OB odour coding which is discussed in section 14.1. The results in this chapter show that near-complete bulbar lesions result in total anosmia with mice neither able to discriminate or detect odours. Performance in simple discrimination tasks was left intact even with relatively large bulbar lesions with above chance performance observed in all groups (except anosmic). Reductions in performance were observed for the largest non-anosmic lesion group only for non-trigeminal discrimination tasks. Significant deficits in performance were only consistently observed in the small lesion group for familiar odour recognition tasks over the first few trials in the task.

The finding that familiar odour recognition is the only discrimination behaviour affected for all lesion groups suggests that odour memory is particularly sensitive to OB disruption. This deficit in odour recognition was not due to an inability to perform odour discrimination in general as in all lesion groups that showed recognition deficits learning of a novel odour pair was largely unaffected. This result is in agreement with Bracey et al., 2013, who also report transient decreases in performance accuracy for odour recognition tasks (after nasal epithelium lesioning) followed by rapid re-learning. Together, these results suggest that odour recognition is via input matching to previously learned stimulus 'templates', and that these templates are degraded by lesioning resulting in a perception of a previously learned odour as a novel odour. Lesioning has a less drastic effect on the

ability to re-learn this apparently novel odour, thus the rapid increase in performance accuracy within only a few 10s of trials.

While simple odour discrimination was largely unaffected for all lesion groups, this ability was significantly impaired once non-trigeminal odour pairs were introduced. This suggests that some odour pairs can be discriminated based on their differential activation of the trigeminal system. This may account for some of the discrepancies in previous studies, where very large lesions were induced with no loss of discrimination ability, performance was perhaps based rather on trigeminal discrimination. It should be noted, however, that the largest OB lesions did produce complete anosmia so trigeminal activation is evidently not sufficient for odour discrimination and some olfactory component is generally required. Though we did not image the trigeminal nerve after lesion induction, it is unlikely that our method induced damage in the trigeminal nerve; as the spread of lesion was revealed to be relatively local on inspection of the microCT images (figure 14.11) and the nerve is anatomically separated from the bulb in rodents (Bechara et al., 2015)

The results presented reconcile some of the conflicting views on OB redundancy (Lu and Slotnick, 1998, Laurent, 1999, McBride and Slotnick, 2006, Wilson and Mainen, 2006, Johnson and Leon, 2007, Slotnick, 2007, Knott et al., 2012, Bracey et al., 2013). Though it is true that relatively large lesions leave simple olfactory behaviours intact (pure odour discrimination), more complex behaviours involving memory, mixtures and non-trigeminal odours are readily affected by even quite small lesions. This was revealed in these results by a systematic approach to olfactory behaviour in various contexts. The results suggest that OB circuitry required to discriminate between pure odours is relatively redundant, as evidenced by lesioned animals readily learning novel odour pairs. The failure of animals with small lesions to instantly recognise a previously learned odour pair, however, suggests that the retention of odour identity is non-redundant and that minor perturbations to the OB readily affect perception of a previously encountered odour.

20.2. Future work

This study used an irreversible method of OB challenge in the form of excitotoxic lesions. Although the experiments were well controlled with the introduction of sham injected animals and from monitoring pre-surgery performance; an interesting extension to these experiments could be to use some reversible silencing method, e.g. DREADDs or global optogenetic silencing. In this way, performance in olfactory discrimination tasks could be compared pre- and post-challenge within smaller time windows and over repeated inductions and reversals. For example, one could train an animal in a particular task and then silence an area of the bulb on random trials to determine whether performance was degraded in these trials. Furthermore, excitotoxic lesioning is a relatively non-specific method for OB challenge. These other methods could be used to produce more specific manipulations, e.g. by targeting specific cell types for silencing.

21. Perception and representation of odour correlation structure

21.1. Temporal olfactometer

21.1.1. Conclusions and discussion

In chapter 16 a new olfactometer design is introduced for controlling odour signals with fine-scale control of concentration and temporal profile. Using high-speed injection valves and a low air volume manifold, odours can be quickly released into a carrier stream, generating fast frequency pulses of odour with excellent signal fidelity. Due to the high-speed nature of the valves, odour release can be pulse-width modulated to control amount of odour released without affecting the global temporal profile of the pulsed stimulus. I show that these features can be used to generate random step stimuli, and to replicate the signal profiles of odours recorded from naturally occurring plumes.

21.2. Dual-energy photoionisation detection

21.2.1. Conclusions and discussion

In chapter 15 I present a new method for simultaneous recording of individual odour signals at high temporal bandwidth. This method was used to investigate the inherent concentration fluctuation correlations in odour plumes emanating from sources positioned close together in space, revealing a potential mechanism for odour scene segmentation.

One obstacle in this method is that signals recorded simultaneously in a high energy and low energy PID will have different amplitudes, with the signal from the same odour being of lower amplitude in the low energy PID. A primary assumption in this method is that the low energy signal can be linearly mapped onto the high energy signal before the subtraction step. While this assumption generally holds true (figure 15.1, 15.3), variance around the linear fit shows that the mapping is not exact. This is likely because the difference in installed bulb energy between the two PIDs creates some difference in temporal filtering properties during signal recording, i.e. one PID's temporal bandwidth is marginally reduced leading increased rise- and decay-times relative to the other PID.

What effects could this have on the results presented in chapter 15? One argument is that reported correlation values could be an underestimate. If the two calculated signals come from sensors with different temporal response properties, but with the same underlying signal dynamics, then any correlation values will be skewed downwards by temporal filtering. On the other hand, the argument can be made that correlation values are more likely to be overestimated due to this limitation. If differences in temporal filtering between the two sensors is sufficient, an incorrect linear mapping could be calculated for scaling the low energy signal to the high energy signal. The result would be that during the subtraction step either an over- or under-scaled low energy signal would be subtracted from the high energy signal, resulting in residual correlation not due to correlations in the actual odour signals either way. An example of this subtraction error can be seen in e.g. figure 15.1c3 where negative values are observed in the calculated high energy signal. Since in this case only the low energy odour is being observed, for a perfect algorithm the high energy signal would be a flat 0 line, but errors in scaling result in over-subtraction during periods of low energy odour activity. Fortunately, these errors do not seem to bias the individual odour signal calculations and appear to average out to 0, as evidenced by the fluctuation around 0 mean for the example in figure 15.1c3; and by the fact that over all recorded trials, odour integral during low energy odour presentation in the calculated high energy channel was not significantly different from 0 (figure 15.3d, bottom row, low eV).

21.2.2. Future work

The results presented in chapter 15 show that temporal correlations in odour signals are an excellent predictor of source proximity. An interesting avenue for future work is to investigate how global a phenomenon this is in different environments and length scales. For example, in an outdoor environment with dense vegetation and other general obstacles to air flow are temporal correlations preserved over the same length scales observed here? Moreover, do temporal correlations exist at the length scales utilised by animals that track odours over larger distances?

Given that the mapping between the low energy and high energy signal is not strictly linear, future work could focus on a more sophisticated mapping of one signal to the other. For example, if the difference in signals arises from some constant differences in temporal filtering between the two detectors, then a convolution kernel could be calculated to map the signals onto each other. Alternatively, a filter could be approximated by using a machine-learning method to produce a history-dependent filter for signal mapping, as is sometimes used in generalised-linear models to predict spike rate from input stimulus (Campagner et al., 2016).

Photoionisation detection was chosen as the detection method due to its high-temporal bandwidth relative to other detection methods, for example metal oxide sensors (Liwei et al., 2011, Ziyatdinov et al., 2011). Is there any other detection method that would better enable multi-odour resolution in simultaneous plumes? One possible approach would be to use planar-laser induced fluorescence (PLIF), a method in which a laser light sheet is used to illuminate a medium (e.g. a plume in gas or liquid) which then fluoresces (Lozano et al., 1992). The fluorescence can be captured with a detector and collection optics and used to infer features of the plume in a 2D plane, e.g. relative concentration. The advantage over PID measurements is that a 2D image can be captured over time, rather than just the signal at a single point in space. PLIF is, however, disadvantaged in terms of its lack of transportability as it requires a powerful laser and optics to be calibrated, whereas PID recording is relatively simple to set up.

21.3. Perception of odour correlation

21.3.1. Conclusions and discussion

In chapter 17 I show that mice can discriminate between correlated and anti-correlated odour stimuli at frequencies up to 48 Hz. This performance is stable in the face of a battery of controls. Random introduction of new valves to training did not affect mouse performance, suggesting they were truly using odour cues alone to perform the task. Performance was not particularly biased to any correlation structure or valve subgroup as evidenced by the rate of performance in counterbalanced groups performing with different rewarded correlation structures and valve subgroups. Careful calibration of the stimulus olfactometer was used to ensure no extraneous cues other than odour correlation structure could be used to solve the task. Simulating performance to these extraneous cues showed that the performance levels reached by mice in the task could not be explained by learning of variables other than temporal correlation. I also show that - as evidenced by reaction time changes during different task frequencies - a greater degree of stimulus integration over time is required for good performance at higher correlation frequencies; and that performance cannot be explained by the animals simply performing onset detection. Taken together, these results indicate that mice do have some perception of the correlation structure of odour stimuli.

What strategies might mice use to detect temporal correlations? The most obvious suggestion is that they speed up their sniff cycle as task frequency increases in order to sample each pulse of the stimulus individually, though this seems unlikely for a number of reasons. Firstly, in this mechanism mice would have to sniff at twice as fast as the task frequency to discriminate the stimuli - a 5Hz correlated pulse has the same amount of release of both odours as an anti-correlated pulse in a 200ms pulse window, but in a 100ms window the amounts can be differentiated. Secondly, in a natural setting there is no fixed frequency in an odour plume so even if animals adjust their sniff frequency in this particular task, this does not give strong evidence that it would be the strategy in more naturalistic behaviour. Finally, the perceptual threshold for this task is 48Hz which is significantly higher than the maximum sniff rate in mice (up to ~12Hz, Wesson et al., 2008a).

A more likely scenario is that temporal dynamics in the odour stimulus are percep-

tible within a single sniff (sub-sniff processing). In this case animals would still be able to detect temporal correlation structure at frequencies greater than their respiration rate, though there is limited evidence for this kind of sub-sniff processing. It is generally thought that perception of odours does not change particularly on timescales shorter than a single respiration cycle (Kepecs et al., 2006), although there is evidence that fine-scale timing of odour input relative to each sniff cycle is perceptible (Smear et al., 2013).

21.3.2. Future work

In these experiments I have focused on discrimination between perfectly correlated vs. perfectly anti-correlated stimuli. This was chosen as it is the most explicit representation of the task of interest and presented a way of determining baseline correlation discrimination performance. Furthermore, the stimulus profiles are based on periodic, repeating pulses at a certain frequency. This in contrast to odour signal profiles in natural environments as has already been seen in chapter 15. To further probe perception of temporal features in olfaction these two factors should be taken into account. A future experiment could involve a 2-AFC choice task in which correlation between the odour stimuli randomly varied between -1 (anti-correlated) and 1 (correlated) and mice are asked to report whether the stimulus is more correlated or more anti-correlated with a left/right lick. This experiment is analogous to a kinetogram psychophysical test in vision test, and could be used to build a psychometric curve describing the degree to which fine-scale differences in correlation profile can be detected by mice. Experiments could also use more naturally inspired stimuli, either taken directly from plume recordings or generated based on a statistical model of these recordings, to ask whether correlation discrimination is still robust when correlation structure frequency is dynamic in time.

A key point of interest is the sampling strategy that animals use to perform correlation discrimination. The evidence presented in the reaction time data suggests that longer sampling times are needed for higher frequencies, but how does interaction with the stimulus via the sniff cycle change for different frequencies and for different correlation profiles? Do animals need to adjust their respiration rate, or

can different versions of the task be performed at high accuracy with static respiration frequency? Ideally we would like to be able to continuously monitor respiration while animals perform the correlation discrimination task in AutonoMouse to answer these questions. One approach would be to redesign the behaviour port such that in order to initiate a trial animals would have to push their snout into a small, confined nose-poke. This nose-poke would contain the odour delivery port as well as a flow or pressure sensor to monitor respiration. An issue with this approach is that flow/pressure sensors generally must be very precisely positioned next to the nostril (or implanted via a cannula) in mice in order to record meaningful respiration data (Fukunaga et al., 2012, Smear et al., 2013, Resulaj and Rinberg, 2015). Very small head movements by the mice could potentially distort the data. Another approach would be to use an implanted sniff sensor such as a thermocouple inserted nasally or through the dorsal nasal bone. The disadvantage here is that, unless the signals could be somehow wirelessly received, the wire connection between the sensor and acquisition device would have to be somehow automatically connected every time the animal enters the behaviour port, and then disconnected on exit. Wireless recording of respiration rate can be achieved with an implanted pressure sensor in the jugular, along with a battery pack and transmitter that relays pressure signals to an external antennae (*Stellar Telemetry, TSE Systems, Germany*), though this is an extremely invasive method and requires relatively risky surgical methods. A non-invasive method could also be used, such as high-speed thermal imaging of the nostril while the animal is in the port - though this would also require the animal to move minimally during sampling of the stimulus. Alternatively, following training animals could be removed from the system entirely and made to repeat the task in a head-fixed behavioural rig. In this scenario stimuli could be delivered exactly as before in AutonoMouse and respiration could be precisely monitored with a carefully positioned flow sensor. The disadvantage here is that the stress of implanting a head fixation bar and the water restriction necessary to motivate animals to perform the task outside of AutonoMouse might impair performance after the transfer.

21.4. Representation of odour correlation

21.4.1. Discussion and conclusions

The finding that mice can discriminate temporal correlations in odour signals is here further validated by the discovery of projection cells in the OB that encode differences in correlation structure. The population of odour responsive recorded M/TCs displayed heterogeneous responses to each of the odours used to build the correlation stimuli. A fraction of these odour responsive cells showed robust response differences between different correlation structures. Furthermore, linear classifiers trained on trial-to-trial responses to the stimuli reached comparable (or higher) accuracy to animals trained in AutonoMouse on the same stimuli.

Olfactory transduction and processing, especially in mammalian models has been classically considered a low temporal bandwidth process. This is because a number of steps occur in olfactory transduction in mammals that are though to act as a filter on fine-scale temporal structure. First, odours must be drawn into the nose across the convoluted structure of the olfactory turbinates which may break up the pattern of odor dispersion in the inhaled air packet. Next, odour molecules must diffuse through a mucosal layer on the nasal epithelium. Finally, the odours must bind to ORs in OSNs. This binding process will presumably happen over a variable timescale depending on the binding kinetics between the particular volatile and OR. How then can the early olfactory system can encode temporal information in odour signals at frequencies up to ~40Hz?

The most intuitive explanation is that olfactory transduction and OSN response has a temporal fidelity greater than 40Hz. Studies in insect olfaction have confirmed that this is at least biologically plausible (Szyszka et al., 2014) with early olfactory receptor structures quite capable of tracking rapid odour pulses in this frequency range. Insect olfaction, however, generally involves antennae that are in direct contact with the air as opposed to mammalian olfaction in which the path from inhalation to OSNs is more complex. Moreover, it appears that mammalian OSNs (regardless of the transmission time of odours through the nose) are not capable of responding with a great degree of temporal fidelity: in OSNs exposed to pulses of odour, responses tracked pulse frequency only up to ~5Hz (Ghatpande

and Reisert, 2011)[1]. Another possibility is that single OSNs do not respond with exact response fidelity to pulsed stimuli, but instead produce a 'step' response in which response amplitude increases on every odour pulse without returning to baseline firing. This would allow OSNs to encode stimulation frequency even if their response termination period is longer than the time between odour pulses. This mechanism also seems unlikely, firstly as the dynamic range of OSNs is relatively narrow (Reisert and Matthews, 2001, Rospars et al., 2003) and secondly because OSN spiking in response to increasing concentration is not monotonic. Instead firing rate increases with odour concentration up to a certain level and then begins to decrease at higher concentrations (Shibuya and Shibuya, 1963, Reisert and Matthews, 2001, Rospars et al., 2003, Reisert et al., 2007).

An alternative model is that odour pulse frequency is encoded at the level of populations of OSNs rather than being faithfully tracked by each individual neuron. Consider a population of OSNs individually endowed with poor temporal resolution for resolving odour pulses. Suppose that each odour pulse that enters the nose only contains enough odour molecules to activate some fraction of them, say 5%, and once they are activated they will display some excitation with a long decay back to baseline. Although these cells are occupied, the next odour pulse that enters the nose may, by chance, activate some other 5% of OSNs such that now 10% of cells are excited. This process can continue until all OSNs are occupied (although depending on the time for the odours to be cleared and OSN firing to return to baseline it may continue indefinitely as OSN groups are 'reset'). The OSNs can now respond with higher temporal fidelity as a group as regardless of their individual fidelity the output of the population will be a step response that increases for each odour pulse. The fidelity of this step response depends only on the response delay of OSNs which is typically quite short, at around 30ms for dissociated neurons (Reisert and Zhao, 2011) and 160ms in intact epithelium (Grosmaitre et al., 2006). Furthermore, due to the convergence of OSNs of

[1] It should be noted here that this study used *ex vivo* dissociated OSNs, the process of which may affect their response properties compared to their *in vivo* responses. It should also be pointed out that in this study responses to the first 2Hz pulse appear consistently larger in amplitude than the response to the first 5Hz pulse. This is a curious finding since the pulses are the same length. The authors argue that at 5Hz the interaction between pulse frequency and response termination in OSNs causes the amplitude of the entire stimulus response to have a dampened amplitude, but this does not explain the difference in amplitude for the first pulses.

the same type onto the same glomerular foci in the OB, there already exists a mechanism for reading out this OSN population response: the M/TC projection neurons which are synapsed onto by OSN axon bundle terminals. If this were true, the M/TCs in the imaging results presented should display a step response at the odour stimulus pulse frequency. This does not seem to be the case in our imaging data, however consider that 1) the response kinetics of the fluorescent reporter may not be sufficiently fast to see this response and 2) there may be some transformation at the OSN to M/TC synapse that filters the step response, e.g. non-linearly transforming it to rate of post-synaptic spiking.

This model may account for how olfactory information at high-temporal bandwidth can be transmitted through the mammalian olfactory system at the receptor stage, but it still remains to be explained how the OB circuit uses this information to distinguish correlated from anti-correlated odour presentation at a given frequency. The mechanism for this is likely to involve lateral interactions between glomeruli and their associated projection neurons, such that the relative timing of odour pulses can be compared. These lateral interactions could well be mediated by the inhibitory interneuron network in the bulb.

21.4.2. Future work

A key focus of future work will be determining the full pathway of early olfactory system coding of temporal information, from transduction through to OB response. Ideally, we would like to first record responses to pulsed odour stimuli at different frequencies *in vivo,* for both OSNs and M/TCs. Additionally, it would be beneficial to use a recording method with higher temporal fidelity than 2p imaging (patch-recording, extracellular silicon probe recording) in order to uncover any complex spatiotemporal responses to the stimuli. One possibility would be to use the same stimulation procedure used for the 2p imaging results presented, but record from OSN axon bundles from a genetically defined glomerulus expressing a fluorescent protein as a guide (as in e.g. Smear et al., 2013). The same kinds of recording could also be made from M/TCs in the glomerulus at which the axons terminate. This would allow for analysis of the temporal resolution of responses to incoming odour temporal patterns in the input stage of olfaction, as well as any response transformations between OSNs and the projection cells of the bulb.

As mentioned above, the neural mechanism for determining correlation structure in incoming odour stimuli is likely to involve the bulb's lateral interactions between glomeruli and their projections. The primary mediator of these interactions is inhibitory interneurons of various types, juxtaglomerular cells in the glomerular layer and granule cells in the external plexiform layer. These cell types can be targeted with genetic methods (e.g. as in Fukunaga et al., 2014), to express optogenetic proteins or to generate conditional knock-outs. An interesting avenue for future work would be to determine, using these genetic tools, which interneuron cell types might be involved in correlation discrimination. For example, animals expressing a light-gated chloride channel in their GCs could be trained on the task in AutonoMouse with an implanted light fiber. The fiber could be randomly activated on certain trials to determine if performance was significantly worse on those trials than on normal trials, implicating GCs as mediators of the mechanism by which correlation information is processed.

22. Summary and conclusion

The topic of temporal information in olfaction has largely been overlooked in the literature, partly due to the absence of any experimental apparatuses capable of fine-scale control of odour signals at high temporal bandwidth; and also perhaps due to the perception of olfaction as a sense without the same degree of temporal bandwidth as, for example, audition or somatosensation. Previous work in these fields, however, has shown approaching an understanding of a sensory system's function is greatly accelerated by also investigating the statistics of its natural sensory input in an appropriate natural scene for the model system of choice. Whisker system research in rodents, for example, concerned itself in early publications with investigations into somatosensory pathway neuron responses to so called 'ramp-and-hold' stimuli (Gibson and Welker, 1983a,b, Simons and Carvell, 1989, Lichtenstein et al., 1990, Shoykhet et al., 2000). Based on this work, neurons were readily classified into various types according to whether they responded to the onset of stimuli or fired spikes throughout, as well as their directional selectivity. Later work was inspired by the observation of the fast, complex whisker movements seen in behaving animals as they palpitated objects with their whiskers. When complex 'white-noise' patterns of whisker stimulation and other naturally inspired stimuli were delivered to individual whiskers, a tremendous reliability and temporal precision of neuronal response was revealed (Jones et al., 2004, Arabzadeh et al., 2005, Bale et al., 2015, Campagner et al., 2016). There is an analogy to olfaction research here, in which the majority of studies in rodents utilise artificial 'square-pulse' stimuli similar to the ramp-and-hold stimuli used in early whisker system research[1].

[1] This equivalence holds in part, but it should be noted that a general aim of whisker system research was always to understand the encoding of whisker mechanics and movement by neurons in the somatosensory pathway. In olfaction, where a large majority of work is concerned with how the olfactory system encodes odour identity or concentration (rather than

As introduced in chapter 3, the natural scene of olfaction cannot be described by odour identity alone and there is a rich temporal component to odour transmission in the environments of macroscopic organisms. In this work, I confirm experimentally a key theoretical prediction on the nature of temporal information in natural odour scenes; namely that mixed odours evolve odour plumes in which the concentration fluctuations of each odour are highly correlated with each other in time , whereas the same odours emanating from separate sources will not display these correlations (Hopfield, 1991, Moore and Atema, 1991, Fort and Rospars, 1992, Murlis, 1992, Hendin et al., 1998, Hopfield, 1999, Weissburg et al., 2002, Vergassola et al., 2007). This correlation structure is shown to be an excellent predictor of the source origin of odours in the environment, and is therefore a good candidate mechanism for the segmentation of odour objects from each other and from background atmospheric odorants in olfactory processing. Using a high-throughput, systematic approach I also show that temporal correlations between odours are detectable and discriminable by mice. This shows for the first time in mammals that correlation detection is a biologically plausible mechanism for odour scene segmentation. Further, I show that correlation discrimination occurs at frequencies well above the respiration rate in mice. The classical view of olfaction is that a single respiration cycle or sniff is the functional unit of olfactory processing (Kepecs et al., 2006), whereas this result suggests that sub-sniff processing is possible. Generally, this result also indicates that mammalian olfaction operates at a much higher temporal bandwidth than previously thought. In chapter 18 I identify a population of OB projection neurons that account for the ability of mice to discriminate correlation structure in odour stimuli. These M/TCs differentially encode correlated / anti-correlated odour stimuli in their response with reliability and accuracy comparable with mouse behaviour.

In realising these aims I developed several hardware solutions that facilitated the experiments presented here, but that are also likely to be of general use in neuroscience research. AutonoMouse is a high-throughput, automated system for behavioural training and testing in mice. I show here that it is capable of training large cohorts of mice simultaneously in various behavioural tasks and at comparable accuracy to manual and semi-automated training. The system has a

temporal features), it is perhaps more appropriate that these kinds of stimuli are used as the primary aim is to standardise odour delivery across stimulations.

number of advantages over these latter techniques, primarily the throughput of data collection; the ability to motivate mice to complete behavioural tasks without severe water restriction; and that fact that an experimenter need not be present for much of the time during an experiment. This system was used to complete the behavioural study on correlation discrimination, and also used to perform a systematic, large-scale study of olfactory phenotype following OB challenge - yielding results that clarify a number of contentious points in the olfactory literature regarding the redundancy of OB coding for odour identity (Lu and Slotnick, 1998, Laurent, 1999, McBride and Slotnick, 2006, Wilson and Mainen, 2006, Johnson and Leon, 2007, Slotnick, 2007, Knott et al., 2012, Bracey et al., 2013).

I also present a new, scalable olfactometer design capable of generating almost arbitrary odor signal profiles and complex mixtures with a relatively compact apparatus. This olfactometer enabled the completion of the experiments regarding odour correlation discrimination and representation of that correlation in the brain, and has a number of potential uses in future exploration of olfactory processing. Finally, in chapter 16 I introduce a new method for recording of multiple odours simultaneously, using dual-energy photoionisation detection. Although this has been technically possible previously (e.g. with metal oxide sensors), this new technique massively improves the temporal bandwidth of multiple odour recording.

The finding that mammalian olfaction can process and perceive temporally structured information suggests that it is capable of implementing the kinds of sensory algorithms proposed by Hopfield, 1991, 1999. Namely, detection of temporal features should allow olfaction to efficiently perform odour scene segmentation, and guide navigation behaviours. More generally, this suggests a prominent role for olfaction in the formation of cognitive 'maps' (Jacobs, 2012): internal representations of the surrounding environment. Place cells in the hippocampus are thought to be a major component of the brain's internal representation of the environment. These cells are generally thought to encode an animal's position in space (O'Keefe and Conway, 1978, Moser et al., 2015), though recent work suggests they may instead encode multiple continuous variables about the environment (Aronov et al., 2017). It has been known for some time that visual cues can contribute to the formation of this hippocampal map (O'Keefe and Conway, 1978, Muller and Kubie, 1987, Cressant et al., 1997). Visual in-

formation is, however, clearly not the only component in map formation (Save et al., 2000). For example, place cell fields form similar receptive field patterns in blind rats compared to sighted counterparts (Save et al., 1998). One of the sensory modalities likely to contribute to internal cognitive map formation is olfaction - especially in highly olfactory and nocturnal animals such as mice and rats. There are certainly projections from olfactory centres to hippocampal areas (Vanderwolf, 1992, Gourevitch et al., 2010, Sosulski et al., 2011) and it has been shown that olfactory cues contribute to stable place field formation in rats (Zhang and Manahan-Vaughan, 2013). Together, these findings present an interesting avenue for further research. How is temporal odour information relayed first to higher olfactory areas such as piriform cortex and olfactory tubercle, and how is it transformed/processed as it moves downstream? Additionally, how does this information contribute to cognitive map formation in the projections from olfactory centres to the hippocampus?

In this thesis I have focused on a particular group of temporal signals observed in natural olfactory scenes: temporal correlations between odours. There are, of course, other temporal features in olfactory scenes that would merit further analysis. In particular, the role of fluctuations in odour concentration with regards to navigation have been discussed extensively elsewhere (Hopfield, 1991, Murlis, 1992, Hopfield, 1999, Vickers, 2000, Weissburg et al., 2002, Vergassola et al., 2007). A key prediction of these studies is that odour concentration fluctuations are progressively filtered as an odour plume travels and odorised air becomes more dispersed and mixed with surrounding clean air. Therefore, close to an odour source fluctuations would be rapid, intermittent and have high variance. Far away from a source, fluctuations would be slow and with lower variance. If animals could detect the differences in these fluctuation statistics, they could navigate to the source of an odour without time-averaging to determine absolute odour concentration at a particular point in space (as the classical interpretation of chemotaxis suggests). This, in theory, could result in much more rapid olfactory navigation than trying to determine concentration gradients as the features of these fluctuations are approximately instantaneous features. Previous work has shown that bilateral sampling is important for olfactory orienting behaviour (Gardiner and Atema, 2010, Catania, 2013, Esquivelzeta Rabell et al., 2017) and the interpretation of these studies has been that the two nostrils compare odour

concentration differences to orient towards odour source. It is equally, possible, however that the nostrils (and thereby the two hemispheres of the early olfactory system) are in fact comparing temporal feature properties.

In summary, in this thesis I have shown that mammalian olfaction operates at a higher temporal bandwidth than previously thought. This was achieved through analysis of natural transmission of odour signals and identifying potentially informative temporal features of these signals. I show that mice are capable of perceiving temporal correlations in odour signals at high frequencies and that these correlations are represented in neurons of the early olfactory system. In general, these findings suggest that a deeper understanding of olfactory neural circuit function can be achieved through continued exploration of olfactory stimulus space in the temporal domain.

Part V.

End Matter

Personal Acknowledgements

First and foremost I would like to express my sincere gratitude to my supervisor Dr. Andreas T. Schaefer for the continuous support of my PhD project and all the research in the lab, for his insight, patience and advice. Andreas' guidance has been instrumental in all aspects of my research life including experimental ideas, presentations and writing to name but a few. I would also like to highlight his willingness to provide helpful discussion and feedback at all times throughout my project. His extensive knowledge and enthusiasm for science has been a constant inspiration and motivation.

I would also like to thank Dr. Rasmus S. Petersen for giving me my first opportunities in research, introducing me to the field and helping me gain experience both in his lab and externally. Working in Rasmus' lab - as well as his continuing guidance and encouragement - spurred me on to continue in research and pursue a PhD. I would also like to thank current and former members of the Petersen lab, in particular Dr. Michael Bale, for useful discussion and advice.

My sincere thanks to my thesis committee: Dr. Troy Margrie, Dr. Denis Burdakov and Dr. Victor Tybulewicz for their insightful comments and help with the progression of my project.

Thanks also to Dr. Jan Herb for his support and mentorship in the early portion of my PhD.

To my labmates in the neurophysiology division (both at the NIMR and the Crick) I would like to express my gratitude for all the stimulating discussion, both in and out of the lab, and for all the fun we have had in the last 4 years. I could not have hoped for a better group of colleagues and friends to spend these years with. Special thanks must be mentioned for William Wray, Rebecca Jordan, Dr. Tobias Ackels and the Crickets for some particularly memorable times.

I also wish to thank my friends Robert Bedford and James Ashworth for their support throughout University, in particular during all the late-nights over exam periods, and all the good times in between.

Last but not least, I would like to thank my mother, father and brother - Fiona, Jonathan and Joseph - for their enduring emotional support and without whom this would not have been possible. I am also grateful to all my family, whose interest and encouragement will always be appreciated.

Experimental Acknowledgements

Dr. Tobias Ackels performed all 2-photon imaging experiments in chapter 18 and performed the analysis shown in figure 18.1 and figure 18.4.

Dr. Debanjan Dasgupta and Dr. Tobias Ackels performed all the odour signal recordings in chapter 15 and built the experimental apparatus used to gather these results.

Dr. Izumi Fukunaga contributed to early prototypes of the olfactometer described in chapter 16.

Dr. Andreas Schaefer, Dr. Jan Herb and Dr. Thorsten Bus designed, built and implemented the first iterations of the AutonoMouse system presented in chapter 13. The results of the lesion study (chapter 14) were gathered in collaboration with Dr. Jan Herb.

Dr. Andreas Schaefer, Dr. Tobias Ackels and Cristina Marin provided useful discussion and feedback on this thesis.

The concept for the dual-energy photo-ionisation method was conceived of by myself, Dr. Andreas Schaefer, Dr. Tobias Ackels and Dr. Debanjan Dasgupta.

Isabell Whitely performed the microCT segmentation in the lesion study.

Bibliography

N M Abraham, H Spors, A Carleton, T W Margrie, T Kuner, and A T Schaefer. Maintaining accuracy at the expense of speed: stimulus similarity defines odor discrimination time in mice. *Neuron*, 44(5):865–876, 2004.

N M Abraham, V Egger, D R Shimshek, R Renden, I Fukunaga, R Sprengel, P H Seeburg, M Klugmann, T W Margrie, A T Schaefer, and T Kuner. Synaptic inhibition in the olfactory bulb accelerates odor discrimination in mice. *Neuron*, 65(3):399–411, 2010.

N M Abraham, D Guerin, K Bhaukaurally, and A Carleton. Similar odor discrimination behavior in head-restrained and freely moving mice. *PloS one*, 7(12): e51789, 2012.

R Apfelbach, C D Blanchard, R J Blanchard, R A Hayes, and I S McGregor. The effects of predator odors in mammalian prey species: a review of field and laboratory studies. *Neuroscience and biobehavioral reviews*, 29(8):1123–1144, 2005.

E Arabzadeh, E Zorzin, and M E Diamond. Neuronal encoding of texture in the whisker sensory pathway. *PLoS biology*, 3(1):e17, 2005.

R C Araneda, A D Kini, and S Firestein. The molecular receptive range of an odorant receptor. *Nature neuroscience*, 3(12):1248–1255, 2000.

R C Araneda, Z Peterlin, X Zhang, A Chesler, and S Firestein. A pharmacological profile of the aldehyde receptor repertoire in rat olfactory epithelium, 2004.

A C Arevian, V Kapoor, and N N Urban. Activity-dependent gating of lateral inhibition in the mouse olfactory bulb. *Nature Neuroscience*, 11(1):80–87, 2008.

V Aroniadou-Anderjaska, F M Zhou, C A Priest, M Ennis, and M T Shipley. Tonic and synaptically evoked presynaptic inhibition of sensory input to the rat ol-

factory bulb via GABA(B) heteroreceptors. *Journal of neurophysiology*, 84(3): 1194–1203, 2000.

D Aronov, R Nevers, and D W Tank. Mapping of a non-spatial dimension by the hippocampal-entorhinal circuit. *Nature*, 543(7647):719–722, 2017.

T C Baker, M A Willis, K F Haynes, and P L Phelan. A pulsed cloud of sex pheromone elicits upwind flight in male moths. *Physiological Entomology*, 10 (3):257–265, 1985.

J P Balcombe, N D Barnard, and C Sandusky. Laboratory routines cause animal stress. *Contemporary topics in laboratory animal science / American Association for Laboratory Animal Science*, 43(6):42–51, 2004.

M. R. Bale, D. Campagner, A. Erskine, and R. S. Petersen. Microsecond-Scale Timing Precision in Rodent Trigeminal Primary Afferents. *Journal of Neuroscience*, 35(15):5935–5940, 2015.

Arkarup Banerjee, Fred Marbach, Francesca Anselmi, Matthew S. Koh, Martin B. Davis, Pedro Garcia da Silva, Kristen Delevich, Hassana K. Oyibo, Priyanka Gupta, Bo Li, and Dinu F. Albeanu. An Interglomerular Circuit Gates Glomerular Output and Implements Gain Control in the Mouse Olfactory Bulb. *Neuron*, 87 (1):193–207, 2015.

D C Barnes, R D Hofacer, A R Zaman, R L Rennaker, and D A Wilson. Olfactory perceptual stability and discrimination. *Nature neuroscience*, 11(12):1378–80, 2008.

B Bathellier, D L Buhl, R Accolla, and A Carleton. Dynamic ensemble odor coding in the mammalian olfactory bulb: sensory information at different timescales. *Neuron*, 57(4):586–598, 2008.

A Bechara, C Laumonnerie, N Vilain, C F Kratochwil, V Cankovic, N A Maiorano, M A Kirschmann, S Ducret, and F M Rijli. Hoxa2 Selects Barrelette Neuron Identity and Connectivity in the Mouse Somatosensory Brainstem. *Cell Reports*, 13(4):783–797, 2015.

C M Bekkevold, K L Robertson, M K Reinhard, A H Battles, and N E Rowland. Dehydration Parameters and Standards for Laboratory Mice. *Journal of the American Association for Laboratory Animal Science*, 52(3):233–239, 2013.

U Bhattacharyya and U Singh Bhalla. Robust and rapid air borne odor tracking without casting. *eNeuro*, 2015.

Stephanie Bisulco and Burton Slotnick. Olfactory discrimination of short chain fatty acids in rats with large bilateral lesions of the olfactory bulbs. *Chemical senses*, 28(5):361–70, 2003.

A R Blaustein. Sexual Selection and Mammalian Olfaction. *The American Naturalist*, 117(6):1006–1010, 1981.

N Bodyak and B Slotnick. Performance of mice in an automated olfactometer: odor detection, discrimination and odor memory. *Chemical senses*, 24(6):637–45, 1999.

T Bozza, P Feinstein, C Zheng, and P Mombaerts. Odorant receptor expression defines functional units in the mouse olfactory system. *The Journal of neuroscience : the official journal of the Society for Neuroscience*, 22(8):3033–3043, 2002.

Thomas Bozza, John P McGann, Peter Mombaerts, and Matt Wachowiak. In vivo imaging of neuronal activity by targeted expression of a genetically encoded probe in the mouse. *Neuron*, 42(1):9–21, 2004.

E F Bracey, B Pichler, A T Schaefer, D J Wallace, and T W Margrie. Perceptual judgements and chronic imaging of altered odour maps indicate comprehensive stimulus template matching in olfaction. *Nature Communications*, 4(2100): 2100, 2013.

L Buck and R Axel. A novel multigene family may encode odorant receptors: a molecular basis for odor recognition. *Cell*, 65(1):175–187, 1991.

L B Buck. Information coding in the vertebrate olfactory system. *Annual review of neuroscience*, 19:517–544, 1996.

T J Bussey, T L Padain, E A Skillings, B D Winters, A J Morton, and L M Saksida. The touchscreen cognitive testing method for rodents: How to get the best out of your rat. *Learning & Memory*, 15(7):516–523, 2008.

Daniel a Butts, Chong Weng, Jianzhong Jin, Chun-I Yeh, Nicholas a Lesica, Jose-Manuel Alonso, and Garrett B Stanley. Temporal precision in the neural code and the timescales of natural vision. *Nature*, 449(7158):92–5, 2007.

Q Cai, M Keck, M R Mcreynolds, J D Klein, K Greer, K Sharma, J B Hoying, J M Sands, and Heddwen L Brooks. Effects of water restriction on gene expression in mouse renal medulla : identification of 3 HSD4 as a collecting duct protein. 5051:218–224, 2006.

D Campagner, M H Evans, M R Bale, A Erskine, and R S Petersen. Prediction of primary somatosensory neuron activity during active tactile exploration. *eLife*, 5, 2016.

K C Catania. Stereo and serial sniffing guide navigation to an odour source in a mammal. *Nature communications*, 4:1441, 2013.

A Celani, E Villermaux, and M Vergassola. Odor Landscapes in Turbulent Environments. *Physical Review X*, 4(4):041015, 2014.

V Chen and B P Halpern. Retronasal but not oral-cavity-only identification of purely olfactory odorants. *Chemical senses*, 33(2):107–18, 2008.

W R Chen, W Xiong, and G M Shepherd. Analysis of Relations between NMDA Receptors and GABA Release at Olfactory Bulb Reciprocal Synapses. *Neuron*, 25(3):625–633, 2000.

T A Cleland and C Linster. Concentration tuning mediated by spare receptor capacity in olfactory sensory neurons: A theoretical study. *Neural computation*, 11(7):1673–1690, 1999.

T A Cleland and C Linster. Computation in the olfactory system. *Chemical senses*, 30(9):801–13, 2005.

J E Cometto-Muñiz, W S Cain, and M H Abraham. Determinants for nasal trigeminal detection of volatile organic compounds. *Chemical Senses*, 30(8):627–642, 2005.

T Connelly, A Savigner, and M Ma. Spontaneous and sensory-evoked activity in mouse olfactory sensory neurons with defined odorant receptors. *Journal of Neurophysiology*, 110(1):55–62, 2013.

A Cressant, R U Muller, and B Poucet. Failure of centrally placed objects to control the firing fields of hippocampal place cells. *The Journal of neuroscience : the official journal of the Society for Neuroscience*, 17(7):2531–2542, 1997.

S M Crouzet and T Serre. What are the Visual Features Underlying Rapid Object Recognition? *Frontiers in psychology*, 2:326, 2011.

Kevin M. Cury and Naoshige Uchida. Robust Odor Coding via Inhalation-Coupled Transient Activity in the Mammalian Olfactory Bulb. *Neuron*, 68(3):570–585, 2010.

C T David, J S Kennedy, and A R Ludlow. Finding of a sex pheromone source by gypsy moths released in the field. *Nature*, 303(5920):804–806, 1983.

M de Bruyne, P J Clyne, and J R Carlson. Odor coding in a model olfactory organ: the Drosophila maxillary palp. *The Journal of neuroscience : the official journal of the Society for Neuroscience*, 19(11):4520–4532, 1999.

M de Bruyne, K Foster, and J R Carlson. Odor coding in the Drosophila antenna. *Neuron*, 30(2):537–552, 2001.

D De Saint Jan, D Hirnet, G L Westbrook, and S Charpak. External Tufted Cells Drive the Output of Olfactory Bulb Glomeruli. *Journal of Neuroscience*, 29(7): 2043–2052, 2009.

S H DeVries and D A Baylor. Synaptic circuitry of the retina and olfactory bulb. *Cell*, 72 Suppl:139–49, 1993.

Adam Dewan, Rodrigo Pacifico, Ross Zhan, Dmitry Rinberg, and Thomas Bozza. Non-redundant coding of aversive odours in the main olfactory pathway. *Nature*, 497(7450):486–489, 2013.

R L Doty, W E Brugger, P C Jurs, M A Orndorff, P J Snyder, and L D Lowry. Intranasal trigeminal stimulation from odorous volatiles: Psychometric responses from anosmic and normal humans. *Physiology and Behavior*, 20(2):175–185, 1978.

W Drongelen. Unitary recordings of near threshold responses of receptor cells in the olfactory mucosa of the frog. *The Journal of physiology*, 277:423–435, 1978.

Patricia Duchamp-Viret and André Duchamp. Odor processing in the frog olfactory system. *Progress in Neurobiology*, 53(5):561–602, 1997.

V Egger, K Svoboda, and Z F Mainen. Mechanisms of lateral inhibition in the olfactory bulb: efficiency and modulation of spike-evoked calcium influx into granule cells. *The Journal of neuroscience : the official journal of the Society for Neuroscience*, 23(20):7551–7558, 2003.

M Elhilali and S A Shamma. A cocktail party with a cortical twist: How cortical mechanisms contribute to sound segregation. *The Journal of the Acoustical Society of America*, 124(6):3751–3771, 2008.

M Ennis, F M Zhou, K J Ciombor, V Aroniadou-Anderjaska, A Hayar, E Borrelli, L A Zimmer, F Margolis, and M T Shipley. Dopamine D2 receptor-mediated presynaptic inhibition of olfactory nerve terminals. *Journal of neurophysiology*, 86(6):2986–2997, 2001.

J Esquivelzeta Rabell, K Mutlu, J Noutel, P Martin Del Olmo, and S Haesler. Spontaneous Rapid Odor Source Localization Behavior Requires Interhemispheric Communication. *Current biology : CB*, 27(10):1542–1548.e4, 2017.

J C Fort and J P Rospars. Modelling of the qualitative discrimination of odours in the first two layers of olfactory system by Jutten and Herault algorithm. *Comptes rendus de l'Academie des sciences. Serie III, Sciences de la vie*, 315(9):331–336, 1992.

N A Francis and P O Kanold. Automated Operant Conditioning in the Mouse Home Cage. *Frontiers in Neural Circuits*, 11(March):1–6, 2017.

J Frasnelli, C Wohlgemuth, and T Hummel. The influence of stimulus duration on odor perception. *International journal of psychophysiology : official journal of the International Organization of Psychophysiology*, 62(1):24–29, 2006.

Johannes Frasnelli, Genevieve Charbonneau, Olivier Collignon, and Franco Lepore. Odor localization and sniffing. *Chemical Senses*, 34(2):139–144, 2009.

Rainer W. Friedrich and Sigrun I. Korsching. Combinatorial and chemotopic odorant coding in the zebrafish olfactory bulb visualized by optical imaging. *Neuron*, 18(5):737–752, 1997.

I Fukunaga, J T Herb, M Kollo, E S Boyden, and A T Schaefer. Independent control of gamma and theta activity by distinct interneuron networks in the olfactory bulb. *Nat Neurosci*, 17(9):1208–1216, 2014.

Izumi Fukunaga, Manuel Berning, Mihaly Kollo, Anja Schmaltz, and Andreas T. Schaefer. Two Distinct Channels of Olfactory Bulb Output. *Neuron*, 75(2):320–329, 2012.

J M Gardiner and J Atema. The function of bilateral odor arrival time differences in olfactory orientation of sharks. *Current Biology*, 20(13):1187–1191, 2010.

M N Geffen, B M Broome, G Laurent, and M Meister. Neural encoding of rapidly fluctuating odors. *Neuron*, 61(4):570–86, 2009.

T V Getchell and M L Getchell. Peripheral mechanism of olfaction: Biochemistry and neurophysiology. In *Neurobiology of taste and smell*, chapter 5, pages 91–124. Krieger Publishing Company, 1 edition, 1991.

A S Ghatpande and J Reisert. Olfactory receptor neuron responses coding for rapid odour sampling. *The Journal of Physiology*, 589(9):2261–2273, 2011.

J M Gibson and W I Welker. Quantitative studies of stimulus coding in first-order vibrissa afferents of rats. 1. Receptive field properties and threshold distributions. *Somatosensory Research*, 1(1):51–67, 1983a.

J M Gibson and W I Welker. Quantitative studies of stimulus coding in first-order vibrissa afferents of rats. 2. Adaptation and coding of stimulus parameters. *Somatosensory research*, 1(2):95–117, 1983b.

D. H. Gire, K. M. Franks, J. D. Zak, K. F. Tanaka, J. D. Whitesell, A. A. Mulligan, R. Hen, and N. E. Schoppa. Mitral Cells in the Olfactory Bulb Are Mainly Excited through a Multistep Signaling Path. *Journal of Neuroscience*, 32(9):2964–2975, 2012.

B Gourevitch, L M Kay, and C Martin. Directional coupling from the olfactory bulb to the hippocampus during a go/no-go odor discrimination task. *Journal of neurophysiology*, 103(5):2633–2641, 2010.

X Grosmaitre, A Vassalli, P Mombaerts, G M Shepherd, and M Ma. Odorant responses of olfactory sensory neurons expressing the odorant receptor MOR23: a patch clamp analysis in gene-targeted mice. *Proceedings of the National Academy of Sciences of the United States of America*, 103(6):1970–1975, 2006.

O Gschwend, N M Abraham, S Lagier, F Begnaud, I Rodriguez, and A Carleton. Neuronal pattern separation in the olfactory bulb improves odor discrimination learning. *Nature neuroscience*, 18(10):1474–1482, 2015.

P Gupta, D F Albeanu, and U S Bhalla. Olfactory bulb coding of odors, mixtures and sniffs is a linear sum of odor time profiles. *Nature neuroscience*, (October 2014):1–14, 2015.

Lewis B. Haberly and Joseph L. Price. The axonal projection patterns of the mitral and tufted cells of the olfactory bulb in the rat. *Brain Research*, 129(1):152–157, 1977.

E A Hallem, M G Ho, and J R Carlson. The molecular basis of odor coding in the Drosophila antenna. *Cell*, 117(7):965–979, 2004.

T Hasegawa, H Fujimoto, K Tashiro, M Nonomura, A Tsuchiya, and D Watanabe. A wireless neural recording system with a precision motorized microdrive for freely behaving animals. *Scientific Reports*, 5(1):7853, 2015.

A Hasler, A T Scholz, and R M Horrall. Olfactory imprinting and homing in salmon. *American scientist*, 66(3):347–355, 1978.

A Hayar. Olfactory Bulb Glomeruli: External Tufted Cells Intrinsically Burst at Theta Frequency and Are Entrained by Patterned Olfactory Input. *Journal of Neuroscience*, 24(5):1190–1199, 2004a.

A Hayar. External Tufted Cells: A Major Excitatory Element That Coordinates Glomerular Activity. *Journal of Neuroscience*, 24(30):6676–6685, 2004b.

O Hendin, D Horn, and M V Tsodyks. Associative memory and segmentation in an oscillatory neural model of the olfactory bulb. *Journal of computational neuroscience*, 5(2):157–169, 1998.

J F Hopfield and A Gelperin. Differential conditioning to a compound stimulus and its components in the terrestrial mollusc Limax maximus. *Behavioral Neuroscience*, 103(2):329–333, 1989.

J. J. Hopfield. Olfactory computation and object perception. *Proceedings of the National Academy of Sciences*, 88(15):6462–6466, 1991.

J J Hopfield. Odor space and olfactory processing: collective algorithms and neural implementation. *Proceedings of the National Academy of Sciences of the United States of America*, 96(22):12506–12511, 1999.

W E Howard, R E Marsh, and R E Cole. Food detection by deer mice using olfactory rather than visual cues. *Animal behaviour*, 16(1):13–17, 1968.

S J Huston, M Stopfer, S Cassenaer, Z N Aldworth, and G Laurent. Neural Encoding of Odors during Active Sampling and in Turbulent Plumes. *Neuron*, 88 (2):403–418, 2015.

Ximena Ibarra-Soria, Maria O. Levitin, Luis R. Saraiva, and Darren W. Logan. The Olfactory Transcriptomes of Mice. *PLoS Genetics*, 10(9), 2014.

Y Imanaka and H Takeuchi. Spiking properties of olfactory receptor cells in the slice preparation. *Chemical senses*, 26(8):1023–1027, 2001.

J S Isaacson. Mechanisms governing dendritic gamma-aminobutyric acid (GABA) release in the rat olfactory bulb. *Proceedings of the National Academy of Sciences of the United States of America*, 98(1):337–42, 2001.

J S Isaacson and B W Strowbridge. Olfactory reciprocal synapses: Dendritic signaling in the CNS. *Neuron*, 20(4):749–761, 1998.

L F Jacobs. From chemotaxis to the cognitive map: the function of olfaction. *Proceedings of the National Academy of Sciences of the United States of America*, 109 Suppl:10693–700, 2012.

C E Jahr and R A Nicoll. Dendrodendritic inhibition: demonstration with intracellular recording. *Science (New York, N.Y.)*, 207(4438):1473–1475, 1980.

C E Jahr and R A Nicoll. An intracellular analysis of dendrodendritic inhibition in the turtle in vitro olfactory bulb. *The Journal of physiology*, 326:213–234, 1982.

A Jinks and D G Laing. Temporal processing reveals a mechanism for limiting the capacity of humans to analyze odor mixtures. *Brain research. Cognitive brain research*, 8(3):311–325, 1999.

A Jinks and D G Laing. The analysis of odor mixtures by humans: evidence for a configurational process. *Physiology & behavior*, 72(1-2):51–63, 2001.

B A Johnson and M Leon. Chemotopic odorant coding in a mammalian olfactory system. *Journal of Comparative Neurology*, 503(1):1–34, 2007.

D T Jones and R R Reed. Golf: an olfactory neuron specific-G protein involved in odorant signal transduction. *Science (New York, N.Y.)*, 244(4906):790–795, 1989.

L M Jones, S Lee, J C Trageser, D J Simons, and A Keller. Precise temporal responses in whisker trigeminal neurons. *Journal of neurophysiology*, 92(1): 665–8, 2004.

K A Justus, J Murlis, C Jones, and R T Cardé. Measurement of Odor-Plume

Structure in a Wind Tunnel Using a Photoionization Detector and a Tracer Gas. *Environmental Fluid Mechanics*, 2(1):115–142, 2002.

L M Kay, T Crk, and J Thorngate. A redefinition of odor mixture quality. *Behavioral neuroscience*, 119(3):726–733, 2005.

P F Kent, Maxwell M. Mozell, S J Murphy, and D E Hornung. The interaction of imposed and inherent olfactory mucosal activity patterns and their composite representation in a mammalian species using voltage-sensitive dyes. *The Journal of neuroscience : the official journal of the Society for Neuroscience*, 16(1): 345–353, 1996.

Adam Kepecs, Naoshige Uchida, and Zachary F Mainen. The sniff as a unit of olfactory processing. *Chemical senses*, 31(2):167–179, 2006.

A G Khan, M Sarangi, and U S Bhalla. Rats track odour trails accurately using a multi-layered strategy with near-optimal sampling. *Nature communications*, 3: 703, 2012.

Shu Kikuta, Max L. Fletcher, Ryota Homma, Tatsuya Yamasoba, and Shin Nagayama. Odorant Response Properties of Individual Neurons in an Olfactory Glomerular Module. *Neuron*, 77(6):1122–1135, 2013.

T K Knott, P A Madany, A A Faden, M Xu, J Strotmann, T R Henion, and G A Schwarting. Olfactory discrimination largely persists in mice with defects in odorant receptor expression and axon guidance. *Neural development*, 7(4):17, 2012.

M Kollo, A Schmaltz, M Abdelhamid, I Fukunaga, and A T Schaefer. Silent mitral cells dominate odor responses in the olfactory bulb of awake mice. *Nature neuroscience*, 17(10):1313–5, 2014.

K Kosaka, Y Aika, K Toida, C W Heizmann, W Hunziker, D M Jacobowitz, I Nagatsu, P Streit, T J Visser, and T Kosaka. Chemically defined neuron groups and their subpopulations in the glomerular layer of the rat main olfactory bulb. *Neuroscience research*, 23(1):73–88, 1995.

K Kosaka, K Toida, F L Margolis, and T Kosaka. Chemically defined neuron groups and their subpopulations in the glomerular layer of the rat main olfactory bulb-II. Prominent differences in the intraglomerular dendritic arborization and

their relationship to olfactory nerve terminals. *Neuroscience*, 76(3):775–786, 1997.

K Kosaka, K Toida, Y Aika, and T Kosaka. How simple is the organization of the olfactory glomerulus?: the heterogeneity of so-called periglomerular cells. *Neuroscience research*, 30(2):101–110, 1998.

M Kree, J Duplat, and E Villermaux. The mixing of distant sources. *Physics of Fluids*, 25(9):91103, 2013.

L P S Kuenen and R T Carde. Strategies for recontacting a lost pheromone plume: casting and upwind flight in the male gypsy moth. *Physiological Entomology*, 19(1):15–29, 1994.

D G Laing and G W Francis. The capacity of humans to identify odors in mixtures. *Physiology & behavior*, 46(5):809–814, 1989.

G Laurent. A Systems Perspective on Early Olfactory Coding. *Science*, 286 (5440):723–728, 1999.

G Laurent, M Stopfer, R W Friedrich, M I Rabinovich, a Volkovskii, and H D Abarbanel. Odor encoding as an active, dynamical process: experiments, computation, and theory. *Annual review of neuroscience*, 24:263–97, 2001.

A Li, D H Gire, T Bozza, and D Restrepo. Precise Detection of Direct Glomerular Input Duration by the Olfactory Bulb. *Journal of Neuroscience*, 34(48):16058–16064, 2014.

S H Lichtenstein, G E Carvell, and D J Simons. Responses of Rat Trigeminal Ganglion Neurons to Movements of Vibrissae in Different Directions. *Somatosensory & Motor Research*, 7(1):47–65, 1990.

D Y Lin, S D Shea, and L C Katz. Representation of natural stimuli in the rodent main olfactory bulb. *Neuron*, 50(6):937–949, 2006.

C Linster and R Gervais. Investigation of the role of interneurons and their modulation by centrifugal fibers in a neural model of the olfactory bulb. *Journal of computational neuroscience*, 3(3):225–46, 1996.

C Linster and M Hasselmo. Modulation of inhibition in a model of olfactory bulb reduces overlap in the neural representation of olfactory stimuli. *Behavioural brain research*, 84(1-2):117–127, 1997.

S. Liu, A. C. Puche, and M. T. Shipley. The Interglomerular Circuit Potently Inhibits Olfactory Bulb Output Neurons by Both Direct and Indirect Pathways. *Journal of Neuroscience*, 36(37):9604–9617, 2016.

C Liwei, Y Jianhua, and H Oussaadi. Experimental Study on Odor Source Localization System Based on Metal Oxide Gas Sensors. pages 143–146, 2011.

C Lodovichi, L Belluscio, and L C Katz. Functional topography of connections linking mirror-symmetric maps in the mouse olfactory bulb. *Neuron*, 38(2):265–276, 2003.

A Lozano, B Yip, and R K Hanson. Acetone: a tracer for concentration measurements in gaseous flows by planar laser-induced fluorescence. *Experiments in Fluids*, 13(6):369–376, 1992.

X Lu and B M Slotnick. Olfaction in rats with extensive lesions of the olfactory bulbs: implications for odor coding. *Neuroscience*, 84(3):849–66, 1998.

J Ma and G Lowe. Correlated firing in tufted cells of mouse olfactory bulb. *Neuroscience*, 169(4):1715–1738, 2010.

M Ma, W R Chen, and G M Shepherd. Electrophysiological characterization of rat and mouse olfactory receptor neurons from an intact epithelial preparation. *Journal of Neuroscience Methods*, 92(1-2):31–40, 1999.

Foteos Macrides and Stephen P. Schneider. Laminar organization of mitral and tufted cells in the main olfactory bulb of the adult hamster. *Journal of Comparative Neurology*, 208(4):419–430, 1982.

Masato Maesako, Kengo Uemura, Masakazu Kubota, Akira Kuzuya, Kazuki Sasaki, Naoko Hayashida, Megumi Asada-Utsugi, Kiwamu Watanabe, Maiko Uemura, Takeshi Kihara, Ryosuke Takahashi, Shun Shimohama, and Ayae Kinoshita. Exercise is more effective than diet control in preventing high fat diet-induced β-amyloid deposition and memory deficit in amyloid precursor protein transgenic mice. *Journal of Biological Chemistry*, 287(27):23024–23033, 2012.

B Malnic. Combinatorial receptor codes for odors. 1999.

K McBride and B Slotnick. Discrimination between the enantiomers of carvone and of terpinen-4-ol odorants in normal rats and those with lesions of the olfactory bulbs. *The Journal of neuroscience : the official journal of the Society for Neuroscience*, 26(39):9892–901, 2006.

J H McDermott. The cocktail party problem. *Current biology : CB*, 19(22):R1024–7, 2009.

M J Meaney, J Diorio, D Francis, J Widdowson, P La Plante, C Caldji, S Sharma, R Jonathan, S Paul, and M Plotsky. Early environmental regulation of forebrain glucocorticoid receptor gene expression: Implications for adrenocortical responses to stress. *Developmental Neuroscience*, 18(1-2):61–72, 1996.

M K Meijer, R Sommer, B M Spruijt, L F M van Zutphen, and V Baumans. Influence of environmental enrichment and handling on the acute stress response in individually housed mice. *Laboratory Animals*, 41(2):161–173, 2007.

P Mombaerts, F Wang, C Dulac, S K Chao, A Nemes, M Mendelsohn, J Edmondson, and R Axel. Visualizing an olfactory sensory map. *Cell*, 87(4):675–686, 1996.

P A Moore and J Atema. Spatial information in the three-dimensional fine structure of an aquatic odor plume. *The Biological Bulletin*, 181(3):408–418, 1991.

Kensaku Mori, Kiyoshi Kishi, and Hisayuki Ojima. Distribution of local axon collaterals of mitral, displaced mitral, and tufted cells in the rabbit olfactory bulb. *Journal of Comparative Neurology*, 225(4):511–526, 1984.

M B Moser, D C Rowland, and E I Moser. Place cells, grid cells, and memory. *Cold Spring Harbor perspectives in biology*, 7(2):a021808, 2015.

R U Muller and J L Kubie. The effects of changes in the environment on the spatial firing of hippocampal complex-spike cells. *Journal of Neuroscience*, 7 (7):1951–1968, 1987.

J Murlis. Odor Plumes And How Insects Use Them. *Annual Review of Entomology*, 37(1):505–532, 1992.

J Murlis. *Odor Plumes and the Signal They Provide*, pages 221–231. Springer US, Boston, MA, 1997.

J Murlis. Spatial and temporal structures of pheromone plumes in fields and forests. *Langmuir*, 2000.

G J Murphy, L L Glickfeld, Z Balsen, and J S Isaacson. Sensory Neuron Signaling to the Brain: Properties of Transmitter Release from Olfactory Nerve Terminals. *The Journal of Neuroscience*, 24(12):3023 –3030, 2004.

S Nagayama, A Enerva, M L Fletcher, A V Masurkar, K M Igarashi, K Mori, and W R Chen. Differential Axonal Projection of Mitral and Tufted Cells in the Mouse Main Olfactory System. *Frontiers in Neural Circuits*, 4(September):1–8, 2010.

S Nagayama, R Homma, and F Imamura. Neuronal organization of olfactory bulb circuits. *Frontiers in Neural Circuits*, 8(September):1–19, 2014.

Katherine I Nagel and Rachel I Wilson. Biophysical mechanisms underlying olfactory receptor neuron dynamics. *Nature neuroscience*, 14(2):208–16, 2011.

K. Nara, L. R. Saraiva, X. Ye, and L. B. Buck. A Large-Scale Analysis of Odor Coding in the Olfactory Epithelium. *Journal of Neuroscience*, 31(25):9179–9191, 2011.

W T Nickell, M M Behbehani, and M T Shipley. Evidence for GABAB-mediated inhibition of transmission from the olfactory nerve to mitral cells in the rat olfactory bulb. *Brain research bulletin*, 35(2):119–123, 1994.

D Nunes and T Kuner. Disinhibition of olfactory bulb granule cells accelerates odour discrimination in mice. *Nature communications*, 6:8950, 2015.

J F Nunez, P Ferre, R M Escorihuela, A Tobena, and A Fernandez-Teruel. Effects of postnatal handling of rats on emotional, HPA-Axis, and prolactin reactivity to novelty and conflict. *Physiology and Behavior*, 60(5):1355–1359, 1996.

D H O'Connor, N G Clack, D Huber, T Komiyama, E W Myers, and K Svoboda. Vibrissa-based object localization in head-fixed mice. *The Journal of neuroscience : the official journal of the Society for Neuroscience*, 30(5):1947–67, 2010.

J O'Keefe and D H Conway. Hippocampal place units in the freely moving rat: why they fire where they fire. *Experimental brain research*, 31(4):573–590, 1978.

N Onoda and K Mori. Depth distribution of temporal firing patterns in olfactory bulb related to air-intake cycles. *Journal of Neurophysiology*, 44(1):29–39, 1980.

E Orona, E C Rainer, and J W Scott. Dendritic and axonal organization of mitral and tufted cells in the rat olfactory bulb. *The Journal of comparative neurology*, 226(3):346–356, 1984.

G H Otazu, H Chae, M B Davis, and D F Albeanu. Cortical Feedback Decorrelates Olfactory Bulb Output in Awake Mice. *Neuron*, pages 1–17, 2015.

F Papi. Olfactory navigation in birds. *Experientia*, 46(4):352–363, 1990.

A Parabucki, A Bizer, G Morris, M C Smear, and R Shusterman. Odor concentration change detectors in the Olfactory Bulb. *bioRxiv*, pages 1–17, 2017.

I J Park, A M Hein, Y V Bobkov, M A Reidenbach, B W Ache, and J C Principe. Neurally Encoding Time for Olfactory Navigation. *PLOS Computational Biology*, 12(1):e1004682, 2016.

Il Memming Park, Yuriy V Bobkov, Barry W Ache, and José C Príncipe. Intermittency coding in the primary olfactory system: a neural substrate for olfactory scene analysis. *The Journal of neuroscience : the official journal of the Society for Neuroscience*, 34(3):941–52, 2014.

S I Park, D S Brenner, G Shin, C D Morgan, B A Copits, H U Chung, M Y Pullen, K N Noh, S Davidson, S J Oh, J Yoon, K I Jang, V K Samineni, M Norman, J G Grajales-Reyes, S K Vogt, S S Sundaram, K M Wilson, J S Ha, R Xu, T Pan, T Kim, Y Huang, M C Montana, J P Golden, M R Bruchas, R W Gereau IV, and J A Rogers. Soft, stretchable, fully implantable miniaturized optoelectronic systems for wireless optogenetics. *Nat Biotech*, 33(12):1280–1286, 2015.

S Parrish-Aungst, M T Shipley, F Erdelyi, G Szabo, and A C Puche. Quantitative analysis of neuronal diversity in the mouse olfactory bulb. *The Journal of comparative neurology*, 501(6):825–836, 2007.

J Pevsner, R R Reed, P G Feinstein, and S H Snyder. Molecular cloning of odorant-binding protein: member of a ligand carrier family. *Science (New York, N.Y.)*, 241(4863):336–339, 1988.

D W Pfaff and E Gregory. Olfactory coding in olfactory bulb and medial forebrain bundle of normal and castrated male rats. *J Neurophysiol*, 34(2):208–216, 1971.

B. Raman, J. Joseph, J. Tang, and M. Stopfer. Temporally Diverse Firing Patterns in Olfactory Receptor Neurons Underlie Spatiotemporal Neural Codes for Odors. *Journal of Neuroscience*, 30(6):1994–2006, 2010.

K Raming, J Krieger, J Strotmann, I Boekhoff, S Kubick, C Baumstark, and H Breer. Cloning and expression of odorant receptors. *Nature*, 361(6410): 353–356, 1993.

M R Rebello, T S. McTavish, D C Willhite, S M Short, G M Shepherd, and J V Verhagen. Perception of Odors Linked to Precise Timing in the Olfactory System. *PLoS Biology*, 12(12):e1002021, 2014.

J Reisert and H R Matthews. Response properties of isolated mouse olfactory receptor cells. *The Journal of physiology*, 530(Pt 1):113–122, 2001.

J Reisert and H Zhao. Perspectives on: information and coding in mammalian sensory physiology: response kinetics of olfactory receptor neurons and the implications in olfactory coding. *The Journal of general physiology*, 138(3): 303–310, 2011.

Johannes Reisert, King-Wai Yau, and Frank L Margolis. Olfactory marker protein modulates the cAMP kinetics of the odour-induced response in cilia of mouse olfactory receptor neurons. *The Journal of physiology*, 585(Pt 3):731–740, 2007.

K J Ressler, S L Sullivan, and L B Buck. A zonal organization of odorant receptor gene expression in the olfactory epithelium. *Cell*, 73(3):597–609, 1993.

K J Ressler, S L Sullivan, and L B Buck. Information coding in the olfactory system: evidence for a stereotyped and highly organized epitope map in the olfactory bulb. *Cell*, 79(7):1245–1255, 1994.

A Resulaj and D Rinberg. Novel Behavioral Paradigm Reveals Lower Temporal Limits on Mouse Olfactory Decisions. *Journal of Neuroscience*, 35(33):11667–11673, 2015.

M F Revial, G Sicard, A Duchamp, and A Holley. New studies on odour discrimination in the frog's olfactory receptor cells. II. Mathematical analysis of electrophysiological responses. *Chemical Senses*, 8(2):179–194, 1983.

D Rinberg, A Koulakov, and A Gelperin. Speed-accuracy tradeoff in olfaction. *Neuron*, 51(3):351–8, 2006.

D Rokni, V Hemmelder, V Kapoor, and V N Murthy. An olfactory cocktail party: figure-ground segregation of odorants in rodents. *Nat Neurosci*, 17(9):1225–1232, 2014.

B Roland, R Jordan, D L Sosulski, A Diodato, I Fukunaga, I Wickersham, K M Franks, A T Schaefer, and Alexander Fleischmann. Massive normalization of olfactory bulb output in mice with a monoclonal nose. *eLife*, 5(MAY2016):1–25, 2016.

J P Rospars, P Lansky, A Duchamp, and P Duchamp-Viret. Relation between stimulus and response in frog olfactory receptor neurons in vivo. *The European journal of neuroscience*, 18(5):1135–1154, 2003.

Silke Sachse and C Giovanni Galizia. Role of inhibition for temporal and spatial odor representation in olfactory output neurons: a calcium imaging study. *Journal of neurophysiology*, 87(2):1106–1117, 2002.

S Saito and K Murase. Ex vivo imaging of mouse brain using micro-CT with non-ionic iodinated contrast agent: a comparison with myelin staining. *The British journal of radiology*, 85(1019):e973–8, 2012.

Luis R. Saraiva, Ximena Ibarra-Soria, Mona Khan, Masayo Omura, Antonio Scialdone, Peter Mombaerts, John C. Marioni, and Darren W. Logan. Hierarchical deconstruction of mouse olfactory sensory neurons: From whole mucosa to single-cell RNA-seq. *Scientific Reports*, 5(October):1–17, 2015.

E Save, A Cressant, C Thinus-Blanc, and B Poucet. Spatial firing of hippocampal place cells in blind rats. *The Journal of neuroscience : the official journal of the Society for Neuroscience*, 18(5):1818–1826, 1998.

E Save, L Nerad, and B Poucet. Contribution of multiple sensory information to place field stability in hippocampal place cells. *Hippocampus*, 10(1):64–76, 2000.

K Shen, S Tootoonian, and G Laurent. Encoding of mixtures in a simple olfactory system. *Neuron*, 80(5):1246–62, 2013.

G M Shepherd and C A Greer. Olfactory bulb. In *Synaptic organisation of the brain*, chapter 5, pages 159–203. Oxford Univ Press, 5 edition, 1998.

T Shibuya and S Shibuya. Olfactory epithelium: unitary responses in the tortoise. *Science (New York, N.Y.)*, 140(3566):495–496, 1963.

M T Shipley and M Ennis. Functional organization of olfactory system. *Journal of neurobiology*, 30(1):123–176, 1996.

M T Shipley, J H McLean, and M Ennis. Olfactory system. In *The rat nervous system*, chapter 33, pages 899–926. Academix Press, 2 edition, 1995.

M Shoykhet, D Doherty, and D J Simons. Coding of deflection velocity and amplitude by whisker primary afferent neurons: implications for higher level processing. *Somatosensory & motor research*, 17(2):171–80, 2000.

R Shusterman, M C Smear, A A Koulakov, and D Rinberg. Precise olfactory responses tile the sniff cycle. *Nature neuroscience*, 14(8):1039–44, 2011.

D J Simons and G E Carvell. Thalamocortical response transformation in the rat vibrissa/barrel system. *Journal of Neurophysiology*, 61(2):311–330, 1989.

Andrew M. Slater and Lei Cao. A Protocol for Housing Mice in an Enriched Environment. *Journal of Visualized Experiments*, (100):1–8, 2015.

B Slotnick. Olfactory performance of rats after selective deafferentation of the olfactory bulb by 3-methyl indole. *Chemical senses*, 32(2):173–81, 2007.

Burton Slotnick and Natalya Bodyak. Odor discrimination and odor quality perception in rats with disruption of connections between the olfactory epithelium and olfactory bulbs. *The Journal of neuroscience : the official journal of the Society for Neuroscience*, 22(10):4205–16, 2002.

M Smear, A Resulaj, J Zhang, T Bozza, and D Rinberg. Multiple perceptible signals from a single olfactory glomerulus. *Nature neuroscience*, 16(11):1687–1691, 2013.

R E Sorge, L J Martin, K A Isbester, S G Sotocinal, S Rosen, A H Tuttle, J S Wieskopf, Erinn L Acland, Anastassia Dokova, Basil Kadoura, Philip Leger, Josiane C S Mapplebeck, Martina McPhail, Ada Delaney, Gustaf Wigerblad, Alan P Schumann, Tammie Quinn, Johannes Frasnelli, Camilla I Svensson, Wendy F Sternberg, and Jeffrey S Mogil. Olfactory exposure to males, including men, causes stress and related analgesia in rodents. *Nature Methods*, 11 (6):629–632, 2014.

D L Sosulski, M Lissitsyna Bloom, T Cutforth, R Axel, and S R Datta. Distinct representations of olfactory information in different cortical centres. *Nature*, 472(7342):213–216, 2011.

Hartwig Spors and Amiram Grinvald. Spatio-temporal dynamics of odor representations in the mammalian olfactory bulb. *Neuron*, 34(2):301–15, 2002.

Hartwig Spors, Matt Wachowiak, Lawrence B Cohen, and Rainer W Friedrich. Temporal Dynamics and Latency Patterns of Receptor Neuron Input to the Olfactory Bulb. *The Journal of Neuroscience*, 26(4):1247–1259, 2006.

J S Stierle, C G Galizia, and P Szyszka. Millisecond stimulus onset-asynchrony enhances information about components in an odor mixture. *The Journal of*

neuroscience : the official journal of the Society for Neuroscience, 33(14):6060–9, 2013.

J N Stirman, L B Townsend, and S L Smith. A touchscreen based global motion perception task for mice. *Vision Research*, 127:74–83, 2016.

T A Szuts, V Fadeyev, S Kachiguine, A Sher, M V Grivich, M Agrochao, P Hottowy, W Dabrowski, E V Lubenov, A G Siapas, N Uchida, A M Litke, and M Meister. A wireless multi-channel neural amplifier for freely moving animals. *Nat Neurosci*, 14(2):263–269, 2011.

P Szyszka, J S Stierle, S Biergans, and C G Galizia. The speed of smell: odor-object segregation within milliseconds. *PloS one*, 7(4):e36096, 2012.

Paul Szyszka, Richard C Gerkin, C Giovanni Galizia, and Brian H Smith. High-speed odor transduction and pulse tracking by insect olfactory receptor neurons. *Proceedings of the National Academy of Sciences of the United States of America*, 111(47):16925–16930, 2014.

K Toida, K Kosaka, C W Heizmann, and T Kosaka. Chemically defined neuron groups and their subpopulations in the glomerular layer of the rat main olfactory bulb: III. Structural features of calbindin D28K-immunoreactive neurons. *The Journal of comparative neurology*, 392(2):179–198, 1998.

K Toida, K Kosaka, Y Aika, and T Kosaka. Chemically defined neuron groups and their subpopulations in the glomerular layer of the rat main olfactory bulb-IV. Intraglomerular synapses of tyrosine hydroxylase-immunoreactive neurons. *Neuroscience*, 101(1):11–17, 2000.

A Tomaru and T Kurahashi. Mechanisms determining the dynamic range of the bullfrog olfactory receptor cell. *Journal of neurophysiology*, 93(4):1880–8, 2005.

Kazushige Touhara and Leslie B. Vosshall. Sensing Odorants and Pheromones with Chemosensory Receptors. *Annual Review of Physiology*, 71(1):307–332, 2009.

N Uchida and Z F Mainen. Odor concentration invariance by chemical ratio coding. *Frontiers in systems neuroscience*, 1(April):3, 2007.

N Uchida, Y K Takahashi, M Tanifuji, and K Mori. Odor maps in the mammalian olfactory bulb: domain organization and odorant structural features. *Nature neuroscience*, 3(10):1035–1043, 2000.

Naoshige Uchida and Zachary F Mainen. Speed and accuracy of olfactory discrimination in the rat. *Nature neuroscience*, 6(11):1224–9, 2003.

F van Breugel and M H Dickinson. Plume-tracking behavior of flying Drosophila emerges from a set of distinct sensory-motor reflexes. *Current biology : CB*, 24 (3):274–286, 2014.

C H Vanderwolf. Hippocampal activity, olfaction, and sniffing: an olfactory input to the dentate gyrus. *Brain research*, 593(2):197–208, 1992.

R Vassar, J Ngai, and R Axel. Spatial segregation of odorant receptor expression in the mammalian olfactory epithelium. *Cell*, 74(2):309–318, 1993.

R Vassar, S K Chao, R Sitcheran, J M Nunez, L B Vosshall, and R Axel. Topographic organization of sensory projections to the olfactory bulb. *Cell*, 79(6): 981–991, 1994.

M Vergassola, E Villermaux, and B I Shraiman. Infotaxis as a strategy for searching without gradients. *Nature*, 445(7126):406–9, 2007.

N J Vickers. Mechanisms of animal navigation in odor plumes. *The Biological bulletin*, 198(2):203–12, 2000.

N J Vickers. Winging it: moth flight behavior and responses of olfactory neurons are shaped by pheromone plume dynamics. *Chemical senses*, 31(2):155–66, 2006.

N J Vickers, T a Christensen, T C Baker, and J G Hildebrand. Odour-plume dynamics influence the brain's olfactory code. *Nature*, 410(6827):466–470, 2001.

E Villermaux and C Innocenti. On the geometry of turbulent mixing. *Journal of Fluid Mechanics*, 393:123–147, 1999.

V Voikar, G Colacicco, O Gruber, E Vannoni, H Lipp, and D P Wolfer. Conditioned response suppression in the IntelliCage: assessment of mouse strain differences and effects of hippocampal and striatal lesions on acquisition and retention of memory. *Behavioural Brain Research*, 213(2):304–312, 2010.

M Wachowiak and L B Cohen. Presynaptic inhibition of primary olfactory afferents mediated by different mechanisms in lobster and turtle. *The Journal of neuroscience : the official journal of the Society for Neuroscience*, 19(20):8808–8817, 1999.

M Wachowiak and L B Cohen. Representation of Odorants by Receptor Neuron Input to the Mouse Olfactory Bulb, 2001.

M Wachowiak and M T Shipley. Coding and synaptic processing of sensory information in the glomerular layer of the olfactory bulb. *Seminars in cell & developmental biology*, 17(4):411–23, 2006.

Matt Wachowiak, John P McGann, Philip M Heyward, Zuoyi Shao, Adam C Puche, and Michael T Shipley. Inhibition of olfactory receptor neuron input to olfactory bulb glomeruli mediated by suppression of presynaptic calcium influx. *Journal of neurophysiology*, 94(4):2700–2712, 2004.

H Wallraff. Avian olfactory navigation: its empirical foundation and conceptual state. *Animal Behaviour*, 67(2):189–204, 2004.

J W Wang, A M Wong, J Flores, L B Vosshall, and R Axel. Two-photon calcium imaging reveals an odor-evoked map of activity in the fly brain. *Cell*, 112(2): 271–282, 2003.

H Wässle. Parallel processing in the mammalian retina. *Nature Reviews Neuroscience*, 5(10):747–757, 2004.

Michael Wehr and Anthony M. Zador. Balanced inhibition underlies tuning and sharpens spike timing in auditory cortex. *Nature*, 426(6965):442–446, 2003.

M. J. Weissburg, D. B. Dusenbery, H. Ishida, J. Janata, T. Keller, P. J.W. Roberts, and D. R. Webster. A multidisciplinary study of spatial and temporal scales containing information in turbulent chemical plume tracking. *Environmental Fluid Mechanics*, 2(1-2):65–94, 2002.

C T Wentz, J G Bernstein, P Monahan, A Guerra, A Rodriguez, and E S Boyden. A wirelessly powered and controlled device for optical neural control of freely-behaving animals. *Journal of neural engineering*, 8(4):46021, 2011.

D W. Wesson, T N. Donahou, M O. Johnson, and M Wachowiak. Sniffing behavior of mice during performance in odor-guided tasks. *Chemical Senses*, 33(7):581–596, 2008a.

Daniel W. Wesson, Ryan M. Carey, Justus V. Verhagen, and Matt Wachowiak. Rapid encoding and perception of novel odors in the rat. *PLoS Biology*, 6(4): 717–729, 2008b.

C H Wetzel, H J Behrendt, G Gisselmann, K F Stortkuhl, B Hovemann, and H Hatt. Functional expression and characterization of a Drosophila odorant receptor in a heterologous cell system. *Proceedings of the National Academy of Sciences of the United States of America*, 98(16):9377–9380, 2001.

M A. Willis and T C. Baker. Effects of intermittent and continuous pheromone stimulation on the flight behaviour of the oriental fruit moth, Grapholita molesta. *Physiological Entomology*, 9(3):341–358, 1984.

R I Wilson and Z F Mainen. Early events in olfactory processing. *Annual Review of Neuroscience*, 29(1):163–201, 2006.

S S Wolfson and M S Landy. Examining edge- and region-based texture analysis mechanisms. *Vision research*, 38(3):439–446, 1998.

T B Woolf, G M Shepherd, and C A Greer. Local information processing in dendritic trees: subsets of spines in granule cells of the mammalian olfactory bulb. *The Journal of neuroscience : the official journal of the Society for Neuroscience*, 11(6):1837–1854, 1991.

G A. Wright and M G.A. Thomson. Odor perception and the variability in natural odor scenes. *Recent Advances in Phytochemistry*, 39(C):191–226, 2005.

C A Yao, R Ignell, and J R Carlson. Chemosensory coding by neurons in the coeloconic sensilla of the Drosophila antenna. *The Journal of neuroscience : the official journal of the Society for Neuroscience*, 25(37):8359–8367, 2005.

M Yokoi, K Mori, and S Nakanishi. Refinement of odor molecule tuning by dendrodendritic synaptic inhibition in the olfactory bulb. *Proceedings of the National Academy of Sciences of the United States of America*, 92(8):3371–5, 1995.

J M Young, C Friedman, E M Williams, J A Ross, L Tonnes-Priddy, and Barbara J Trask. Different evolutionary processes shaped the mouse and human olfactory receptor gene families. *Human molecular genetics*, 11(5):535–546, 2002.

C R Yu, J Power, G Barnea, S O'Donnell, H E V Brown, J Osborne, R Axel, and J A Gogos. Spontaneous neural activity is required for the establishment and maintenance of the olfactory sensory map. *Neuron*, 42(4):553–566, 2004.

H A Zariwala, A Kepecs, N Uchida, J Hirokawa, and Z F Mainen. The limits of deliberation in a perceptual decision task. *Neuron*, 78(2):339–51, 2013.

S Zhang and D Manahan-Vaughan. Spatial Olfactory Learning Contributes to Place Field Formation in the Hippocampus. *Cerebral cortex (New York, N.Y. : 1991)*, pages 1–10, 2013.

A Ziyatdinov, J M B Calvo, M Lechón, S Bermúdez i Badia, P F M J Verschure, S Marco, and A Perera. Odour Mapping Under Strong Backgrounds With a Metal Oxide Sensor Array. *AIP Conference Proceedings*, 1362(1):232–233, 2011.

Nomenclature

2-AFC	2-Alternative forced choice
2H	2-Heptanone
2P	2-Phenylethanol
αT	Alpha-terpinene
AA	Isopentyl acetate (also known as amyl acetate)
ACP	Acetophenone
ACSF	Artificial cerebrospinal fluid
AON	Anterior olfactory nucleus
B	Blank (mineral oil)
BNC	Bayonet Neill-Concelman (a type of RF coaxial cable jack)
bOSN	Bursting olfactory sensory neuron
cAMP	Cyclic adenosine monophosphate
cc	Correlation coefficient
Cinn.	Cinnamaldehyde
CN	Eucalyptol (also known as Cineol)
CSF	Cerebrospinal fluid
CT	Computed tomography

DAQ	Data acquisition
dF/F	Change in fluorescene relative to baseline fluorescence
DREADD	Designer receptor exclusively activated by designer drugs
EB	Ethyl butyrate
EPL	External plexiform layer
ET	External tufted (cell)
EU	Eugenol
eV	Electron volt
FC	Flow controller
GABA	γ-aminobutyric acid
GC	Granule cell
GL	Glomerular layer
GNG	Go/no-go
Guaj	Guajacol
GUI	Graphical user interface
ID	Identifier
IR	Infra-red
JG	Juxtaglomerular (cell)
MC	Mitral cell
MFC	Mass flow controller
NMDA	N-Methyl-D-aspartic acid
NTM	Non-trigeminal mixture

NTS	Non-trigeminal simple
O1	Odour 1
O2	Odour 2
OB	Olfactory bulb
OR	Olfactory receptor
OSN	Olfactory sensory neuron
P	Phenylethyl alcohol
PBS	Phosphate-buffered saline
PCA	Principal component analysis
PCI	Peripheral component interconnect
PD	Pulse duty
Pel.	Pelargonic acid
PFA	Paraformaldehyde
PG	Periglomerular (cell)
PID	Photoionisation detector
PLIF	Planar-laser induced fluorescence
PN	Principal neuron
PP	Pre-pulse
PWM	Pulse-width modulation
RFID	Radio-frequency identification
ROI	Region of interest
S+	Rewarded behavioural trial in go/no-go paradigm

S-	Unrewarded behavioural trial in go/no-go paradigm
SD	Standard deviation
sSA	Superficial short axon (cell)
TC	Tufted cell
TTC	Trials to criterion
UV	Ultraviolet
V	Vanillin
Val.	Valeric acid
VHS	Very high speed (valve)